CONTROL AND MANAGEMENT STRATEGY OF AUTONOMOUS VEHICLE FUNCTIONS

A Dissertation

by

CHANG WON KIM

Submitted to the Office of Graduate Studies of
Texas A&M University
in partial fulfillment of the requirements for the degree of

DOCTOR OF PHILOSOPHY

December 2010

Major Subject: Mechanical Engineering

CONTROL AND MANAGEMENT STRATEGY OF AUTONOMOUS VEHICLE FUNCTIONS

A Dissertation

by

CHANG WON KIM

Submitted to the Office of Graduate Studies of
Texas A&M University
in partial fulfillment of the requirements for the degree of

DOCTOR OF PHILOSOPHY

Approved by:

Chair of Committee,	Reza Langari
Committee Members,	Swaroop Darbha
	Won-jong Kim
	Yoonsuck Choe
Head of Department,	Dennis L. O'Neal

December 2010

Major Subject: Mechanical Engineering

ABSTRACT

Control and Management Strategy of Autonomous Vehicle Functions.

(December 2010)

Chang Won Kim, B.S., Pusan National University, Korea;

M.S., Pusan National University, Korea

Chair of Advisory Committee: Dr. Reza Langari

In this research, an autonomous vehicle function management methodology is studied. In accordance with the traffic situation, the decision making level chooses the optimal function that guarantees safety and minimizes fuel consumption while the control level is implemented via neuromorphic strategy based on the brain limbic system. To realize the decision making strategy, the Analytic Hierarchy Process (AHP) is used by considering driving safety, driving speed, and fuel efficiency as the objectives. According to the traffic situation and predefined driving mode, Lane Change Maneuver (LCM) and Adaptive Cruise Control (ACC) are chosen as the alternative functions in the AHP framework.

The adaptive AHP is utilized to cope with dynamically changing traffic environment. The proposed adaptive AHP algorithm provides an optimal relative importance matrix that is essential to make decisions under a varying traffic situation and driving modes. The simulation results show that proposed autonomous vehicle function management structure produces optimal decisions that satisfy the driving

preference. The stability of BLS based control is also investigated via Cell-to-Cell Mapping.

In this research, autonomous vehicle functions such as Lane change maneuver and Adaptive cruise control are developed by means of BLS based control. The simulation results considered various traffic situations that an autonomous vehicle can encounter. To demonstrate the suggested control method Cell-to-Cell Mapping is utilized. Subsequently, the autonomous vehicle function management strategy is developed by Applying AHP and an adaptive AHP strategy is developed to cope with various traffic situations and driving modes. The suggested method is verified numerical simulations.

In his heart a man plans his course, but the LORD determines his steps

(Proverbs 16: 9)

ACKNOWLEDGEMENTS

First of all, I would like to thank God for leading me to this unique experience and making me trained under good circumstances.

I convey my sincere appreciation to my committee chair, Dr. Reza Langari, and my committee members, Dr. Won-jong Kim, Dr. Swaroop Darbha, and Dr. Yoonsuck Choe, for their guidance and support throughout the process of this research. Especially, Dr. Langari helped me to grow up as a researcher from a normal graduate student. His encouragement and careful concern drove me to this status.

I would like to express special thanks to my supporters in Korea. They encouraged me to go through all challenging circumstances, especially my brothers, my uncle, pastor Seok, Museop, Haejin, Jinho, Jong, and Wonyeoung. Thanks also go to my church families who shared joy and sorrow together.

Finally, I would like to convey my deepest gratitude to my parents and wife, Hyejin, for their encouragement and continual love during the whole process.

TABLE OF CONTENTS

Page

Page

LIST OF FIGURES

Page

Page

LIST OF TABLES

1. INTRODUCTION

Increasing number of vehicles has resulted in safety issues affecting the transportation sector [1] [1]. Moreover, recent research indicates that driver error contributes to up to 75% of all roadway crashes among vehicle defects, environment, and road conditions [2] because of the human's limited perception about the environment, limited concentration on driving. To reduce the impact of these accidents, additional safety measures in vehicle design have been proposed [3]. An alternative solution in this respect is via the concept of intelligent transportation system (ITS). In particular, advanced vehicle control technology has been proposed towards the goal of a fully autonomous vehicle. The objectives of the unmanned vehicle are not only to achieve safety, but also to improve fuel efficiency and enhance driving comfort. To fulfill these goals, several functions such as stability control, adaptive cruise control, collision mitigation, lane keeping assistance and lane change support etc., have been proposed by a number of researchers [4-9].

While autonomous vehicles provide a viable approach to improve vehicle safety by relying on artificial intelligent control strategies, the vast majority of existing vehicles and even recently launched vehicles remain almost entirely dependent on human driving. Therefore driving safety and efficient reinforcing facilities are developed and installed in

---

This dissertation follows the style and format of *IEEE Transactions on Vehicular Technology.*

[1] World Health Organization (WHO) predicts that traffic accident will be ranked third in the order of disease burden by the year 2030[1].

an autonomous vehicle, and the necessity of managing these functions in accordance with traffic environments is emerging. Optimal management of multiple autonomous vehicle functions will reinforce active safety by reducing driving error. To this end, in this research, lane change maneuver and adaptive cruise control strategies are developed using a Brain Limbic System (BLS) based control while the individual functions are managed by an Analytic Hierarchy Process. These are discussed at more length below.

1.1 Brain Limbic System Based Control

The previously explained autonomous vehicle functions are realized by a neuromorphic based control, especially emotion. Traditionally, emotion has been regarded as something that is irrational. However, scientists have recently learned about the positive aspects of human emotions. Moreover, for a number of years, the emotional signal processing in the brain limbic system has been the subject of research in cognitive science. Mowrer [10] described a two-process model of learning through Amygdalo-Orbitofrontal system. In the suggested learning system, the incoming stimuli are analyzed by the stimulus emotional system, and the analyzed results are manipulated as an emotional cue for stimulus-response learning. Rolls [11] elucidated the mechanism of the emotion and its application to the neural basis of emotion. LeDoux [12] and Rolls [13] explained the function of amygdala in the emotional process. In particular, Moren and Balkenius [14], [15] developed the computational model of the process of generating emotions in the human brain and verified the model using basic simulations. Subsequently the applications of the brain limbic system model appeared in the control

engineering literatures. Lucas et al. [16] introduced an intelligent controller model, which they christened Brain Emotional Learning, or BEL. Mehrabian and Lucas [17] designed a robust adaptive controller for stable uncertain nonlinear systems with BEL. Chandra and Langari [18] analyzed the BEL based approach, which they referred to as the brain limbic system, or BLS, by using methods of nonlinear systems theory. Shahmirzadi, et al. [19] compared the BEL based control with sliding mode control for rollover prevention of tractor-semitrailers. BEL (or BLS) has also been evaluated in a range of other systems [20] – [27]. These studies have demonstrated the performance of BLS as an adaptive control methodology, which I believe that this control strategy is also applicable to the vehicle driving situation in view of the disturbances affecting the vehicle performance.

1.2 Lane Change Maneuver in an Autonomous Vehicle

In the vehicle dynamics control framework, two major control problems have to be solved. One is spacing control and the other is lateral control. The former function is to keep the longitudinal space between vehicles at a prescribed level while the latter is to maintain the vehicle on a set reference path via steering control [28].

Lane change support is one of the functions needed to realize the notion of an intelligent or autonomous vehicle. To this end, Chee and Tomizuka [29] used four trajectories for the lane change maneuver, which are designed using transition time as the performance index. They implemented this function via linear quadratic (LQ) control as well as frequency shaped linear quadratic (FSLQ) control. An infrastructure guided

lane change using an additional cross-over marker reference, and free lane change using a yaw-rate sensor are investigated by Tan et al. [30]. Hatipoglu et al. [31] proposed a virtual yaw reference and the utilization of a robust switching controller to generate steering commands. Feng et al. [32] made usage of fuzzy-neural networks (FNN) and genetic algorithms (GA) to accomplish lane change maneuvers. You et al. [33] have presented a robust vehicle controller using a 2-DOF loop shaping design procedure in highway driving environment. Naranjo et al. [34] introduced an overtaking system that uses a fuzzy controller. The control structure mimics human behavior and reactions during overtaking maneuvers. Abe [35] presented a human driver model based controller with respect to the looking-ahead distance and vehicle speed. This model is widely seen as an effective basis for autonomous or semi-autonomous vehicle control.

1.3 Adaptive Cruise Control in an Autonomous Vehicle

The other autonomous vehicle function that is considered in this research is Adaptive Cruise Control (ACC). ACC was introduced as an extension of conventional cruise control by including the detection of a vehicle in front of the ACC-equipped car, and inter-vehicle distance regulation with respect to the relevant target. By using a LIDAR (Light Detection And Ranging), which is located on the front of the vehicle, or cameras mounted on the front of the vehicle one can scan for other vehicles or objects in front of the ACC-equipped vehicle. The ACC-equipped vehicle decelerates when approaching a vehicle and accelerates again to the preset velocity when traffic condition

allows this, therefore providing the ACC equipped the capacity to improve driving safety and efficiency.

Since ACC-equipped vehicles must follow a preceding vehicle at a desired distance, a number of inter-vehicle distance spacing policies have been suggested in the literature. These range from constant distance policy to constant time gap (headway) policy, and modified velocity dependent gap policy [36-38]. However, constant time gap policy, the inter-vehicular spacing varies linearly with vehicle velocity, is utilized in the majority of ACC research. In particular, Ioannou and Chien [39] proposed a control law for an AICC (Autonomous Intelligent Cruise Control) system based on constant time headway safety distance. More recently, Liang and Peng [40] developed an optimal ACC algorithm that minimizes the range and range error for all the vehicles in a string considering a two-level methodology. In this two-level approach, which is commonly used in ACC research, the higher level computes the desired acceleration/deceleration rate and the lower lever controls the throttle/brake to generate the prescribed action. Likewise, Swaroop and Hedrick [41] provided a framework for establishing conditions for string stability and a metric for analyzing the performance of a platoon resulting from different ACC algorithms. Similarly, Santhanakrishnan and Rajamani have developed a framework for design and evaluation of spacing policies by considering string stability, traffic flow stability, and traffic flow capacity [38]. Bageshwar et al. [42] proposed optimal control based on the model predictive framework to achieve a spacing control law. Nonlinear reference model based control approach providing dynamic solutions consistent with the safety constraint and comfort specifications is developed in [7]. And

Ferrara and Vecchio [43] have suggested a second order sliding mode control to achieve ACC. More recently, Tsai et al. [44] developed a fuzzy longitudinal control system for achieving adaptive cruise control (ACC) and Stop&Go control.

1.4 Analytic Hierarchy Process

After autonomous vehicle functions are developed. Subsequently, a multi objective decision making theory, so called, Analytic Hierarchy Process (AHP) is utilized as the higher level decision maker for integration of active safety features such as adaptive cruise control or autonomous lane change function. AHP was developed by Thomas L. Saaty in the 1970s [45-46]. This methodology is applied widely in a broad range of areas ranging from public policy to business management, industrial process scheduling, healthcare, and educational administration. Normally, the AHP is a structured method that is used in decision making for complex problems. The decision maker is helped by the AHP to choose the best alternative, which satisfies the given needs. In particular, by considering the traffic situation that the vehicle encounters, this layer decides “which function will be applied when” to ensure safe and efficient driving.

1.5 Contributions

The eventual goal of this research is to developing an autonomous vehicle. Even though a lot of human assistant systems have been developed, those functions do not perform an autonomous driving. Figure 1.1 displays the autonomous vehicle developing direction. Lane change maneuver (LCM), adaptive cruise control (ACC), forward

collision avoidance system (FCAS), and lane keeping system (LKS) are considered as the autonomous vehicles main functions, the decision is made by human (driver) in semi autonomous vehicle system while the computer makes decision in fully autonomous vehicle.

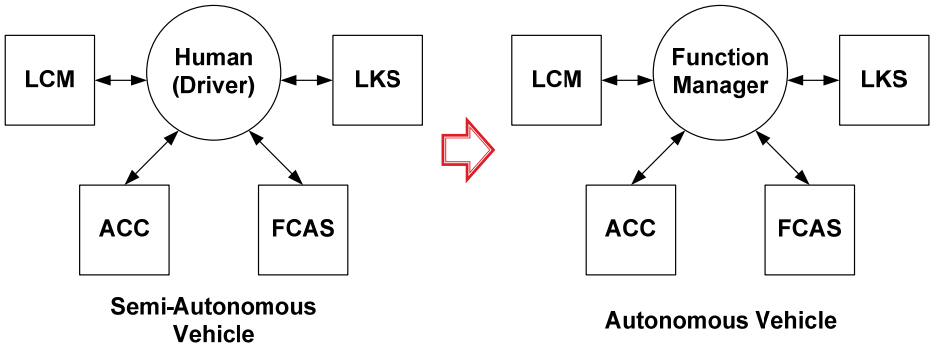

Figure 1.1 An autonomous vehicle.

In order to achieve the goal, two of the functions such as LCM and ACC are developed by Brain Limbic System based control. Subsequently, the functions are managed by Analytic Hierarchy Process to select an optimal function among the available autonomous vehicle functions.

The contributions of this research are stated below;

- BLS based control application to LCM and ACC development
- BLS based control stability analysis via Cell-to-Cell Mapping method
- Application of AHP to an autonomous vehicle function management
- An adaptive AHP for various traffic situations and driving modes.

1.6 Outline of the Dissertation

In Section 2, the detail functions and design and application strategy of brain limbic system based control is stated.

In Section 3, BLS based control method is applied to lane change maneuver function. After design the controller, the results are compared with the human driver model introduced by Abe [35]. In the simulation, without and with disturbance cases are considered by defining the disturbance of wind load, cornering stiffness uncertainty, and mass change.

In Section 4, BLS based control is utilized for adaptive cruise control. The results of BLS based ACC are compared with conventional method [41] and fuzzy logic method [44] by considering various traffic situations such as highway normal, highway emergency, downtown traffic light, and downtown traffic congestion case.

In Section 5, the stability of BSL based control is investigated by Cell-to-Cell Mapping method. LCM model is used to demonstrate the stability of the controller. The cell map displays stable initial conditions within a vehicle operation range showing the stability of the designed control system.

In Section 6, the detail of Analytic Hierarchy Process is explained. To cope with various traffic conditions and driving modes an adaptive AHP algorithm is suggested. The simulation demonstrates the performance of adaptive AHP.

Finally, the conclusions and futures works are given in Section 7.

2. BRAIN LIMBIC SYSTEM BASED CONTROL

2.1 Brain Limbic System

In this research, Brain limbic system (BLS) based control is utilized to implement the lane change maneuver and adaptive cruise control. Thus the key aspects of Brain Limbic System (BLS) based control framework are summarized in this Section. The human brain limbic system learns appropriate reactions to the external stimuli by processing the sensory input representing the external stimuli as well as an internal cue capturing the emotional impact of the collection of stimuli. By mimicking the emotional learning process occurring in the human brain, a control system can be devised to achieve a desired goal, i.e. accomplishing lane change or the adaptive cruise control in autonomous or semi autonomous driving.

Amygdala, orbitofrontal cortex, sensory cortex, and thalamus are the main components of brain limbic system for the emotional processing and learning. Amygdala and the orbito-frontal cortex (OFC) participate in generating the emotional response in the human brain. In this emotional learning process, the amygdala learns the appropriate relations between neutral and emotionally charged stimuli while the OFC tries to inhibit inappropriate links as the task is accomplished. The thalamus functions as a communicator between the cortical and the other parts of the loop. The sensory cortex manipulates the sensed input to produce SI from the definition of raw sensory input.

2.2 Brain Limbic System Based Control

Moren and Balkenius [14-15] developed a computational model of the brain limbic system (BLS) process as shown in Figure 2.1.

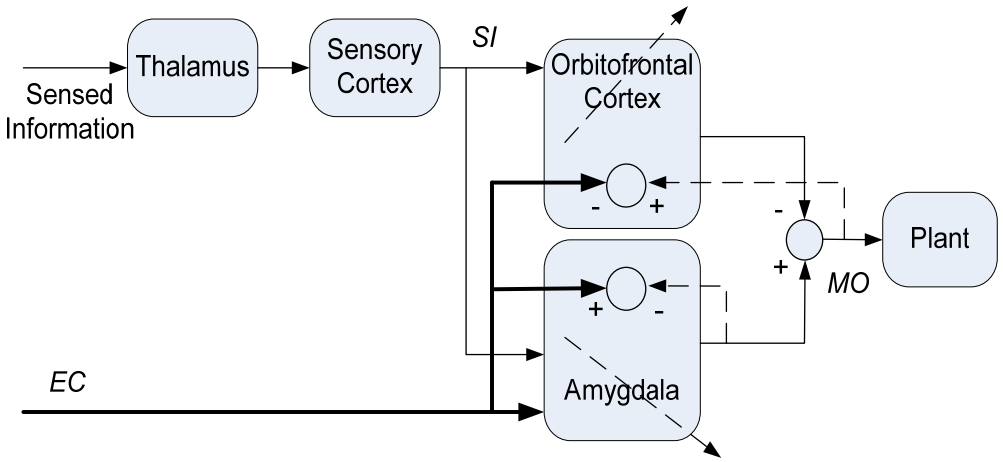

Figure 2.1 A computational model of the BLS controller.

Equations (2.1) through (2.5) describe a simplified model of the process:

$$MO = \sum_i A_i - \sum_i OC_i \tag{2.1}$$

$$A_i = G_{A_i} \cdot SI_i \tag{2.2}$$

$$OC_i = G_{OC_i} \cdot SI_i \,, \tag{2.3}$$

where MO represents the model output (i.e. the output of the computational model representing the brain limbic system) and the subscript i represents the i^{th} sensing stream. G_{A_i} and G_{OC_i} represent the gains of amygdala and the OFC, respectively (with

respect to the given sensing stream). The sensory input is denoted by SI_i and the emotional cue by EC.

In brief, this strategy is inspired by biology, where, based on both good and bad experiences, the amygdala constantly learns the associations between the sensory input signals and the emotional signal and tends to behave based on the learned associations. On the other hand, the OFC's inhibitory signals act to prevent any inappropriate actions to be issued by the amygdala (and hence, by the total model) when it is found inappropriate.

$$\Delta G_{A_i} = \alpha \cdot SI_i \cdot \max\left(0, EC - \sum_i A_i\right) \tag{2.4}$$

The Amygdaloid gains, G_{A_i}, are learned proportionally to the difference between the reinforcement (EC) and the output signal of the amygdala nodes. Here α is a learning rate, selectable between 0 (no learning) and 1 (instant adaptation). In practice, it is usually set at a fairly low value. The learning of the system is a function of the learning rate α, the difference between the strength of the emotional cue and the current output of the amygdala nodes, and the strength of the stimulus signal SI. The stronger the stimulus and the larger the difference between EC and amygdala output, the faster the learning occurs. This subsystem can never unlearn a connection by taking maximum value between 0 and the difference between EC and $\sum_i A_i$; once learned, it is permanent, giving the system the ability to retain emotional connections for as long as necessary.

$$\Delta G_{OC_i} = \beta \cdot SI_i \left(\sum_i A_i - \sum_i OC_i - EC \right), \tag{2.5}$$

Unlike the amygdala model, the learning occurring in OFC is not constrained to be monotonic; β is the learning rate of OFC. Because BLS is an online learning algorithm, it is influenced by the learning rate of each subsystem. In view of this issue, we set the learning rate of the amygdala to be lower than that of OFC to avoid impulsive decisions on the part of the controller. In other words, the system operates more carefully in view of the larger OFC learning rate. The OFC tracks the mismatch between the system's predictions and the actual received reinforcement, and learns to inhibit the system output in proportion to the mismatch. By the observation of (2.4)-(2.5), it is noted that the Amygdaloid gains are not affected when EC is zero; however the OFC gains rapidly increases and inhibits the output. After ΔG_{A_i} and ΔG_{OC_i} are obtained, the output signal of the amygdala, A_i, and that of OFC, OC_i, are calculated by (2.2)-(2.3).

As shown in equations (2.4) and (2.5), SI and EC perform significant roles in BLS. The emotional cue signal, EC, is internally generated. The form of this signal is defined by the designer with respect to the purpose of control. In brain limbic system (BLS) design, the most important task is finding a suitable SI and EC for specific objective. As the objective is accomplished, the EC value should have a tendency to increase (or otherwise to decrease).

2.3 Summary

The research on BLS was started from the effort to figure out the linkage between the stimulus and the resulting emotion. At first, the emotion based learning was neglected because people thought emotion is not reliable. However, the supporting researches demonstrated the advantages of BLS based learning system and it’s robust on uncertainties. In this Section, Brain Limbic System and its mechanism as an adaptive controller is discussed.

3. BRAIN LIMBIC SYSTEM BASED LANE CHANGE MANEUVER

3.1 Lateral Vehicle Dynamics

In this Section, BLS based application to lane change maneuver is discussed. The lane changing maneuver is studied under the consideration of the lateral dynamics of the vehicles [28], [35], [47]-[49]. It is assumed that there is a longitudinal control scheme that maintains the vehicle speed at a set value during the lane change maneuver. Figure 3.1 shows the coordinates of the vehicle and the forces that affect it. To describe the position of a vehicle, vehicle (body) fixed coordinate is utilized.

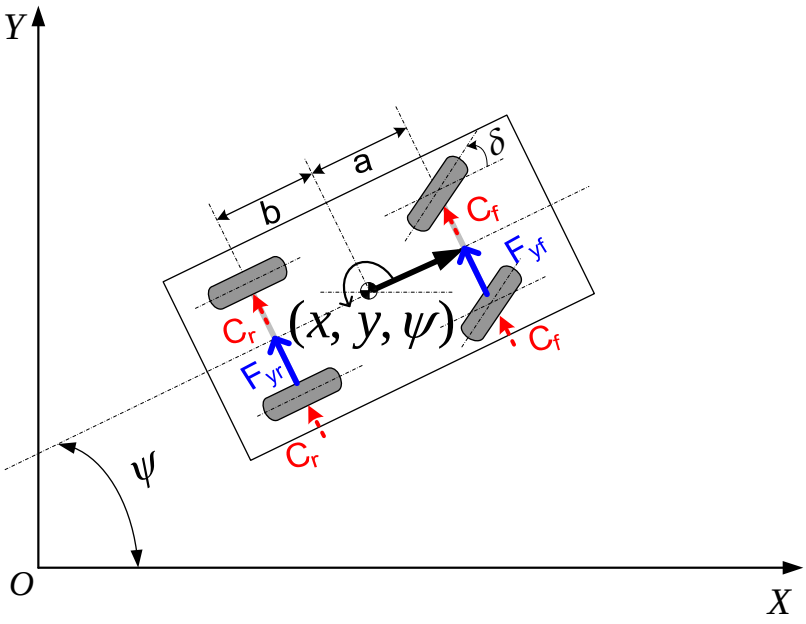

Figure 3.1 Schematic model of lateral vehicle dynamics.

The configuration of the vehicle is composed of three components in the global coordinate system, *x*, *y*, and ψ . By definition, ψ is the vehicle yaw angle, i.e. the angle between the vehicle's longitudinal direction and the coordinate's *X* axis. As shown in Figure 3.1, while the vehicle is driven, the lateral direction forces of front and rear tires, F_{yf} and F_{yr} , are generated by the cornering stiffness $\left(C_f, C_r\right)$ and the side slip angles:

$$F_{yf} = C_f \cdot \alpha_f \tag{3.1}$$

$$F_{yr} = C_r \cdot \alpha_r , \tag{3.2}$$

where the side -slip angles, α_f and α_r are given by

$$\alpha_f = \delta - \frac{v_y + a\dot{\psi}}{v_x} \tag{3.3}$$

$$\alpha_r = -\frac{v_y - b\dot{\psi}}{v_x} . \tag{3.4}$$

Here δ is the steering angle and v_y is the lateral velocity of the vehicle. Additionally, *a* and *b* are defined as the distance from the mass center of the vehicle to the lines of actions of the lateral forces acting on the vehicle. Likewise, v_x represents the longitudinal velocity of the vehicle that is assumed to be constant during the lane change.

After the front and rear forces are defined, the following relationship is derived from Newton's law under body fixed coordinates:

$$m\left(\dot{v}_y + v_x\dot{\psi}\right) = 2F_{yf} + 2F_{yr} . \tag{3.5}$$

From the moment equation

$$I\frac{d^2\psi}{dt^2} = 2aF_{yf} - 2bF_{yr}. \tag{3.6}$$

By substituting (3.3), (3.4) into (3.5)-(3.6)

$$\begin{aligned} m\,\dot{v}_y &= 2C_f\left(\delta - \frac{v_y + a\dot{\psi}}{v_x}\right) + 2C_r\left(-\frac{v_y - b\dot{\psi}}{v_x}\right) - mv_x\dot{\psi} \\ &= -2\frac{\left(C_f + C_r\right)}{mv_x}v_y - \left(2\frac{\left(aC_f - bC_r\right)}{v_x} + mv_x\right)\dot{\psi} + 2C_f\delta \end{aligned} \tag{3.7}$$

$$\begin{aligned} I\frac{d^2\psi}{dt^2} &= 2aC_f\left(\delta - \frac{v_y + a\dot{\psi}}{v_x}\right) - 2bC_r\left(-\frac{v_y - b\dot{\psi}}{v_x}\right) \\ &= -\frac{2\left(aC_f - bC_r\right)}{v_x}v_y - \frac{2\left(a^2C_f + b^2C_r\right)}{v_x}\dot{\psi} + 2aC_f\delta. \end{aligned} \tag{3.8}$$

By dividing (3.7) and (3.8) by the vehicle mass and yaw moment inertia the final vehicle lateral dynamics is obtained.

$$\dot{v}_y = -2\frac{\left(C_f + C_r\right)}{mv_x}v_y - \left[2\frac{\left(aC_f - bC_r\right)}{mv_x} + v_x\right]\dot{\psi} + \frac{2C_f\delta}{m} \tag{3.9}$$

$$\ddot{\psi} = -\frac{2\left(aC_f - bC_r\right)}{Iv_x}v_y - \frac{2\left(a^2C_f + b^2C_r\right)}{Iv_x}\dot{\psi} + \frac{2aC_f}{I}\delta. \tag{3.10}$$

Note that the vehicle gross mass m and the rotational moment I are assumed given. This vehicle model is derived in body fixed coordinate, in order to observe the vehicle motion in global perspective, the following relationship is utilized.

$$\dot{x} = v_x\cos\psi - v_y\sin\psi \tag{3.11}$$

$$\dot{y} = v_x\sin\psi + v_y\cos\psi. \tag{3.12}$$

3.2 BLS Based LCM Design

In this subsection, application of the brain limbic system based control to an autonomous vehicle function, i.e. lane change maneuver, is discussed. Figure 3.2 shows the structure of lane change control for an autonomous vehicle. There are two concepts in controlling lateral vehicle dynamics. One approach is via a looking ahead system using the vehicle's sensors and the other is using sensors installed on the road center [30].

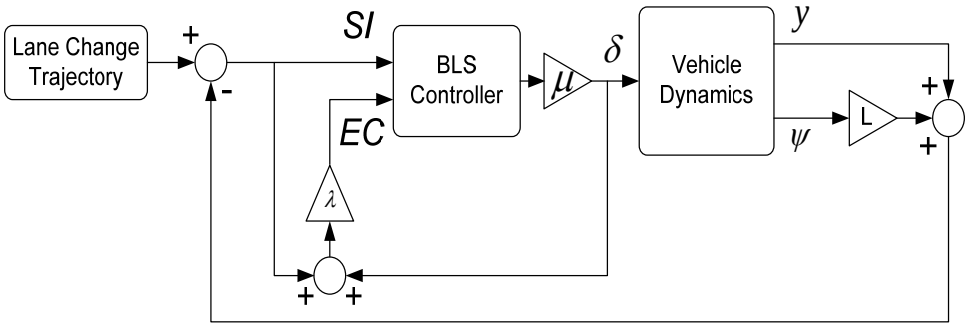

Figure 3.2 An autonomous vehicle control structure for lane changing maneuver.

In this research, the looking ahead method is employed. Therefore, the measured lateral displacement and yaw angle are used to compute the deviations from the target path of the vehicle during the lane change. The outlook distance is defined as the looking ahead distance. And the distance between the look-ahead point and the lane change trajectory is defined as the error [35]

$$e_{LCM} = y_T - y - L\psi, \tag{3.13}$$

where y_T and y represent the lane change trajectory and lateral position of the vehicle, respectively. Furthermore, it is expected that the looking ahead distance should be comparatively larger as the vehicle's speed increases. As a matter of fact, the looking ahead distance L affects the stability of the system [50]. In particular, a large looking ahead distance makes the vehicle stable while a small one generates oscillations [51]. Therefore, the looking ahead distance is defined with respect to the velocity of the vehicle as [52]

$$L = V \times \frac{1000}{3600}\left[\frac{m}{\sec}\cdot \sec\right]. \tag{3.14}$$

The steering angle, δ, is the input to the vehicle for lane change. To generate the appropriate steering angle, the BLS based controller utilizes the essential internal signals, sensory input (SI) and the emotional cue (EC). Now in terms of the application to the given control problem, the brain limbic system based controller is operated by two input signals SI and EC. In the lane changing maneuver, SI has been designed as the error between the reference path of the vehicle and EC as the summation of the control output and sensory input. By designing these two input signals, the system is expected to produce a smaller EC as it approaches the reference path.

$$SI = e_{LCM} \tag{3.15}$$

$$EC = \lambda\left(u_{LCM} + e_{LCM}\right), \tag{3.16}$$

where λ is a positive constant. Here λ works as a weighting factor to impose a sense of relative importance between SI and EC. By using smaller λ the system generates a slower response through a smaller control output. In contrast, a larger λ makes the

system faster by producing higher control outputs. To select the optimal λ, we consider the performance measure,

$$P = \int_0^{t_f} \left(|e| + |\psi| + |\delta| \right) dt , \tag{3.17}$$

where $|e|$, $|\psi|$, and $|\delta|$ represent the absolute values of error, yaw angle, and steering angle, respectively. Minimizing this measure via a gradient search process, the optimal gain λ is obtained. The actual choice of λ is obtained through trial and error. The steering command δ and the BLS output are given by:

$$\delta = \mu u_{LCM} \tag{3.18}$$

$$u_{LCM} = G_A SI - G_{oc} SI , \tag{3.19}$$

where μ is a positive constant to make the steering angle reasonable, this constant is an amplifier of the BLS output. After the steering command is produced from the BLS, it is used to follow the reference path and to produce EC and SI . By taking the differential form of Amagdala and OFC learning rules introduced in Section 2, and substituting (3.18)-(3.19) into the BLS structure is obtained

$$\dot{G}_A = \alpha \max \{0, (\lambda - 1) G_A - \lambda G_{oc} + \lambda \} e_{LCM}{}^2 \tag{3.20}$$

$$\dot{G}_{OC} = \beta \{ (1 - \lambda) G_A - (1 - \lambda) G_{OC} - \lambda \} e_{LCM}{}^2 . \tag{3.21}$$

It is evident from (3.20) that the gain of the amygdala is always positive. However, the Orbito-frontal Cortex gain can have both positive and negative values.

3.3 Human Driver Model for LCM

To demonstrate the performance of the suggested method in lane change behavior, the human driver model (HDM) based control scheme is introduced by Abe [35]. In Abe's vehicle control method, the vehicle is controlled by a human model, which has the ability to generate steering command with respect to the reference deviation of the vehicle. Because a human operator can not react immediately to the error signal, a time delay, τ_L is considered in the human model as the form of $e^{-\tau_L s}$. He suggested a simplified Ragazzini's [53] linear transfer function of a human controller

$$H(s) = h_{LCM}\left(1+\tau_D s\right)e^{-\tau_L s}. \tag{3.22}$$

To make the human model simpler, Abe [35] justified that a human operator does not have derivative gain, τ_D because looking ahead is itself similar to the derivative control action. Additionally, the delay term is approximated by the small time delay.

$$e^{-\tau_L s} \approx \frac{1}{1+\tau_L}. \tag{3.23}$$

Therefore, simplified and modified transfer function of the human driver model is given by

$$H(s) = \frac{h_{LCM}}{1+\tau_L s}, \tag{3.24}$$

where h_{LCM} represents the human proportional action to the input signal [35]. To get the optimal h value Abe [35] analyzed the driver-vehicle system lane change response by

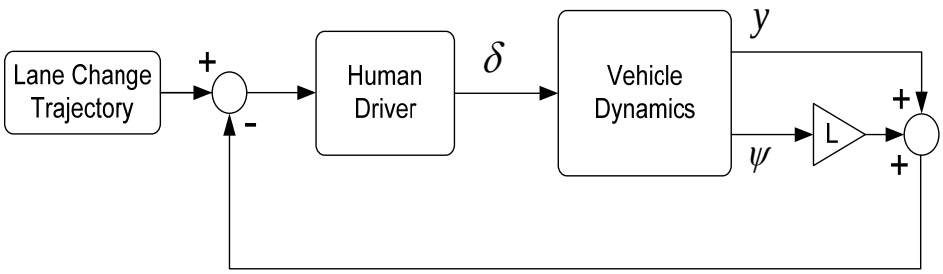

Figure 3.3 Human driver based lane change control structure.

varying h values and finally, they selected $h = 0.02$. Also to obtain the optimal human time delay, $\tau_L = 0.2$, the root-locus of the driver-vehicle system was used in Abe [35]. This same value is adopted here for reference. Figure 3.3 explains the control structure of HDM.

3.4 Overshoot Criterion for Safe Lane Change

In order to avoid collision between neighboring vehicles due to the deviation from the reference path, it is necessary to set a maximum overshoot criterion for the vehicle. The vehicle's yaw angle, ψ, is changed while the vehicle moves to the next lane. Because the movement makes the vehicle rotate towards the direction of the target lane, an additional length that is longer than the vehicle's half width should be factored in. Figure 3.4 explains the overshoot criterion for safe lane change. The bold line represents the lane boundary and the dotted line in the middle is the desired trajectory of the vehicle mass center. When the width of the vehicle is defined as W_v, the angle shown in Figure 3.4, θ_1 and θ_2 are calculated as follows.

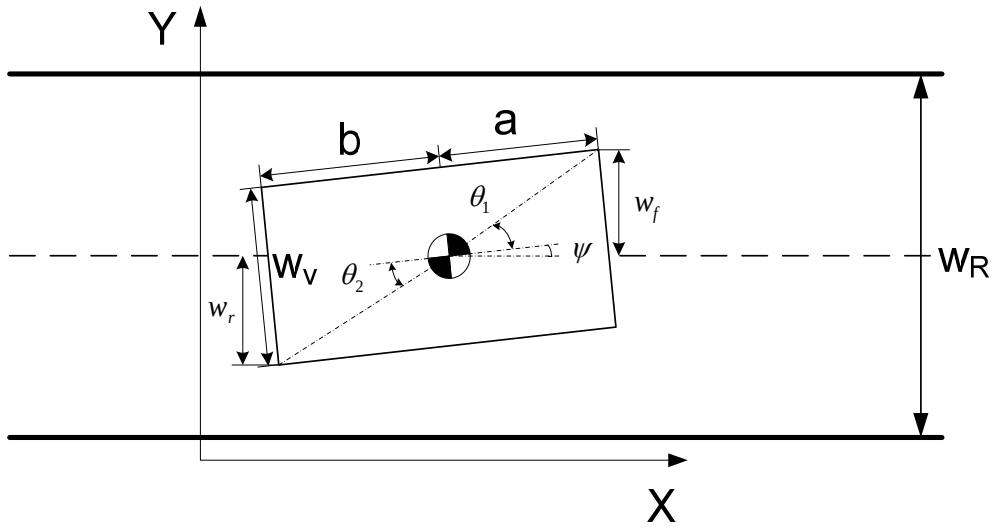

Figure 3.4 Overshoot criterion for safe lane change.

$$\theta_1 = \tan^{-1}\left(\frac{W_v}{2a}\right) \tag{3.25}$$

$$\theta_2 = \tan^{-1}\left(\frac{W_v}{2b}\right). \tag{3.26}$$

By adding the vehicle's yaw angle to the obtained angles, the front and rear lateral lengths of the vehicle from the center of gravity are

$$w_f = \sqrt{a^2 + (W_v/2)^2}\,\sin(\theta_1 + \psi) \tag{3.27}$$

$$w_r = \sqrt{b^2 + (W_v/2)^2}\,\sin(\theta_2 + \psi). \tag{3.28}$$

While the vehicle is rotating, these front and rear lateral vehicle lengths are used to set the overshoot criterion for lane change maneuver. In the view of safety, when a vehicle changes lane, any part of the vehicle should not cross over into the adjoining lane. To guarantee this, the following must be satisfied

$$y_{\max} \le \frac{3}{2} W_R - \max\left(l_f, l_r\right) \tag{3.29}$$

$$OS_{\max} = y_{\max} - W_R, \tag{3.30}$$

where $y_{\max}$ stands for the maximum lateral displacement of the vehicle, $OS_{\max}$ is the maximum allowed overshoot, and W_R is the width of the lane. The overshoot criterion will be used to evaluate the performance of the proposed strategy.

3.5 Simulations

In this subsection, the BLS based lane change control strategy is verified by numerical simulations. For simulation purposes, the vehicle parameters of Honda Accord are borrowed [50]. The minimum lane width in interstate highway standard is chosen as the lane width, W_R [54]. When the discussion about the overshoot criterion is considered with the parameters in Table 3.1, the overshoot of the vehicle path, OS, has to be less than $OS_{\max}$. In other words, if the maximum lateral displacement is larger than $y_{\max}$, the controller is considered to have failed and collision is expected.

Table 3.1 Vehicle parameters (Honda Accord).

a	1.22 m	C_f	60000 N/rad
b	1.62 m	C_r	60000 N/rad
m	1590 kg	W_v	1.847 m
I	2920 $kg\,m^2$	W_R	3.62 m

3.5.1 LCM under Ordinary Condition

The first set of the simulations do not include any disturbances. The dry road condition is considered and the vehicle velocity is set as 100 km/h which is the normal highway speed. The lane change command is given in the form of a step function at 5 seconds of the simulation duration with amplitude of the standard road width, W_R. Figure 3.5 shows the results of the simulation. The steering angle represents the control input to the vehicle for lane change. And the control input of BLS (solid line) is smaller than that of HDM (dotted line). Finally, the lateral movement plots show both methods satisfy the overshoot criterion (the lateral displacement of the vehicle is under 4.24 [meter]) and demonstrate that the performance of BLS is better in terms of maximum

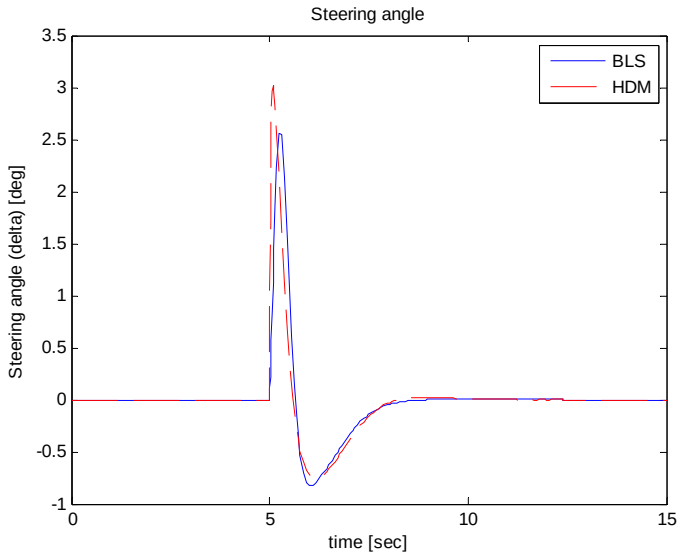

(a) steering angle (δ)

Figure 3.5 Lane change behavior comparison between BLS (brain limbic system based strategy) and HDM (human drive model) under ordinary condition (100km/h).

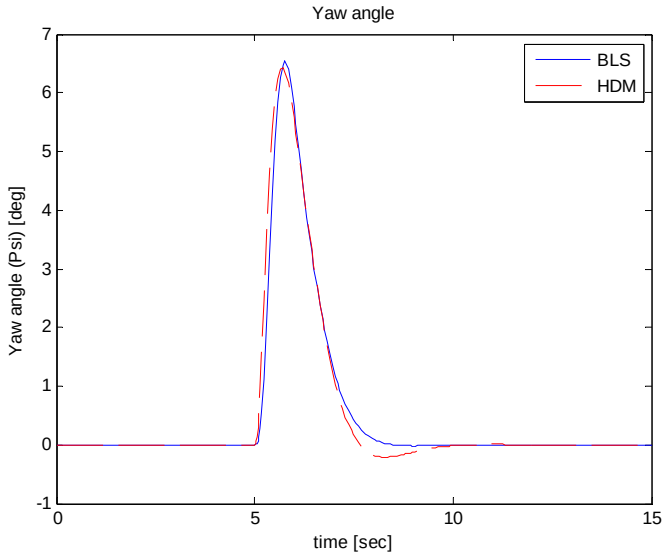

(b) yaw angle (ψ)

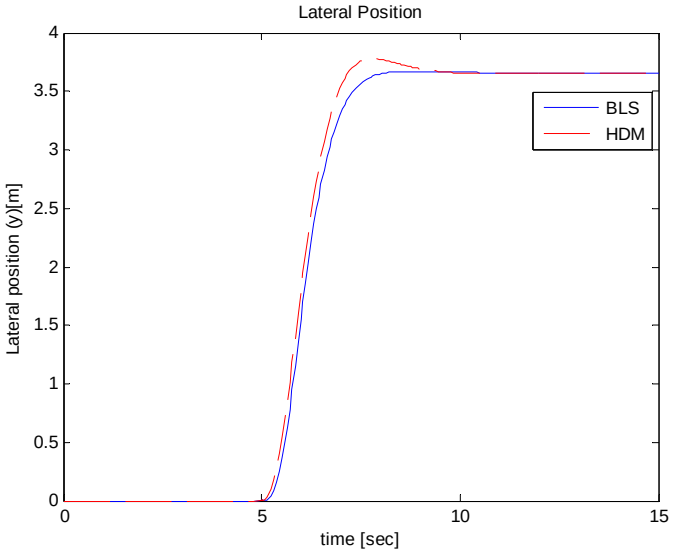

(c) lateral displacement y

Figure 3.5 Continued.

lateral displacement.

3.5.2 Lane Change under Disturbances

The actual driving condition has several unexpected situations and uncertainties. The vehicle can encounter wind, wet road, or even a snowy path. Not only the external factors, but also internal factors such as the tires and mass change can provide uncertainties in vehicle dynamics identification. The cornering stiffness is one of the uncertain parameter that has to be taken into account. To this end, Sienel [55] has reflected on the effect of side-slip angle on cornering stiffness. When the side-slip angle is large, the cornering stiffness changes with the road condition. In order to consider these various conditions, the robustness of the BLS based controller has to be addressed. The following simulations are used to verify this issue.

3.5.2.1 Wind Load

First of all, the wind effect on the driving by using the vehicle dynamics with wind load model is considered. The vehicle shape, the air density, vehicle and wind speed are mainly affected by the wind load that a vehicle has to bear. The lateral dynamics of the vehicle (including an added wind load effect) is as follows

$$\dot{v}_y = -2\frac{\left(C_f + C_r\right)}{mv_x}v_y - \left[2\frac{\left(aC_f - bC_r\right)}{mv_x} + v_x\right]\dot{\psi} + \frac{2C_f\delta}{m} + \frac{Y_w}{m} \tag{3.31}$$

$$\ddot{\psi} = -\frac{2\left(aC_f - bC_r\right)}{Iv_x}v_y - \frac{2\left(a^2C_f + b^2C_r\right)}{Iv_x}\dot{\psi} + \frac{2aC_f}{I}\delta + \frac{l_wY_w}{I}, \tag{3.32}$$

where Y_w represents the wind load and l_w is the distance from vehicle's mass center where the wind load acts [35].

In this simulation, it is assumed that the vehicle experiences wind load during lane changing and normal driving. The first wind load (1600 Newton; 30 m/s) occurs

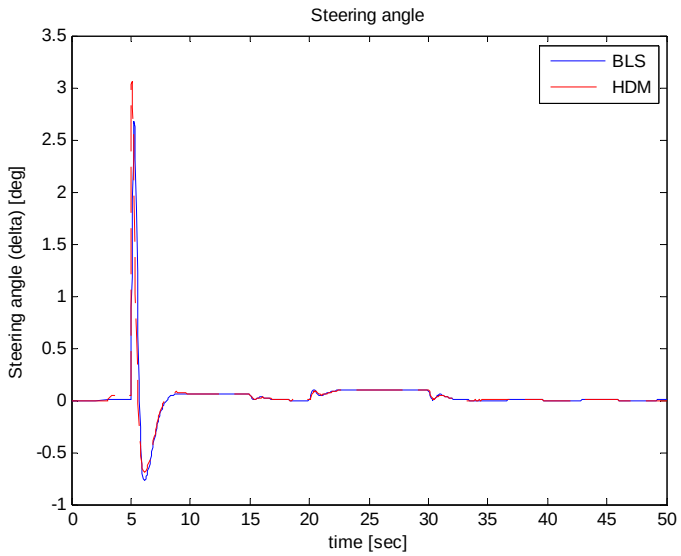

(a) steering angle (δ)

Figure 3.6 Lane change behavior comparison between BLS and HDM under wind blowing condition (100km/h).

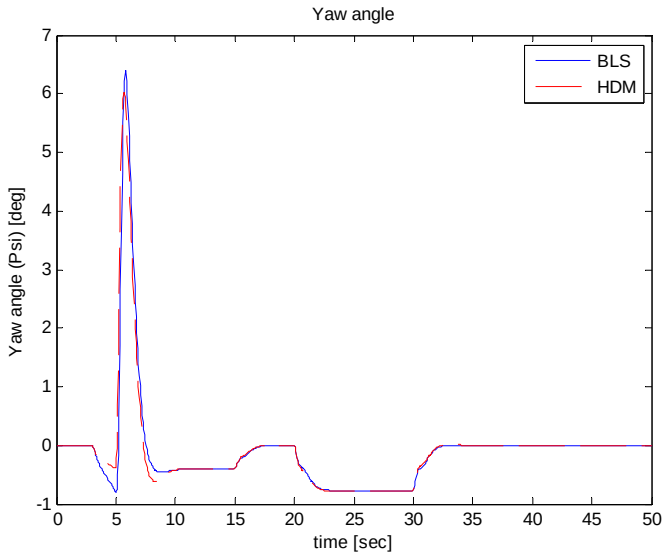

(b) yaw angle (ψ)

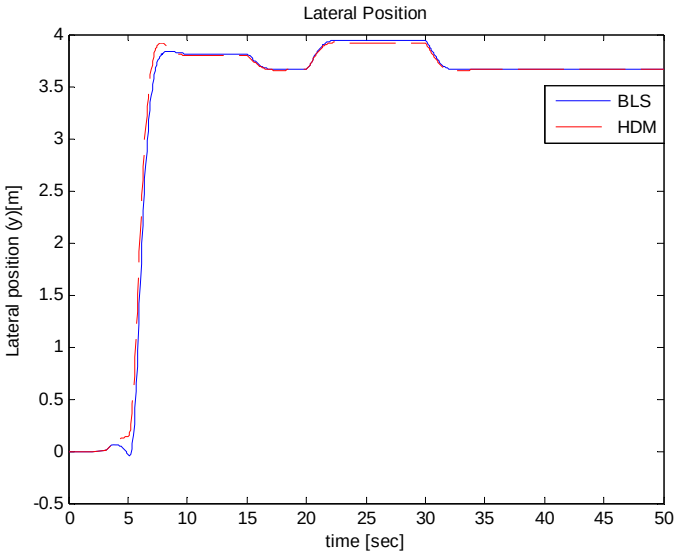

(c) lateral displacement y

Figure 3.6 Continued.

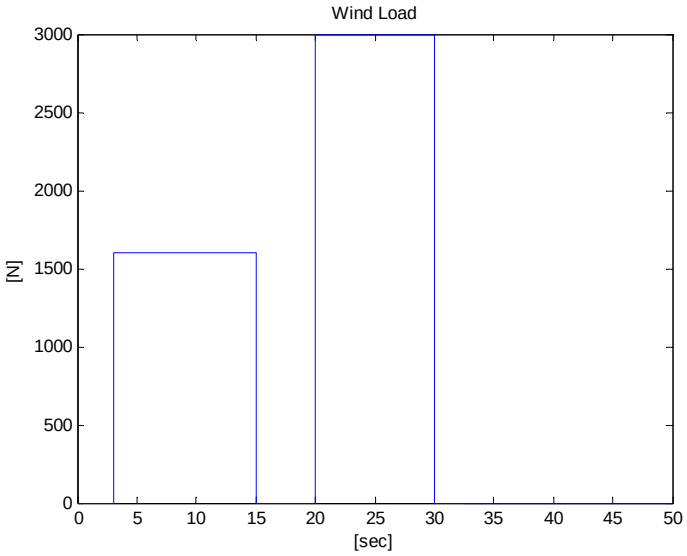

(d) wind load

Figure 3.6 Continued.

from t=3 sec to t=15 sec, and 3000 Newton (50 m/s) of wind load occurs from t=20 sec for 10 seconds as shown in Figure 3.6 (d). The sudden wind load profile applied to the vehicle that is driven at 100km/h. The vehicle's lateral position is offset toward the wind passing direction. Both control strategies successfully control the vehicle under the given wind profile. The comparison results show that the steering input and yaw angle are not quite different; however, the overshoot of BLS is smaller than that of HDM under windy condition.

When the yaw angle is observed, clockwise direction of rotation is observed even though the wind blows from the right-hand side of the vehicle. It is because of the force balance within the vehicle. The engine of a vehicle normally located in front of it. Therefore, the distance from the mass center of a vehicle to the each tire axis is not normally same. The distance unbalance and force unbalance a resultant force is occurs at

NSP (neutral steer point) at $l_N = \frac{bF_{yr} - aF_{yf}}{F_{yf} + F_{yr}}$ in Figure 3.7. Also when wind blows from the side of a vehicle a concentrate force is assumed at the aerodynamic center (AC), l_w . Then there are the following circular motion is observed by the resulting moments;

a. If AC is in front of NSP, CCW motion occurs.
b. If AC with coincide with NSP, no circular motion occurs.
c. If AC is behind the NSP, CW motion occurs.

In the simulation, I used the vehicle parameters of Honda Accord, i.e. $a = 1.22\ m$, $b = 1.62\ m$, $C_f = C_r = 60000\ N/rad$. Therefore the NSP occurs at $l_N = 0.2$ and $l_w = 0.3$, the CW motion is occurred.

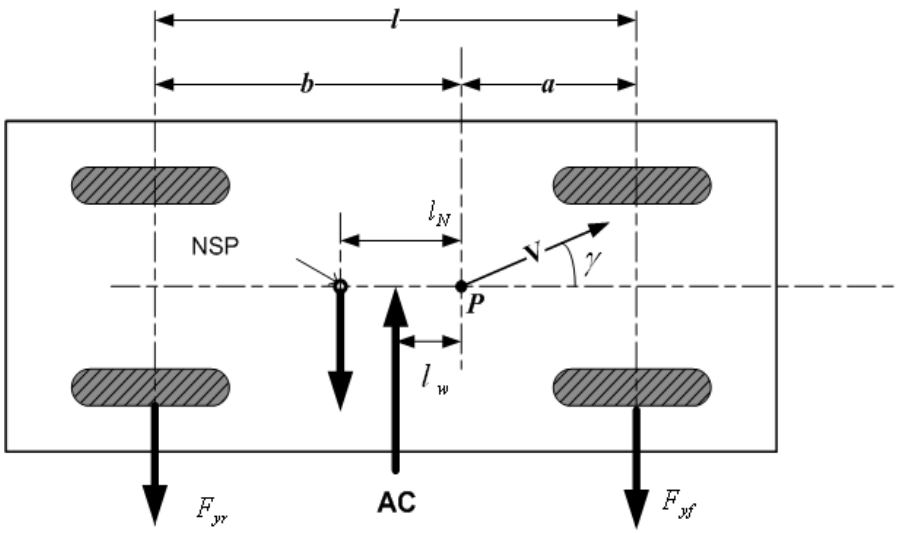

Figure 3.7 Wind disturbance and force balance [35].

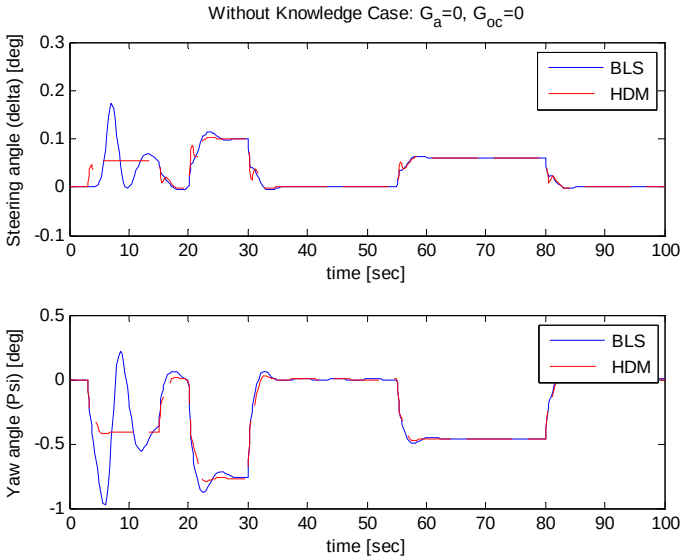

(a) Steering angle and Yaw angle under no knowledge

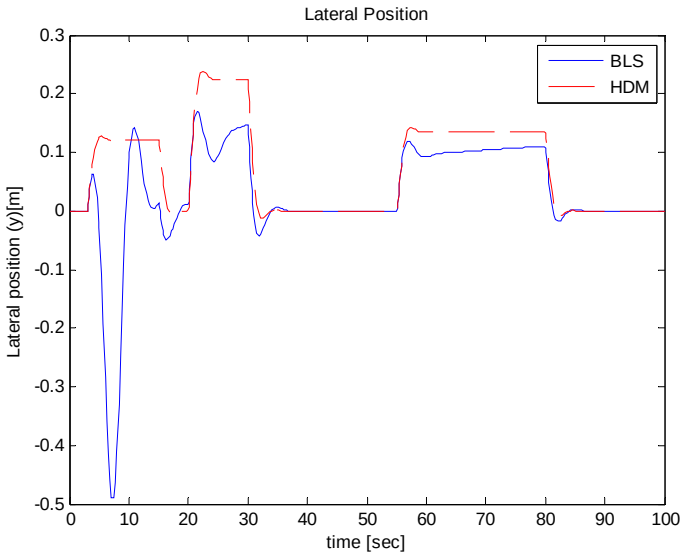

(b) Lateral position of the vehicle.

Figure 3.8 BLS learning under wind disturbance without knowledge case.

Figures 3.8 and 3.9 show the wind disturbance enduring test when there is no lane change maneuver. Especially, Figure 3.8 is the results from the setting without knowledge. Before the BLS system does not experience the windy condition there is no knowledge how to cope with the windy condition. Therefore, the gain of amygdala and OFC are set to zero, i.e. $G_A = 0, G_{OC} = 0$ to apply no knowledge case. At the first few seconds, the BLS system is learning the wind disturbance case while having worse results than that of the HDM control method. However, after the learning process, the results of steering angle and yaw angle are very similar to the counterpart. Additionally, the lateral displacement of BLS based control is better than HDM control. After this simulation, the undated values of amygdala and OFC, i.e. $G_A = 0.0015, \quad G_{OC} = -0.0023$ are obtained. Subsequently, these gains are used as the knowledge about the windy road case. By setting the initial conditions of amygdala and OFC with those values, the same wind disturbance situation is conducted again. Figure 3.9 displays the results and there is no notable learning process observed. This shows that the BLS system gains are undated to appropriate values as the system leans the correct knowledge to accomplish the given task.

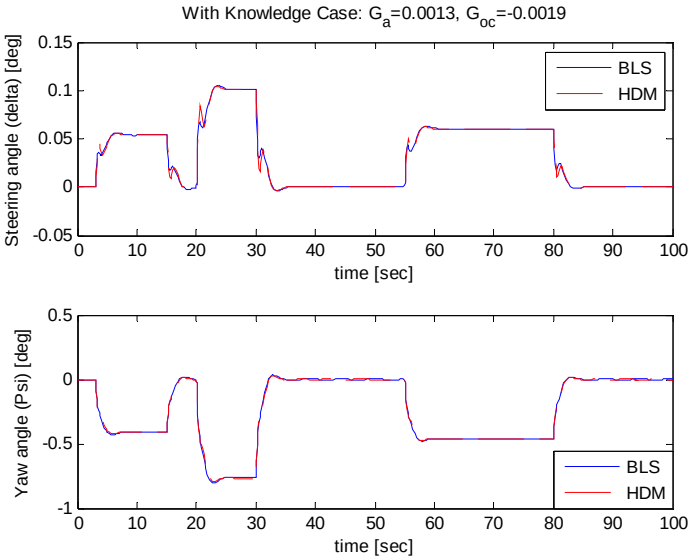

(a) Steering angle and Yaw angle under knowledge

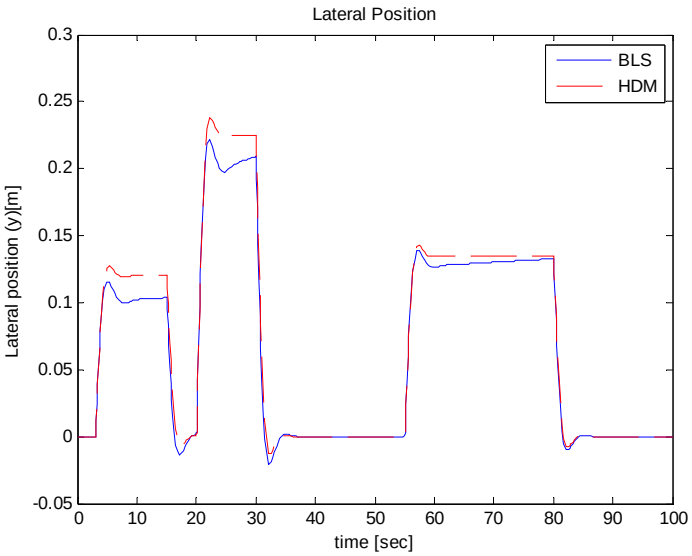

(b) Lateral position of the vehicle.

Figure 3.9 BLS learning under wind disturbance with knowledge case.

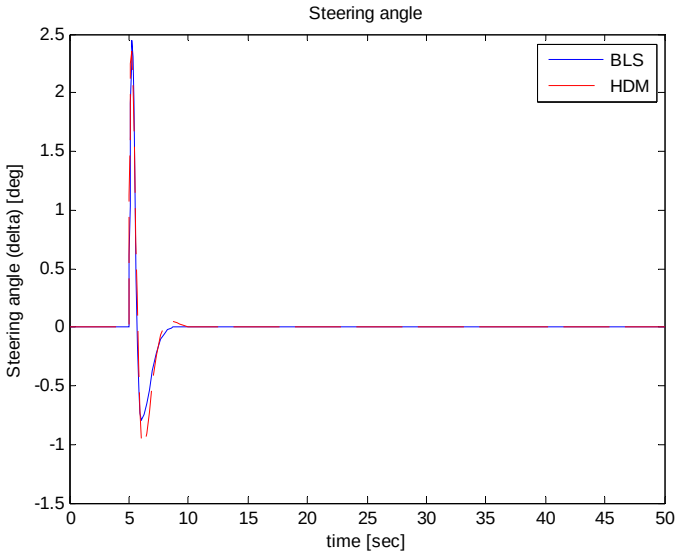

(a) steering angle (δ)

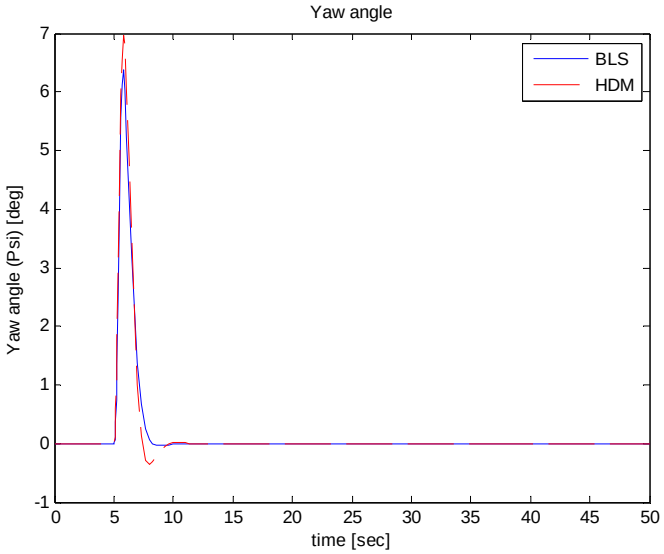

(b) yaw angle (ψ)

Figure 3.10 Lane change behavior comparison between BLS and HDM under cornering stiffness uncertainty (100km/h).

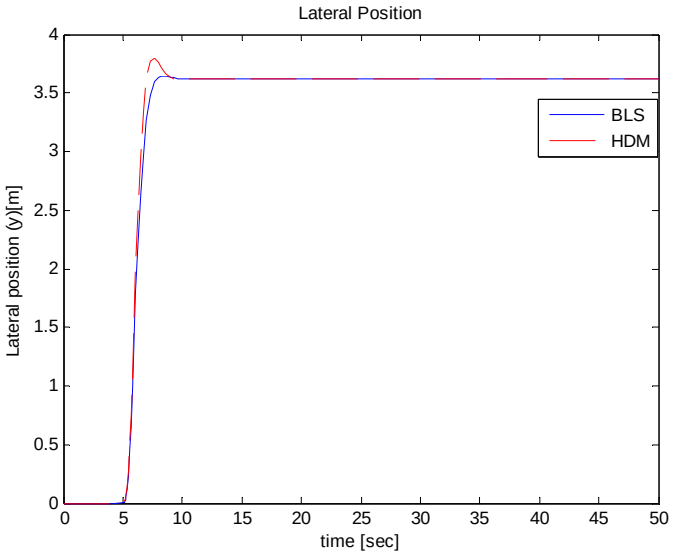

(c) lateral displacement y

Figure 3.10 Continued.

3.5.2.2 Uncertainty of Cornering Stiffness

The cornering stiffness is determined from measuring the lateral force. The uncertainty of cornering stiffness originates from the associated measurement process. And it is assumed that the cornering stiffness varies from -29% to 35% from its nominal value and this range follows other relevant literature [33]. To include the uncertainty in the simulation, random cornering stiffness values within the given ranges is chosen using the ‘rand’ function in Matlab. To this end, 100 different random cornering stiffness values are simulated by means of Monte Carlo simulation method. Figure 3.10 is one of the 100 different simulation results. It shows that BLS produces smaller steering control and yaw angle changes during the lane change maneuver. Also the lateral displacement of the suggested method produces smaller overshoot when it is compared with the HDM

method. Figure 3.11 shows the maximum lateral displacement and the frequency of occurrence of the maximum lateral displacement histogram during the lane change of BLS and HDM, respectively. In particular, 100 simulations were carried out and the statistics provide the frequency of lateral displacement in the histogram and the mean value of the $y_{\max}$ is calculated to compare the performances. In Figure 3.11, the vertical line at the lateral displacement value of 4.24 [meter] represents the displacement for safe lane change. As shown in the figures, the mean of maximum lateral displacements of BLS is 3.64 [meter] and that of HDM is 3.79 [meter] where the targeted lateral displacement is 3.66 [meter]. It demonstrates the safer performance of BLS based control.

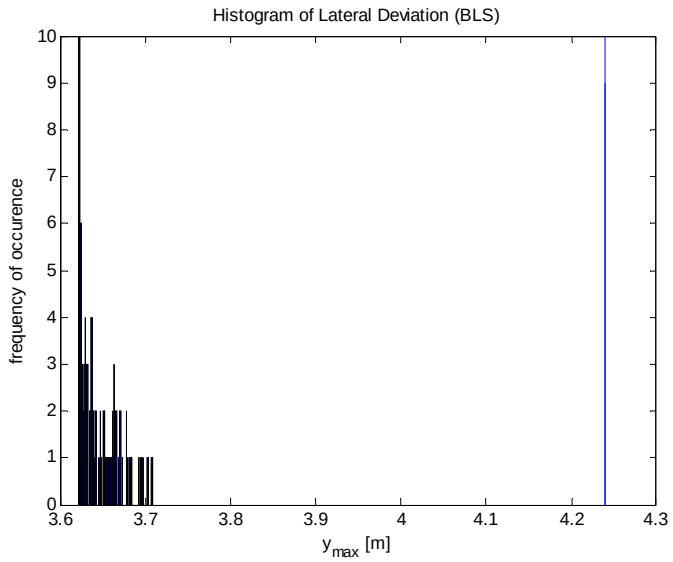

(a) BLS

Figure 3.11 Histogram of lateral deviation under cornering stiffness uncertainty (100km/h).

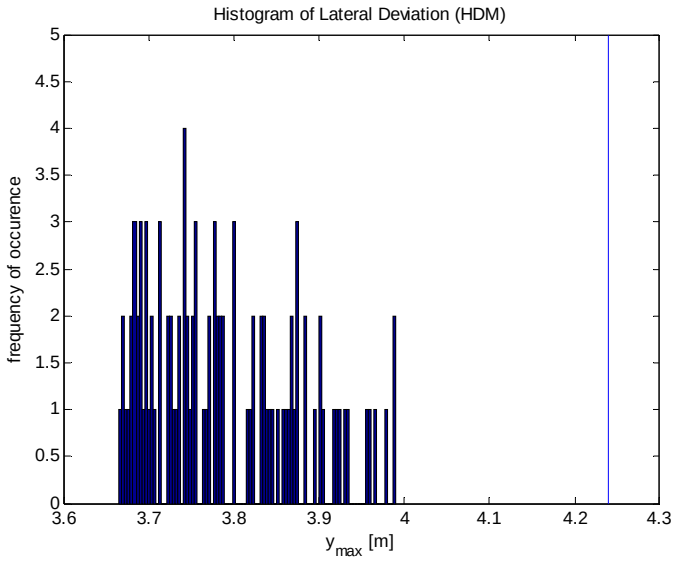

(b) HDM

Figure 3.11 Continued.

3.5.2.3 Wind and Cornering Stiffness

In this part, the disturbances from wind and cornering stiffness are considered together. The same wind profile and variation of the cornering stiffness are used again. Figures 3.12 and 3.13 show the results of this simulation. When the lateral position results are compared, BLS shows less overshoot during lane changing. The $y_{\max}$ histograms show that the mean of BLS is 3.89 [meter] and the mean of HDM is 4.03 [meter]. Also the results show several occurrences of failure of the HDM method that exceed $OS_{\max}$. In this result, it is demonstrated that BLS based method is better than HDM based control in safety aspect.

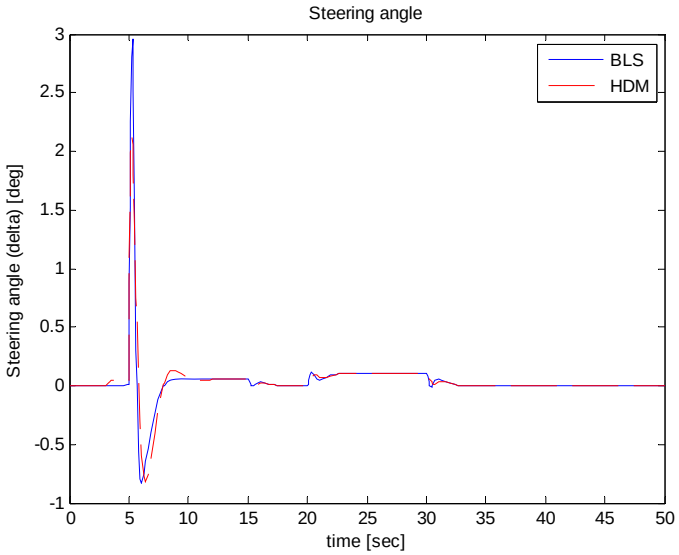

(a) steering angle (δ)

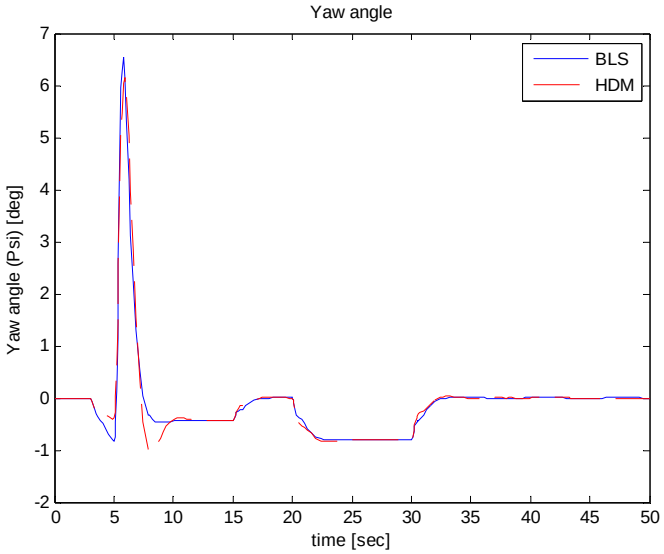

(b) yaw angle (ψ)

Figure 3.12 Lane change behavior comparison between BLS and HDM under wind blowing and uncertain cornering stiffness (100km/h).

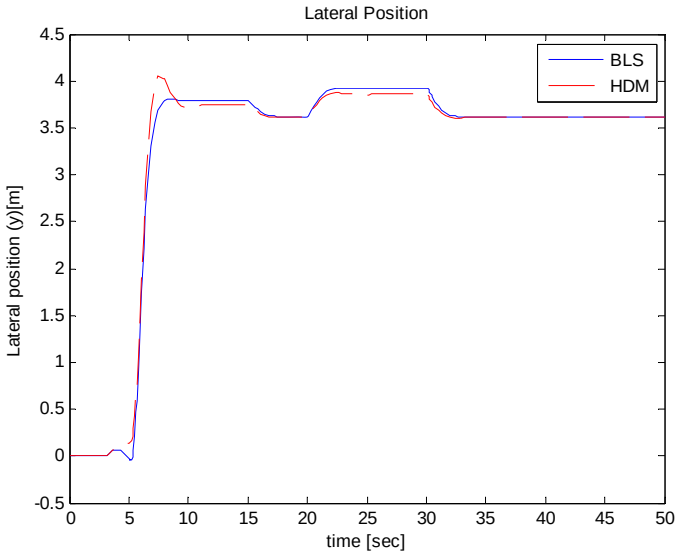

(c) lateral displacement *y*

Figure 3.12 Continued.

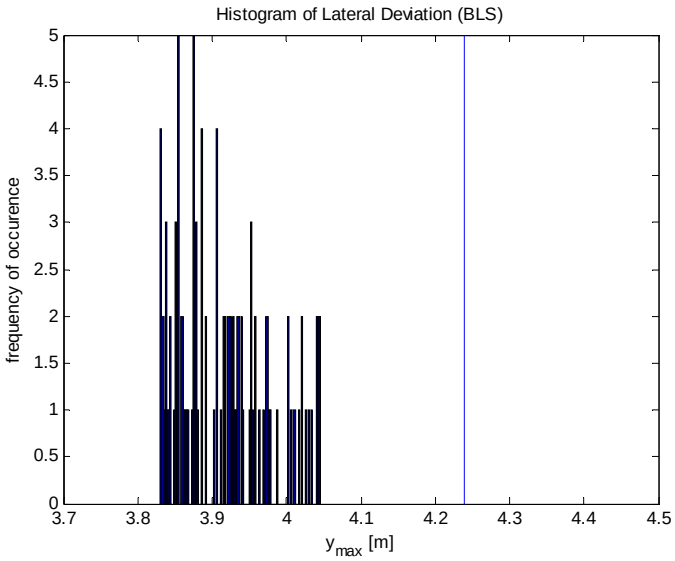

(a) BLS

Figure 3.13 Histogram of lateral deviation under wind blowing and uncertain cornering stiffness (100km/h).

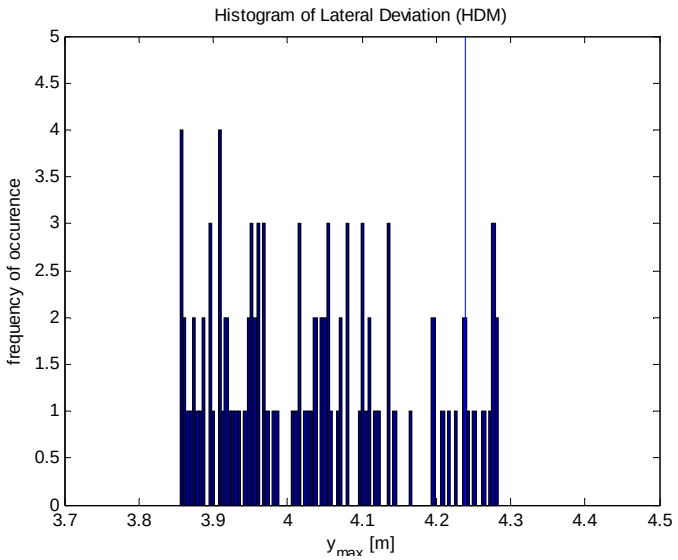

(b) HDM

Figure 3.13 Continued.

3.5.2.4 Wind, Cornering Stiffness, and Mass

The harshest condition is assumed by simultaneously employing all the disturbances in the previous simulations. All the uncertainties and varying rates are maintained. Additionally, the passenger (70kg/person, max 350 kg), the fuel (0.76 kg/liter, max 49.17 kg), and baggage (max 60 kg) are considered by taking account of the maximum load to minimum load (one driver, empty fuel tank, and no baggage condition). To implement this varying mass, the random mass is chosen between the maximum and minimum loading conditions. When the simulation results (Figure 3.14) are compared, the BLS based method is strong in all aspects during the lane change. In

Figure 3.15, the safety of the proposed method is demonstrated again by providing the histograms and the mean $y_{\max}$ of BLS is 3.93 [meter] and that of HDM is 4.01[meter].

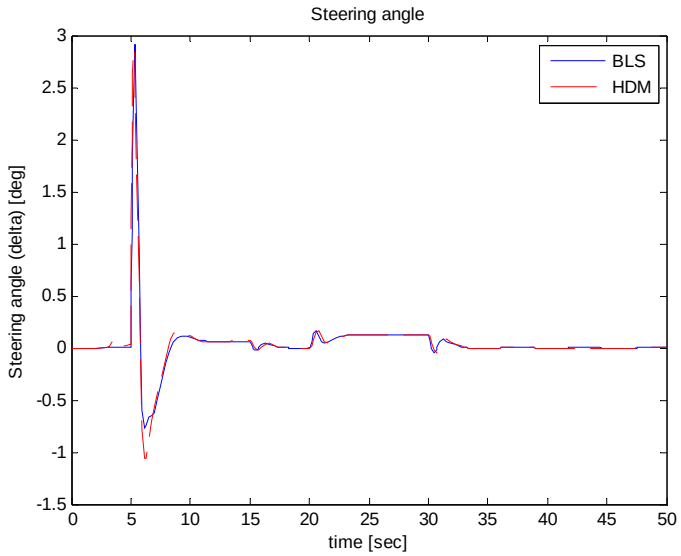

(a) steering angle (δ)

Figure 3.14 Lane change behavior comparison between BLS and HDM under all disturbances (100km/h).

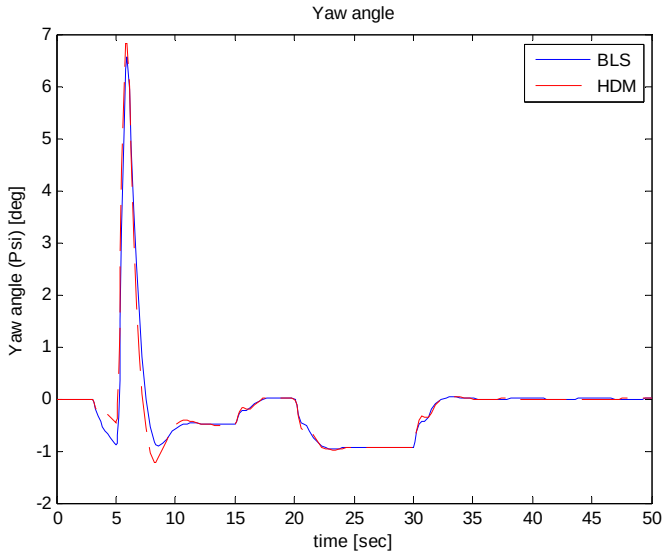

(b) yaw angle (ψ)

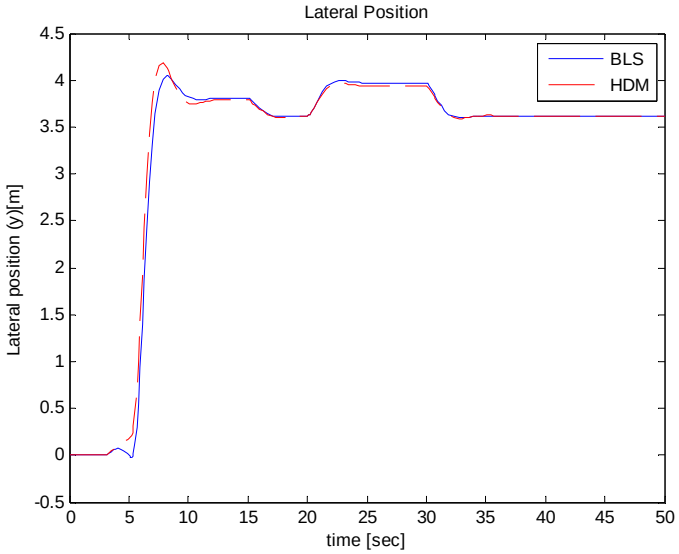

(c) lateral displacement y

Figure 3.14 Continued.

In the first part of the simulation, the BLS based control results have worse performance until it updates the appropriate gains for the amygdala and OFC. The most

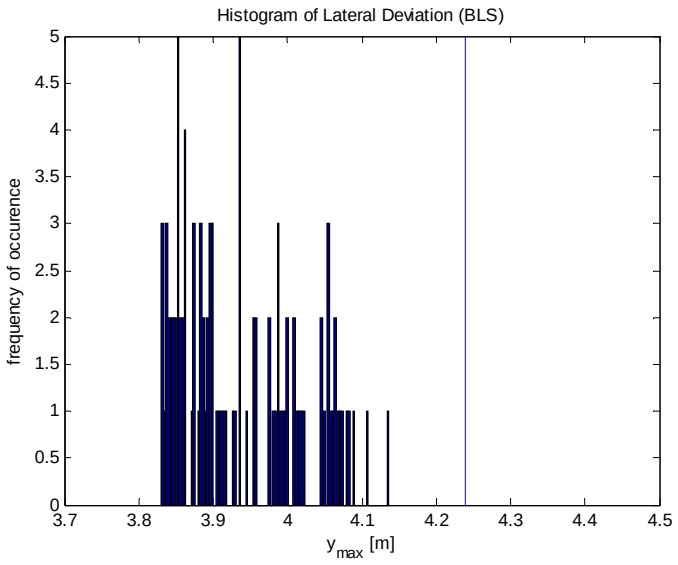

(a) BLS

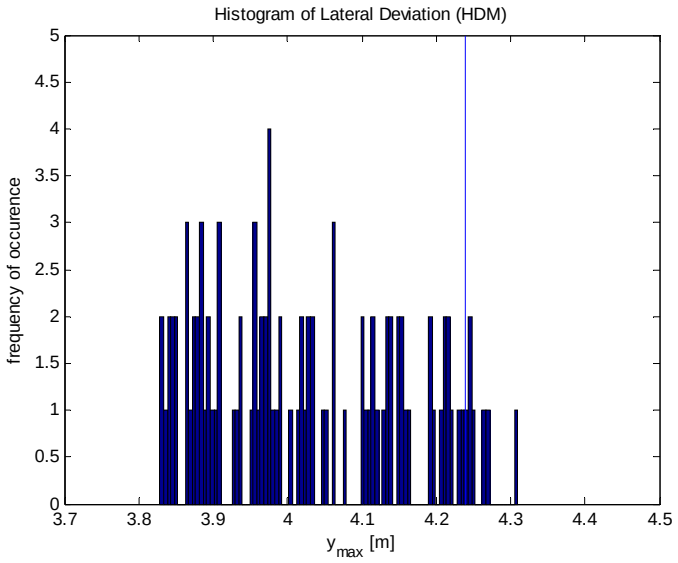

(b) HDM

Figure 3.15 Histogram of lateral deviation under all disturbances (100km/h).

important aspect of the vehicle driving is the safety while driving. The statistical results show that BLS based lane change provides smaller lateral displacement during lane change.

3.6 Summary

In this Section, lane change maneuver for an autonomous vehicle is discussed. It is assumed that the lane change support works after all the required data are given and the lane changing decision is made by a higher level decision maker. The brain limbic system based controller is utilized to accomplish autonomous lane change function under defined environments. To compare the performance of the suggested method, human driver model based controller is introduced. The performance of designed lane change controller is demonstrated by numerical simulations. And the disturbance from wind, cornering stiffness uncertainty, mass change, and mixture of them are considered. From the simulation results, it is concluded that the suggested method is safer than HDM in all simulated cases by showing larger safety margin.

4. BRAIN LIMBIC SYSTEM BASED ADAPTIVE CRUISE CONTROL

4.1 Longitudinal Vehicle Dynamics

Longitudinal vehicle control is utilized to develop adaptive cruise control (ACC) for an autonomous vehicle. Unlike traditional cruise control, ACC has two control modes. One is speed control mode, which is the conventional cruise control itself, and the other is the time gap control mode. When there is no vehicle in front of the ACC-equipped vehicle, the speed control mode comes into operation to maintain the set-up velocity; however, constant time gap control is activated in presence of a vehicle within the desired inter-vehicle distance gap. The transition between the two control modes is determined automatically by this presence [56].

A set of vehicles is considered as depicted in Figure 4.1. In the figure, x and $\dot{x}$ (or v) represent the absolute position and velocity of the ACC-equipped vehicle. Here, the subscript T represents the leading (target) vehicle while the following vehicle is

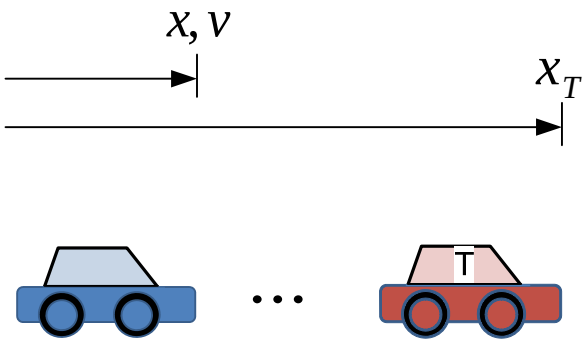

Figure 4.1 Set of adaptive cruise control vehicles.

defined with its location.

To generate the control input at the lower level, vehicle engine and braking system must work together. In this research, the higher level control is focused on by assuming the lower level servo control performs normally. However, the realization of the desired control input is generally limited by the components. Bageshwar, Garrard and Rajamani [42] have suggested a first order time lag model to cover the limitations of control input in the engine and the brake. Therefore the acceleration based vehicle model is derived as follows;

$$\tau \frac{d}{dt} \ddot{x}_i + \ddot{x}_i = u_{ACC}(t), \tag{4.1}$$

where τ is the time delay of the vehicle. And the acceleration of the vehicle has upper and lower boundaries defined as

$$u_{\min} \le u_{ACC}(t) \le u_{\max}, \tag{4.2}$$

where $u_{\min}$ and $u_{\max}$ are the minimum and maximum control inputs, respectively. In this study, it is assumed that $u_{\min} = -5 m/s^2$ and $u_{\max} = 2.5 m/s^2$ as typical values that are also used in other reference [42]. Deceleration is generated by the braking system and the braking force is larger in absolute value than that of the motive forced produced by the accelerator.

4.2 BLS Based ACC Design

In this subsection, the application of the introduced neuromorphic control methodology to an autonomous vehicle is presented. A set of lead and follower vehicles

is considered to evaluate the BLS based ACC. In this set-up, the ACC-equipped vehicle controls the velocity according to the lead (or target) vehicle velocity while maintaining a predefined constant time gap. Figure 4.2 displays the control structure of the BLS based ACC. To implement the suggested control method, it is assumed that the sensors used to measure the relative distance and velocity, and the controlled vehicle's acceleration function perfectly. Therefore, all sensed data pertaining to the vehicles are regarded as accurate[2] [57]. After the ACC-equipped vehicle detects the position and velocity of its target vehicle, the relative distance (e), the relative velocity ($\dot{e}$), and the acceleration of the ACC-equipped vehicle (a_{ACC}) are sent to the signal processor to generate *SI* and *EC* according to the designated form of each signal. The BLS controller subsequently updates the gains of the amygdala and the OFC using the resulting signals such as *SI* and *EC*.

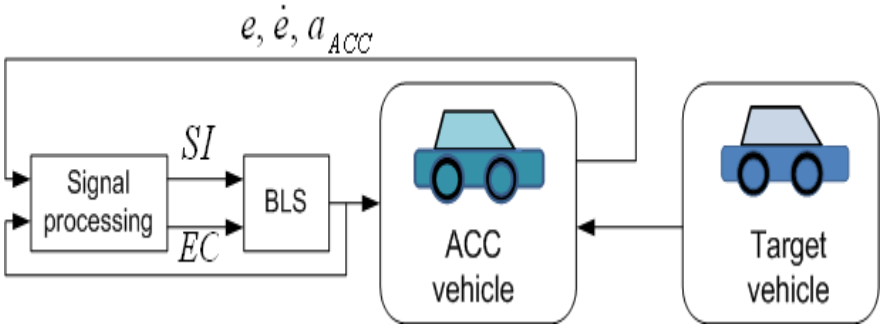

Figure 4.2 BLS control structure for ACC.

[2] R. Sharifi, Y. Kim and R. Langari [57] have developed and applied sensor fault isolation and detection technique that has been applied to engineering applications. The same technique will be utilized to get accurate sensed data and will be incorporated in practical implementation of the proposed approach as the case may require.

As a spacing policy, the constant time gap policy that is varying with the vehicle velocity is employed [43].

$$l = l_0 + h_{ACC} \cdot v, \tag{4.3}$$

where l_0 is the safety inter-vehicle distance when both leading and following vehicles are stopped, l represents the constant time headway distance of the vehicle, and h_{ACC} refers to the time gap of the defined system. The distance, velocity, and spacing error between vehicles are defined as

$$e = x_T - x_{ACC}, \tag{4.4}$$

$$\dot{e} = \dot{x}_T - \dot{x}_{ACC}, \tag{4.5}$$

$$s_e = x_T - x_{ACC} - \left(l_0 + h_{ACC} \cdot v\right). \tag{4.6}$$

BLS is operated by the emotional cues and sensory input, which are designed for specific application. To achieve the objective of ACC, the sensory input, *SI*, and emotional cue, EC, are defined as follows

$$SI = w_1 s_e + w_2 \dot{e} + w_3 a_{ACC}, \tag{4.7}$$

$$EC = SI + u_{ACC}, \tag{4.8}$$

where w_1, w_2, and w_3 are positive gains for spacing error, velocity errors, and the acceleration of the controlled vehicle. In adaptive cruise control, two important things to demonstrate the control performance are the inter-vehicular distance and velocity error. To this end, the following performance measure is defined

$$P = \int_0^{t_f} \left(|s_e| + |\dot{e}|\right) dt, \tag{4.9}$$

while the gins are obtained by trial and error, the performance measure is utilized.

According to the various traffic situations, the gains also need to be changed to get better performance. To cover the various traffic situations, the gain scheduling method is utilized to update the *SI* gains. Table 4.1 shows all *SI* gains with respect to the current preceding vehicle speed and the velocity difference between preceding and ACC vehicle. It is assumed that the velocity change is not larger than 10 km/h, in normal driving condition:

Table 4.1 Parameters of *SI* with respect to the current target velocity and velocity difference.

ΔV (km/h)	V_t (km/h)	w_1	w_2	w_3	ΔV (km/h)	V_t (km/h)	w_1	w_2	w_3
-10 ~ -5	10	6	1	2	0 ~ 5	10	12	1	6
	20	6	1	3		20	12	1	5
	30	5	1	1		30	9	2	2
	40	5	1	2		40	6	1	1
	50	4	1	1		50	4	3	1
	60	4	1	2		60	3	2	1
	70	4	1	2		70	2	3	1
	80	3	1	1		80	2	2	1
	90	2	3	1		90	2	2	1
	100	2	2	1		100	1	2	1
-5 ~ 0	10	10	1	4	5 ~ 10	10	5	2	2
	20	8	1	2		20	5	2	2
	30	7	1	3		30	4	3	1
	40	5	1	1		40	3	3	1
	50	5	1	2		50	3	1	1
	60	4	1	1		60	2	2	1
	70	3	2	1		70	2	1	1
	80	3	1	1		80	1	4	1
	90	2	2	1		90	1	4	1
	100	2	2	1		100	1	3	1

To get this table, four velocity difference regions are defined, i.e. $-10 \le \Delta V_1 < -5$, $-5 \le \Delta V_2 < 0$, $0 \le \Delta V_3 < 5$, $5 \le \Delta V_4 < 10$. And current velocities are define the medium value of region, i.e. 10 represents $5 \le V < 15$. The gain scheduling table is used to update *SI* gains with respect to the encountered traffic situation. From Table 4.1, it is analyzed that as ACC vehicle's velocity is slower the inter-vehicular gain, w_1 is relatively larger than the other gains. Also as the ACC vehicle's velocity is faster the velocity error gain, w_2 is relatively larger than other gains. Therefore it can be concluded that speed control is conducted when the vehicle velocity relatively fast while inter-vehicular distance is focused on under relatively slow velocity. This conclusion is compatible with Francher and Bareket [58]. From these two internally generated signals, BLS based controller updates the gains of the amygdala and the OFC, i.e. G_{A_i} and G_{OC_i}.

4.3 Simulations

In this subsection, numerical simulations and their results are presented to demonstrate the performance of developed controller. Showing highway and city traffic situations, the application of the BLS based ACC is extended to various traffic environments. In the highway traffic environment, it is assumed that there are two disturbances with respect to the driving situation, a normal (albeit complex) road condition and an emergency road condition.

In the normal, complex road condition, various velocity profiles are defined in terms of the relevant speed limits and working zone restrictions that maybe applicable.

The emergency road condition, which requires a sudden stop due to an accident or fallen debris on the road, is also investigated. Additionally, city (downtown) traffic situations are simulated. In the center of a city traffic environment, traffic flow control by traffic signals and traffic congestion are the main contributors to the velocity changes of a vehicle. These situations are covered in downtown traffic simulation. To compare the performance of the suggested method with the fuzzy logic methods and PD control method are simulated under the same condition. The fuzzy rules and membership functions were utilized in [44] is presented in Table 4.2 and Figure 4.3, respectively:

Table 4.2 The rule matrix for the fuzzy longitudinal controller [44].

		Distance Error				
		NL	**NM**	**ZE**	**PM**	**PL**
Relative Speed	**NL**	NL	NL	NM	NM	ZE
	NM	NL	NM	NM	ZE	PM
	ZE	NM	NM	ZE	PM	PM
	PM	NM	ZE	PM	PM	PL
	PL	ZE	PM	PM	PL	PL

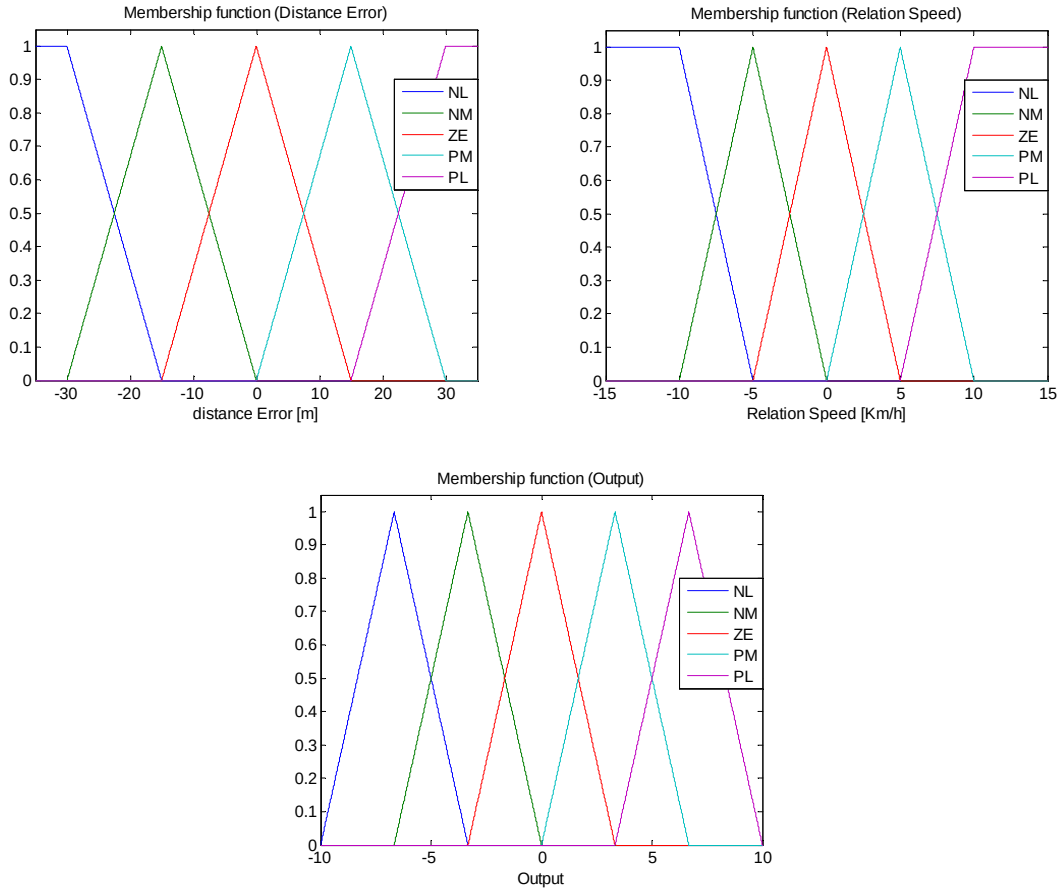

Figure 4.3 Fuzzy sets for the fuzzy longitudinal controller [44].

And Swaroop and Hedrick [41] used the following control law to implement the PD control

$$u_{PD} = -\frac{1}{h_{CTG}}\left(\dot{e}_{ACC} + \lambda S_e\right), \tag{4.10}$$

where, h_{CTG} is constant time gap and λ is a positive constant. $\dot{e}_{ACC}$ and S_e are defined in Equations (4.5)-(4.6).

4.3.1 Highway Normal Condition

Highway normal condition is defined by in terms of several conditions which can occur during normal driving in highway setting. To implement the velocity changes caused by changes in the speed limit and working zones, the lead vehicle velocity profile is defined in Figure 4.4 (b) with dot-dash line. It is assumed that the highway speed limit is changed from 100km/h to 80 km/h and the vehicle then encounters a working zone speed limit of 60km/h. After the working zone, the vehicle speed returns to 100km/h. When ACC maneuver is utilized, the ACC system needs to determine the control modes among speed control, spacing control, and sudden braking [59]. Because the speed control is suitable in the high way normal condition, a relatively large relative velocity gain (w_2) is used. When the results are compared with the result of the PD and fuzzy ACC, the suggested method shows smaller inter-vehicular distance following a perturbation, Figure 4.4 (a). Table 4.3 shows the performance measure of each method.

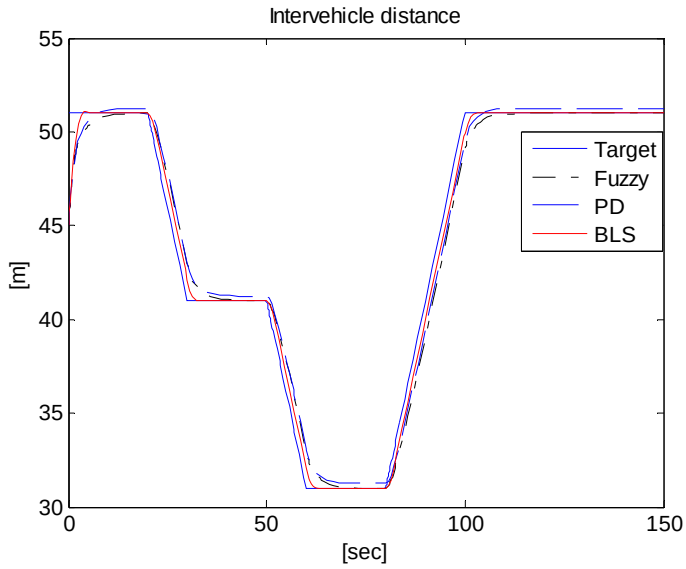

(a) Inter-vehicle distance

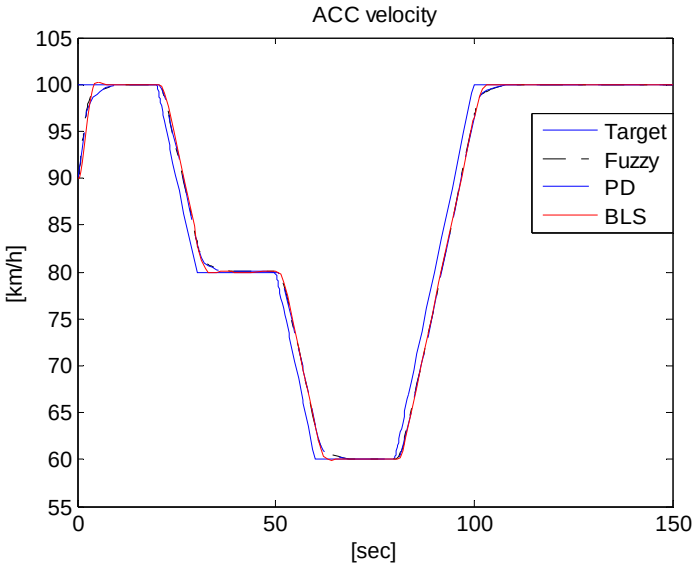

(b) ACC velocity

Figure 4.4 ACC result for highway normal conditions.

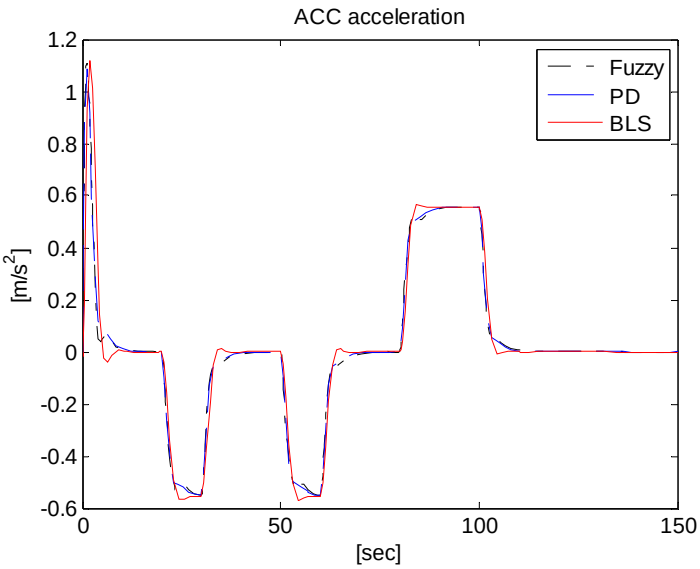

(c) ACC acceleration

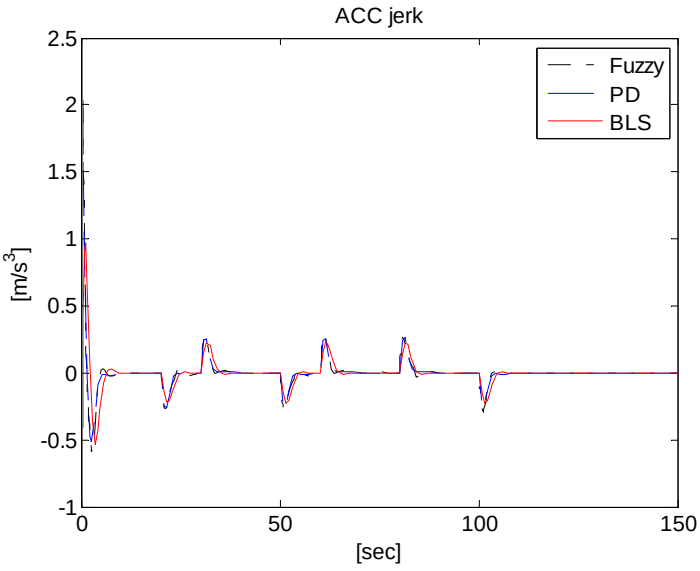

(d) ACC jerk

Figure 4.4 Continued.

Table 4.3 Performance measure for highway normal condition.

	Fuzzy	PD	BLS
$\int_0^{t_f} \lvert S_e \rvert \, dt$	93.01	104.60	**50.76**
$\int_0^{t_f} \lvert \dot{e} \rvert \, dt$	**165.65**	166.69	166.81
P	258.66	271.28	**217.57**

In the inter-vehicular error integration, BLS has the smallest error accumulation while fuzzy logic has smallest velocity error performance. However, the summation of these two measure, P, shows the smallest value in BLS based ACC.

Typically, the acceleration magnitude is used as a comfort metric [59]. In particular, changes the vehicle's longitudinal acceleration is used as an evaluation metric [7]. When the acceleration and its time derivative, jerk, are observed, the BLS based method operates the vehicle more comfortably and indicates a reasonable range of accelerations/decelerations [42] that real vehicles can generate.

4.3.2 Highway Emergency Condition

The highway emergency condition requires a sudden stop to avoid collisions. To implement a sudden stop, the sensory input, *SI* incorporates a relatively large acceleration gain (w_3), thereby enhancing the acceleration/deceleration response of the system. It is assumed that the lead vehicle senses the situation around 100m ahead of its current position on the road. To address the emergency condition, the desired target speed of 100km/h is reduced to 0km/h in 5.56 seconds (in consideration of the deceleration limit also used in other studies [42].) In this scenario, stopping distance and time are important. The result demonstrates that the performance of the suggested

control scheme has shorter stopping time than proportional derivative control law [36] and fuzzy logic control [44] in highway emergency condition, in Figure 4.5 (b).

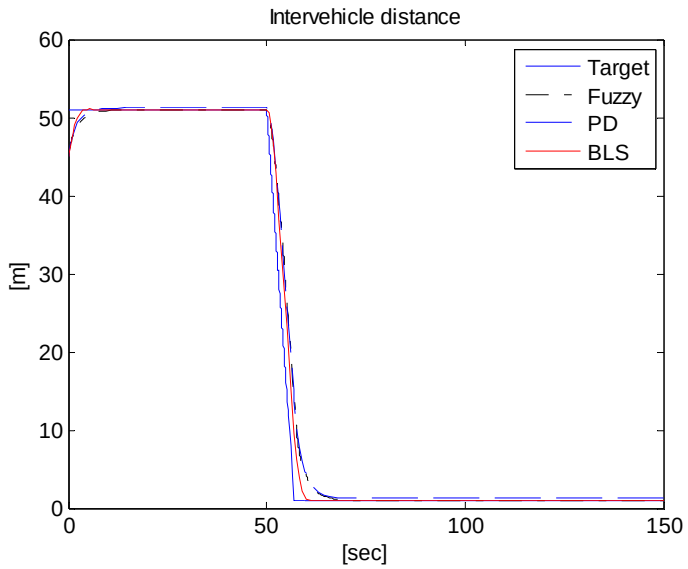

(a)Inter-vehicle distance

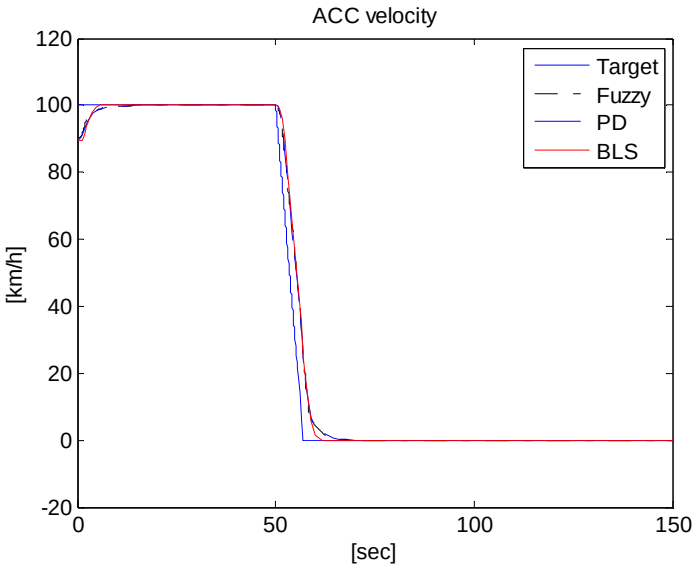

(b) ACC velocity

Figure 4.5 ACC result for highway emergency condition.

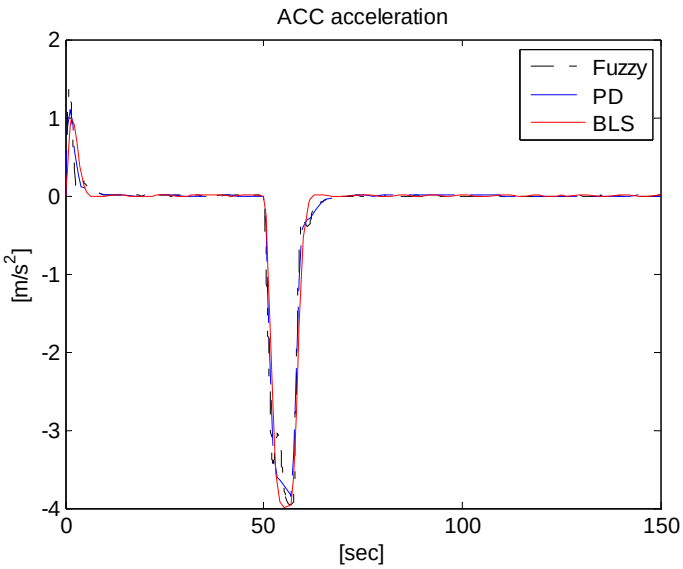

(c) ACC acceleration

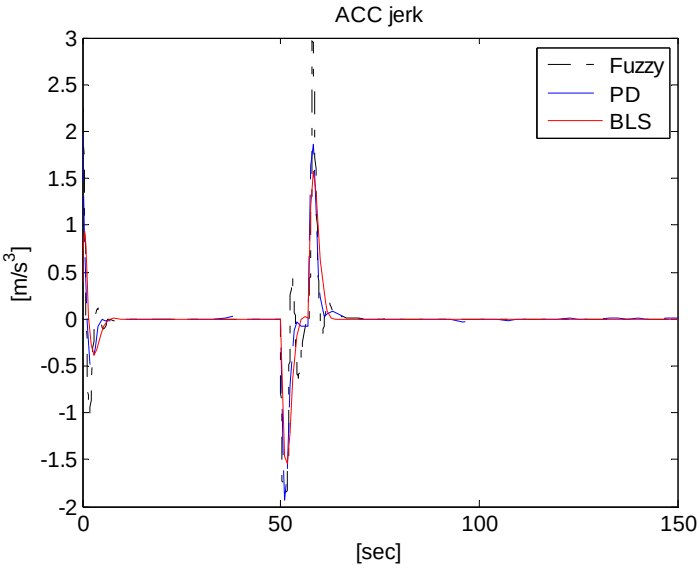

(d) ACC jerk

Figure 4.5 Continued.

Furthermore, the BLS based ACC introduces less jerk and a potentially more comfortable ride for the passengers as shown in Figure 4.5 (d). Table 4.4 shows the performance measure of each method in highway emergency condition. As similar as in

Table 4.4 Performance measure for highway emergency condition.

	Fuzzy	PD	BLS
$\int_0^{t_f} \lvert S_e \rvert \, dt$	106.30	135.85	**67.46**
$\int_0^{t_f} \lvert \dot{e} \rvert \, dt$	**201.63**	203.20	202.58
P	307.93	339.06	**270.04**

the previous simulation, BLS has best performance in following inter-vehicular distance, while Fuzzy has best velocity tracking performance where the performance of each method is very close to each other. Finally, the performance measure, P, shows the best performance in BLS.

4.3.3 Downtown Traffic Light

In this subsection, the performance of the BLS based ACC is considered when the vehicle is driven in a typical city traffic environment where downtown traffic lights are prevalent. In the center of a city, the vehicle must stop at red lights and recover its limit speed when the light turns green. To cope with this situation, a Stop&Go function is developed that emphasizes spacing control by incorporating a relatively large spacing error gain, w_1. The velocity profile is depicted in Figure 4.6 (b). Assuming the speed limit of 40 km/h, the vehicle encounters the red light twice over a period of slightly over two minutes. The results, Figure 4.6 and Table 4.5, demonstrate that all the strategies

perform well in the Stop&Go setting. However, BLS based approach shows a faster response in achieving the required relative distance even though the values of the performance measure are very close to each other.

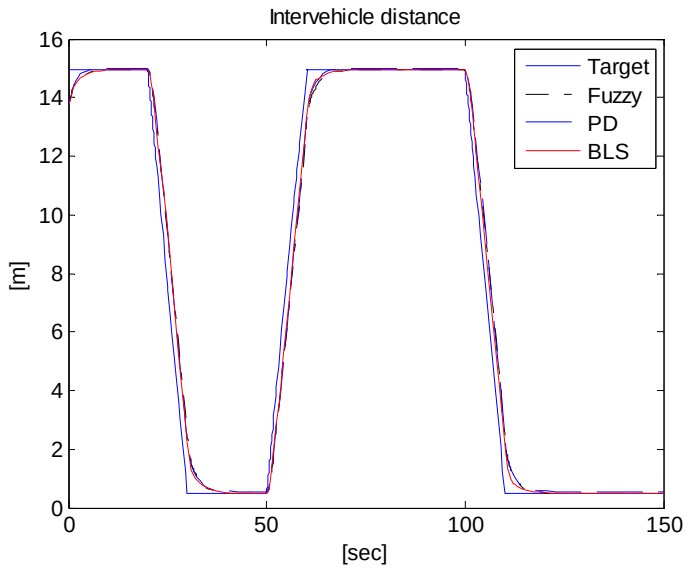

(a)Inter-vehicle distance

Figure 4.6 ACC result for downtown traffic light condition.

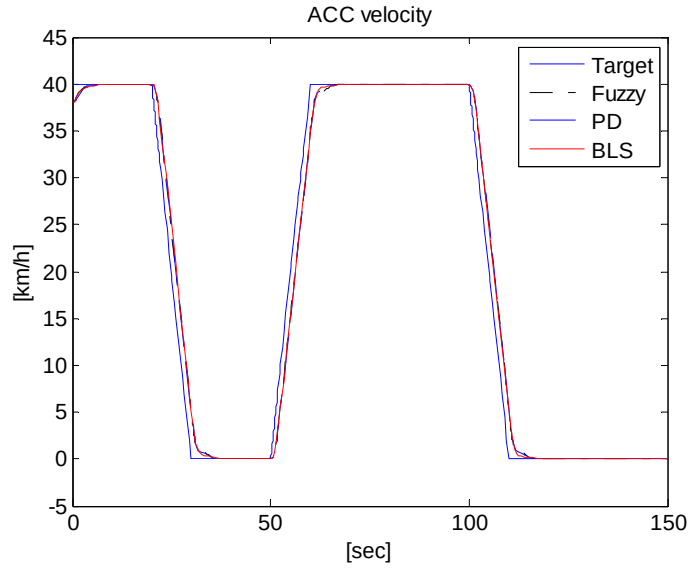

(b) ACC velocity

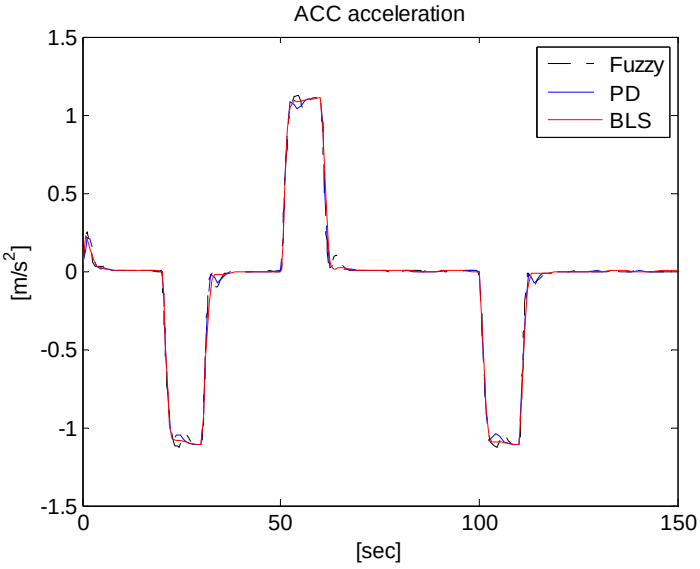

(c) ACC acceleration

Figure 4.6 Continued.

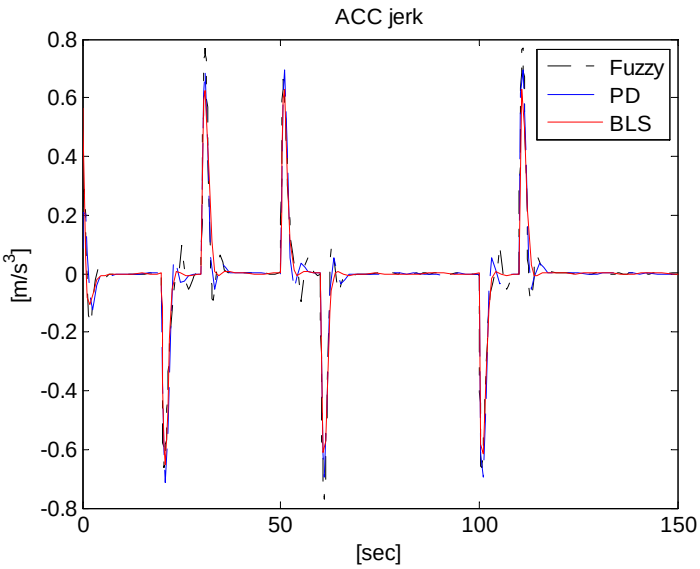

(d) ACC jerk

Figure 4.6 Continued.

Table 4.5 Performance measure for downtown traffic light condition.

	Fuzzy	PD	BLS
$\int_0^{t_f} \lvert S_e \rvert \, dt$	61.56	64.15	**53.63**
$\int_0^{t_f} \lvert \dot{e} \rvert \, dt$	**160.46**	160.72	160.58
P	222.01	224.87	**214.21**

4.3.4 Downtown Traffic Congestion

The rush hour traffic condition is taken into account in this subsection. During the commute time, the vehicle velocity changes frequently. To realize this, a sinusoidal velocity profile is utilized that varies from 25km/h to 0km/h. In this traffic situation, the performance of the BLS based method is better as compared with the conventional

approaches. The results show that the inter-vehicular distance of the BLS based strategy follows the required level with a very small error. Also it is expected that the driver's fatigue is reduced by the proposed ACC system in frequent stop and go situations by using ACC function. When Figure 4.7 and Table 4.6 is analyzed PD control has best performance in velocity tracking, however, by having the smallest inter-vehicular error accumulation, BLS based control has best performance measure value, P.

Table 4.6 Performance measure for downtown traffic jam condition.

	Fuzzy	PD	BLS
$\int_0^{t_f} \lvert S_e \rvert \, dt$	51.42	27.64	**16.00**
$\int_0^{t_f} \lvert \dot{e} \rvert \, dt$	108.94	**99.65**	100.98
P	160.37	127.29	**116.98**

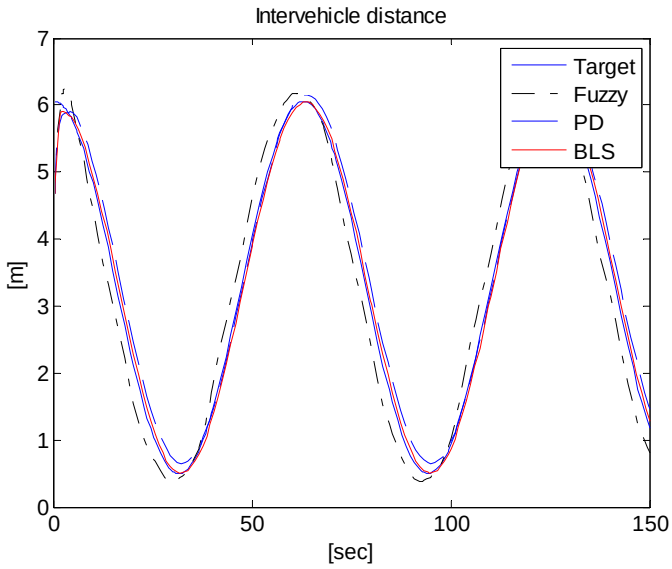

(a)Inter-vehicle distance

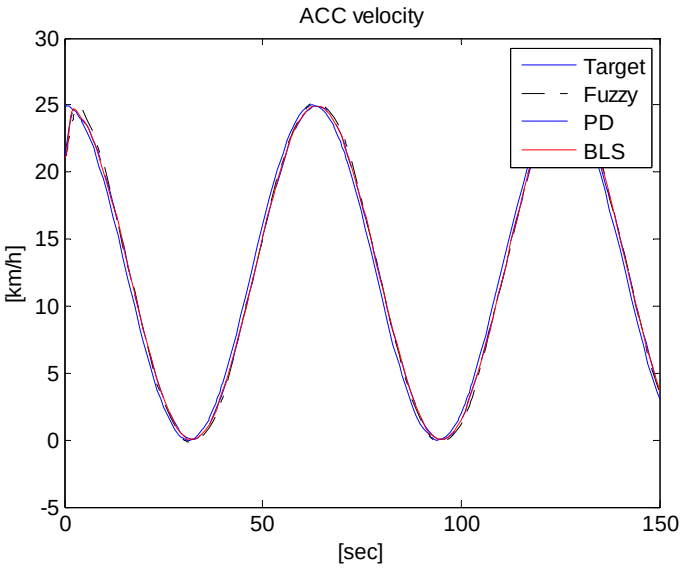

(b)ACC velocity

Figure 4.7 ACC result for downtown traffic jam condition.

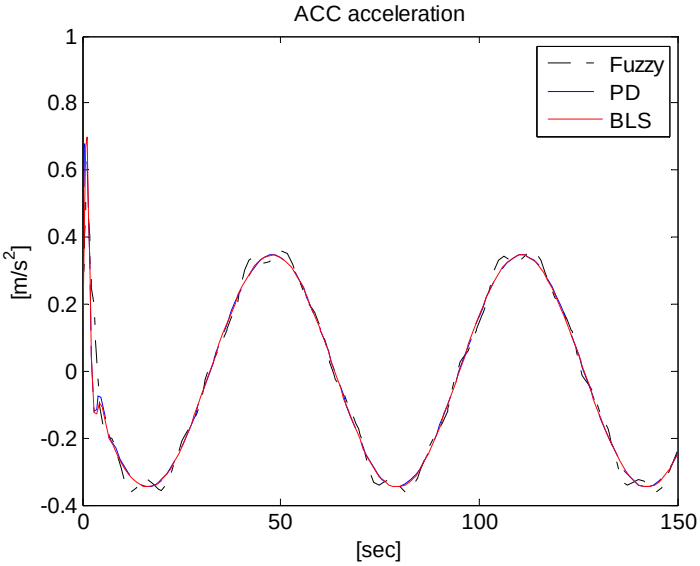

(c) ACC acceleration

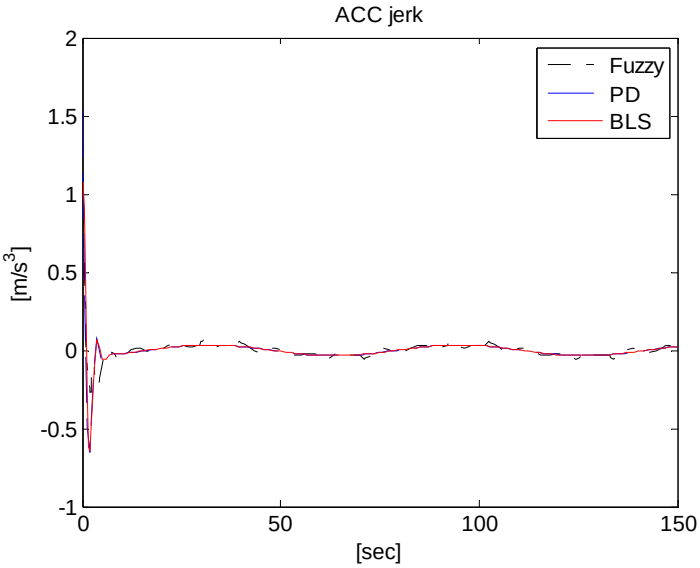

(d) ACC jerk

Figure 4.7 Continued.

4.4 Summary

In this Section, the brain limbic system based controller is utilized to develop the Adaptive cruise control that can be applied in highway and downtown driving environment. Brain limbic system updates the gains of the amygdala and OFC through defined sensory input and emotional cue. And these signals are obtained from the relative distance, velocity, and acceleration of the ACC vehicle. To demonstrate the performance of the suggested method, four different velocity profiles are assumed and compared with constant time gap based PD control and fuzzy logic control. In most traffic situations, the BLS based control shows better inter-vehicle distance tracking performance while fuzzy logic control has better performance in velocity tracking performance. Therefore, it cannot be said that the developed method overwhelms the conventional method. However, the simulation results demonstrate effective performance of the neuromorphic control approach, which is the computational model of brain limbic system, for an autonomous vehicle.

5. CELL-TO-CELL MAPPING: STABILITY ANALYSIS OF BLS BASED CONTROL SYSTEM

5.1 Cell-to-Cell Mapping

In this Section, the stability analysis for BLS based control is discussed. In this research, a bio-inspired learning algorithm, is applied to control problem. Even though it is necessary to investigate the stability, the well-known analytical technique, Lyapunov theory, cannot be used due to the nonlinearity and complicacy of BLS structure. To this end, Shahmirzadi and Langari [60] employed Cell-to-Cell Mapping to investigate the behavior of the BLS based control system.

Cell-to-Cell Mapping is a computational technique for global analysis of nonlinear dynamic systems [61-62]. Cell-to-Cell Mapping technique is based on discretization of a partition of the state space into small grids, called cell. The cells are defined as the initial conditions. And based on the dynamics of the system a Cell-to-Cell Mapping can be evolved. In order to analyze different nonlinear systems such as, a forced zero-stiffness impact oscillator, a fuzzy control system, and a power system Cell-to-Cell Mapping is applied [63-67].

To implement Cell-to-Cell Mapping, the region of interest, a particular region in the state space, (Ω) is discretized into a finite number of cells. A cell in Ω is selected as the initial state (condition). With this initial condition, the subsequent states are evolved based on the dynamics of the system until final states is obtained. After observing all the initial conditions, it can be concluded that there exist two different set of cells, stable

cells and unstable cells. The trajectories of stable cells are staying in the region of interest; however, those of unstable cells are going out from the region of interest. Figure 5.1 shows two different groups of cells. One group of cells (1, 2, 3, 4, and 5) eventually form an orbit; however, the trajectory of the system moving through cell 6 goes outside from the region, Ω. After investigating all the initial states within Ω, a stability map of the system is obtained. And the stable initial conditions are marked with 'o' sign while the unstable initial conditions are marked with 'x' sign.

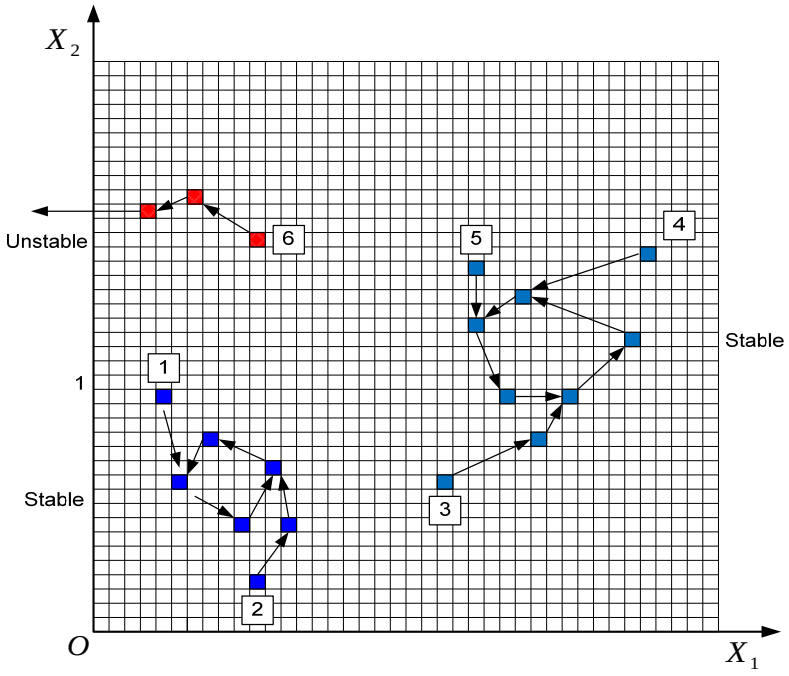

Figure 5.1 Cell to Cell Mapping and two different cell groups.

5.2 Stability Analysis of BLS Based Control

In this subsection, the Cell-to-Cell Mapping method is employed to examine the stability of BLS based control. Especially, the stability of BLS based LCM control is

analyzed. In order to implement BLS based LCM, the sensory input and emotional cue are defined in Section 3 as follows,

$$SI = e_{LCM}\ , \tag{5.1}$$

$$EC = \lambda\left(u + e_{LCM}\right), \tag{5.2}$$

with $\lambda = 1$ and look ahead point error, $e_{LCM} = y_T - y - L\psi$. To analyze the stability of the BLS control system, the reference value zero is set, i.e. $y_T = 0$. And the following lateral vehicle dynamic under the assumptions constant velocity and straight road traveling

$$\dot{v}_y = -2\frac{\left(C_f + C_r\right)}{mv_x}v_y - \left[2\frac{\left(aC_f - bC_r\right)}{mv_x} + v_x\right]\dot{\psi} + \frac{2C_f\delta}{m} \tag{5.3}$$

$$\ddot{\psi} = -\frac{2\left(aC_f - bC_r\right)}{Iv_x}v_y - \frac{2\left(a^2C_f + b^2C_r\right)}{Iv_x}\dot{\psi} + \frac{2aC_f}{I}\delta\ . \tag{5.4}$$

$$\dot{G}_A = \alpha\max\left\{0,\ \lambda\left(G_A - G_{OC} + 1\right) - G_A\right\}SI^2 \tag{5.5}$$

$$\dot{G}_{OC} = \beta\left\{G_A - G_{OC} - \lambda\left(G_A - G_{OC} + 1\right)\right\}SI^2 \tag{5.6}$$

In the BLS based LCM control system, there are six states to examine. To avoid the high calculation load, the BLS gains G_A and G_{OC} are set to zero. It is reasonable because BLS is a kind of learning structure. In other words, before the system experience a certain task, it does not have any knowledge about the task. To this end, other four states are observed to investigate the stability of BLS based control. Therefore the region of interest is defined within the possible vehicle operation ranges for each state, $y, v_y, \psi,$ and $r = \dot{\psi}$.

$$\Omega = \begin{Bmatrix} -1.83 \le y\,[m] \le 1.83, & -5 \le v_y\,[m/s] \le 5 \\ -\pi/6 \le \psi\,[rad] \le \pi/6, & -\pi/6 \le r\,[rad/s] \le \pi/6 \end{Bmatrix} \text{and } G_A = G_{OC} = 0.$$

The range of lateral displacement is obtained from the interstate highway road width 3.66 [m], and the yaw angle range is obtained from the maximum and minimum possible angle of the vehicle.

In order to implement Cell-to-Cell Mapping, the regions of interest of lateral motion and angular motion are discretized with the size of 0.1 cells and 0.01 cells. However, when the results are indicated in the figure, the interval of the initial conditions is set larger to make the figure readable. Therefore, in Figure 5.2 the interval of lateral displacement, lateral velocity, yaw angle, and yaw angle rate is given as 0.5 [m], 0.5 [m/s], $\pi/36$ [rad], and $\pi/36$ [rad/s], respectively. Because each initial condition value is defined as the center position of each cell, all points within the same cell are represented by the center value of corresponding cell.

In this research, we used Cell-to-Cell Mapping for a four states system by assuming the BLS initial gains are zero. In order to display the stable cells, 4-dimensional display method is needed. To this end, the stable cell information is obtained first and the number of stable cell set ($y, v_y, \psi,$ and $\dot{\psi}$) are investigated. By the defined region of interests, 6237 stable cells are obtained out of 31941 cells (from the defined cell interval). To display one set of cells, two of the states, i.e. y and v_y, or ψ and $\dot{\psi}$ are fixed while the other two states are varying. In Figure 5.2 (a), the yaw angle and yaw angle rate are fixed as $\psi = -0.09$ and $\dot{\psi} = 0.171$. When the vehicle is directing negative yaw angle direction, the vehicle stability basin is larger in positive lat-

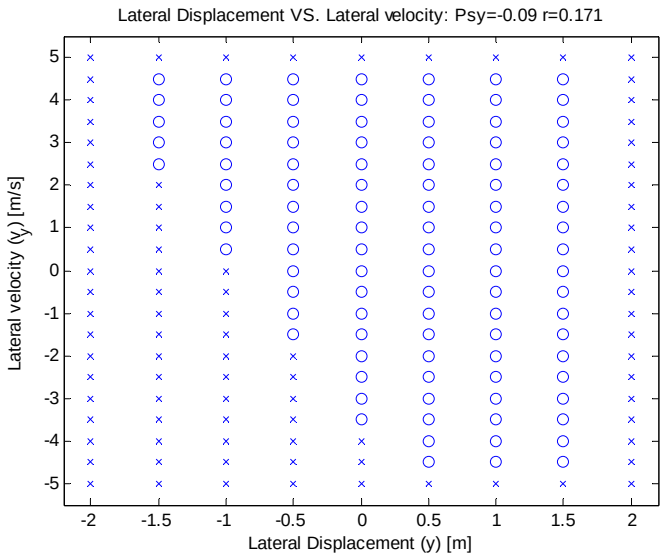

(a) Lateral motion

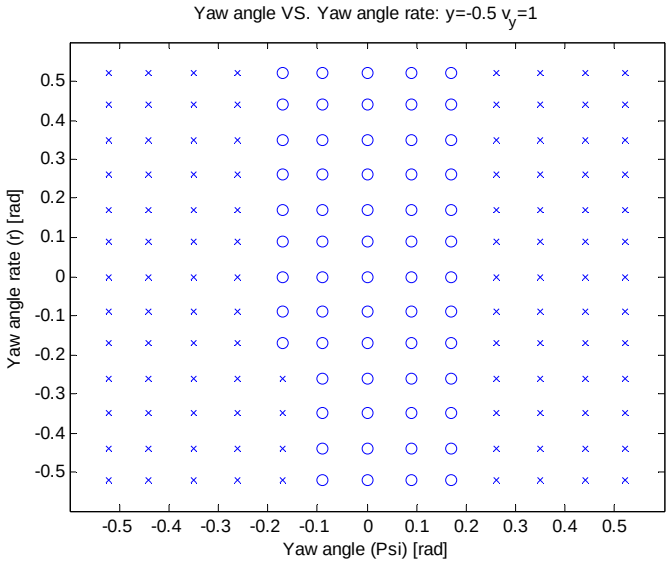

(b) Angular motion

Figure 5.2 Cell-to-Cell Mapping BLS contro results.

eral displacement. From 5.2 (b), the lateral cell map lateral displacement and lateral velocity are fixed as $y = -0.5$ and $v_y = 1$. The resulting plot shows that positive yaw angle area has larger attractive basin when the vehicle is shifted negative direction. If the trajectories are stay in the regions of interest, the corresponding initial conditions are marked with ‘o’. And the other cells are marked with ‘x’. When the cell map is analyzed, the stable range of lateral motion and angular motion are located around the origin, the normal operation range of driving, for each map. Therefore, under the normal driving condition, it can be concluded that the BLS based LCM is stable.

Figure 5.3 displays the BLS based control results when the vehicle’s initial condition is defined as of a stable initial condition and an unstable initial condition. These conditions are selected from Figure 5.2 to investigate the phenomenon with respect to the initial condition, when it is stable or not. The results are indicated in Figure 5.3 (a) are gotten from a stable initial condition and the red dotted line indicates the limit line of the region of interest for each state. Under a stable initial condition, all trajectories are staying in the region and heading to the equilibrium point. However, the results from unstable condition, Figure 5.3 (b), are a little bit different. The responses for lateral displacement, lateral velocity, and the yaw angle rate cross over the region limit. However, they converge to the equilibrium point, eventually. Even though the trajectories are converge to the equilibrium point, these initial conditions are regarded as unstable states because these initial conditions can arouse a collision with the neighboring lane’s vehicle by invading to the next lane.

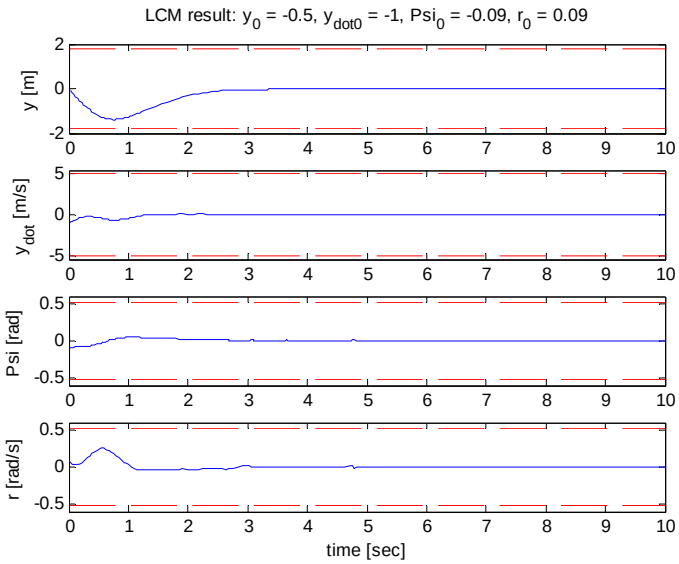

(a) Stable initial condition

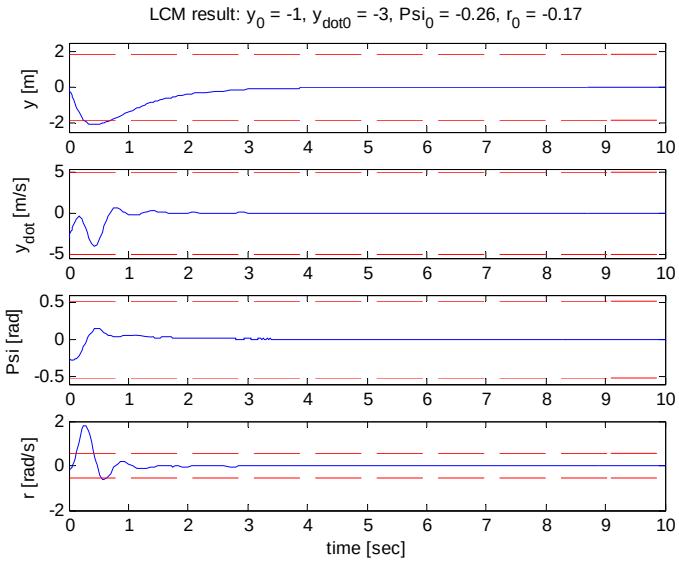

(b) Unstable initial condition

Figure 5.3 BLS based LCM results.

Figures 5.4 and 5.5 are the trajectories of Cell-to-Cell Mapping. Two stable initial conditions and one unstable initial condition as follows,

$y = -0.5,\ \dot{y} = 1, \psi = \pi/36,\ r = \pi/12$ (Stable initial condition)

$y = 1.5,\ \dot{y} = 3, \psi = 5\pi/36,\ r = -\pi/18$ (Unstable initial condition)

$y = 0.5,\ \dot{y} = 1, \psi = -\pi/12,\ r = \pi/36$ (Stable initial condition).

In Figures 5.4 and 5.5, the cell size is defiend as 0.1×0.1 and the results are compared with the real trajectory of correponding initial conditions, which Cell-to-Cell Mapping is not applied initial conditions. The trajectories of stable cells remain in the region of interest, however, the trajectory of unstable cell departures from the region and return to the region of interest. Even though all initial conditions are return to the equilibrium eventually, the unstable trajectory can cause accident with the next lane's vehicle by departuring the region of interst which is the normal vehicle operation boundaries.

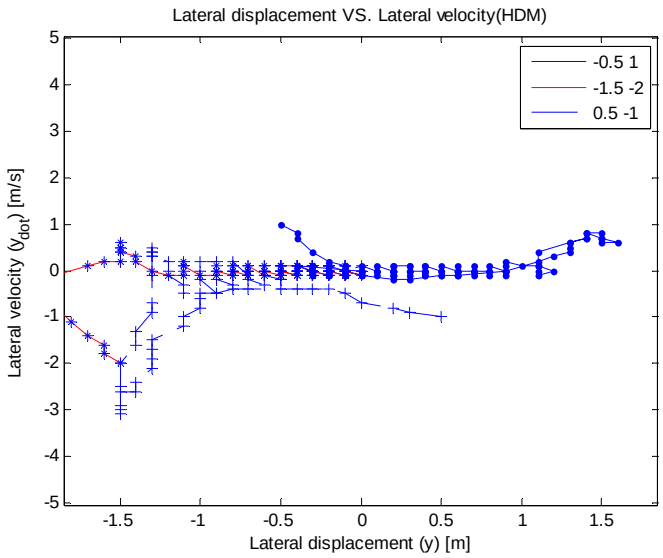

(a) Region of interest

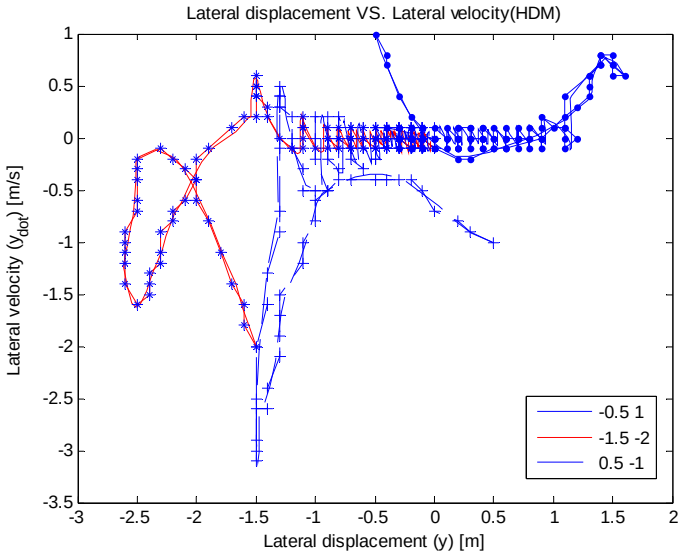

(b) Region of the trajecories

Figure 5.4 Cell-to-Cell Mapping lateral motion trajectories with cell size (0.1×0.1): BLS based control.

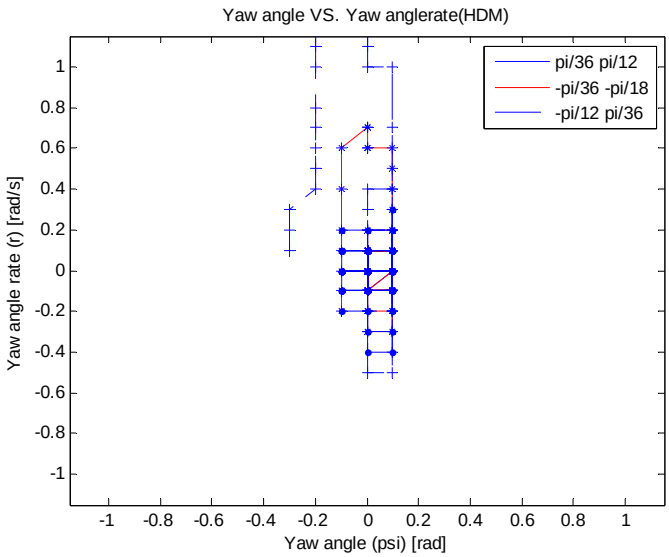

(a) Region of interest

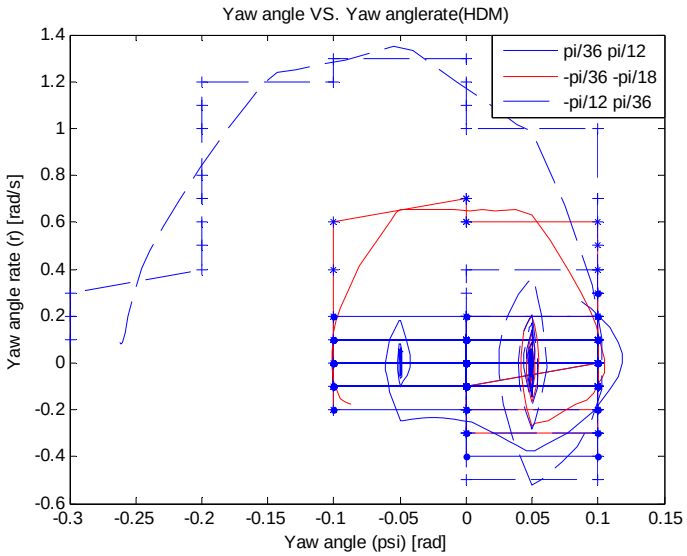

(b) Region of the trajecories.

Figure 5.5 Cell-to-Cell Mapping angular motion trajectories with cell size (0.1×0.1): BLS based control.

Therefore in the sense of Cell-to-Cell Mapping, the initila conditions that the corresponding trajectories are going out from the region of interest defined as unstable cell. Figures 5.6 and 5.7 are the Cell-to-Cell Mapping lateral and angular motion of the BLS based LCM control with smaller cell size, i.e. 0.01×0.01. By defing smaller cell size, the trajectoreis are more closer to the real trajectory and the results are not different from larger cell case. Therefore, it can be concluded that one benefit of Cell-to-Cell Mapping is reducing the number of trajectories that laying on the same cell by defining each cell representing point as the center of the cell.

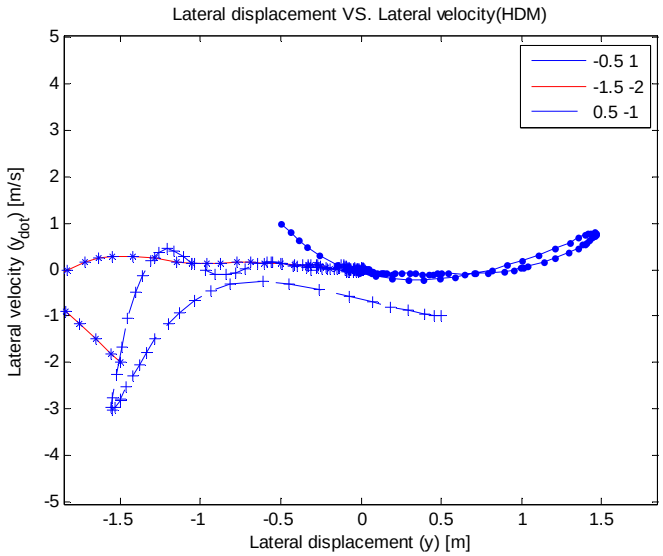

(a) Region of interest

Figure 5.6 Cell-to-Cell Mapping lateral motion trajectories with cell size (0.01×0.01): BLS based control.

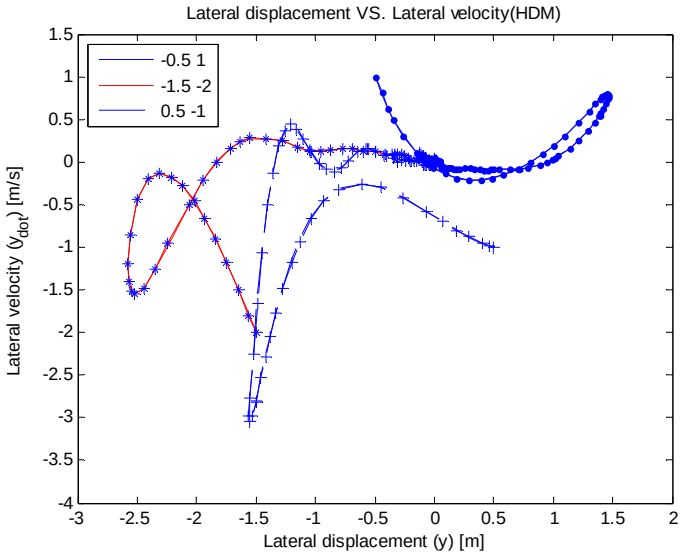

(b) Region of the trajecories

Figure 5.6 Continued.

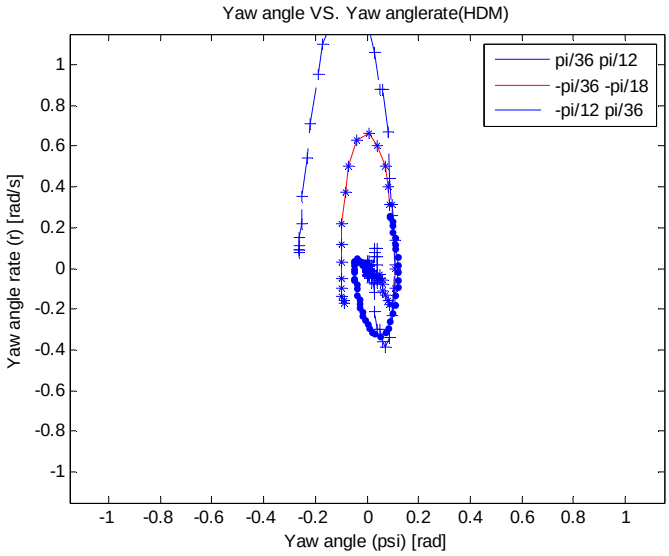

(a) Region of interest

Figure 5.7 Cell-to-Cell Mapping angular motion trajectories with cell size (0.01×0.01): BLS based control.

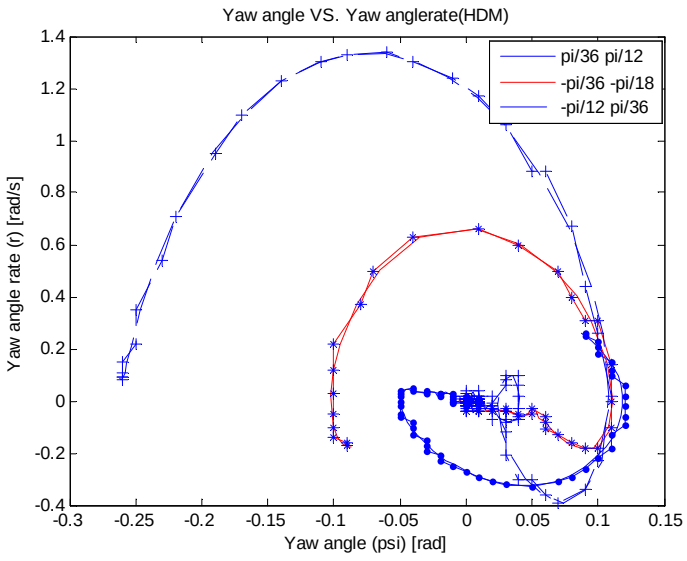

(b) Region of the trajecories

Figure 5.7 Continued.

5.3 Stability Analysis of HDM Based LCM Control

In this subsection, Cell-to-Cell Mapping is applied to human driver model based control which BLS based control results are compared with. The same cell size and the region of interest with BLS based control are defined. The region of interest is ,

$$\Omega = \begin{Bmatrix} -1.83 \le y\,[m] \le 1.83, & -5 \le v_y\,[m/s] \le 5 \\ -\pi/6 \le \psi\,[rad] \le \pi/6, & -\pi/6 \le r\,[rad/s] \le \pi/6 \end{Bmatrix}.$$

To implement Cell-to-Cell Mapping, the regions of interest of lateral motion and angular motion are partitioned with the size of 0.1 cells and 0.01 cells. However, the interval of the initial conditions is made larger to make the figure distinguishable, i.e. the

interval of lateral displacement, lateral velocity, yaw angle, and yaw angle rate is given as 0.5 [m], 0.5 [m/s], 0.2 [rad], and 0.2 [rad/s], respectively.

As stated in the BLS based control stability analysis case, in order to display 4D states, the same method is and the same fixed lateral displacement and lateral velocity set and yaw angle and yaw angle rate set are utilized. Figure 5.8 is the result of HDM based control analysis with respect to the initial conditions. When the stable cell number is investigated the stable cells of HDM based control has 6059 stable cells out of 31941 cells. This number is smaller than that of BLS based control (6237). Larger number of stable initial condition means that BLS based control more margin of stability with respect to the states change. From the cell map, Figure 5.8 (a) and (b), it is observed that HDM based LCM has smaller stability range than that of BLS based control. This supports the better performance of BLS based system again.

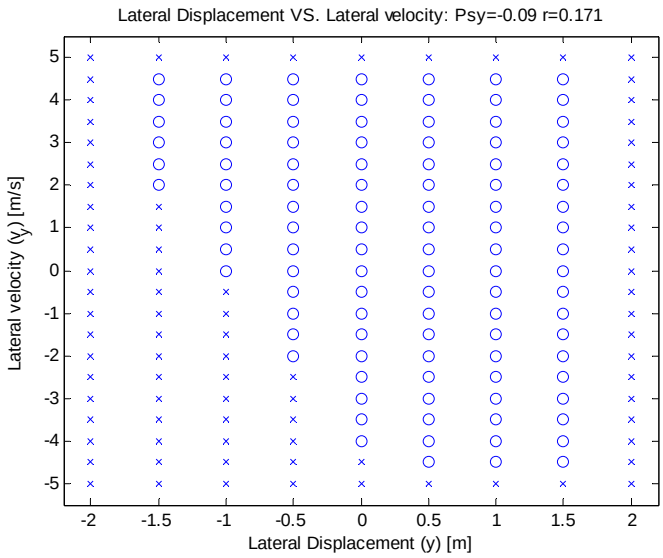

(a) Lateral motion

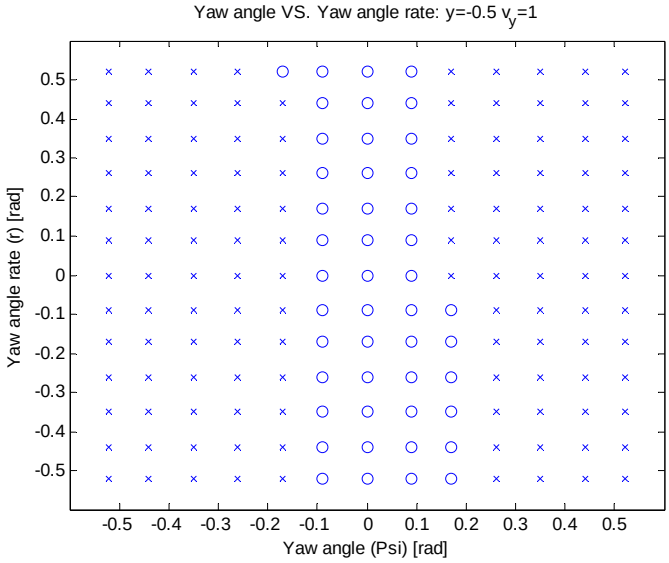

(b) Angular motion

Figure 5.8 Cell-to-Cell Mapping HDM LCM control results.

Figures 5.9 and 5.10 are the trajectories of one stable and two unstable initial conditions as follows,

$y = -0.5,\ \dot{y} = 1, \psi = \pi/36\,,\ r = \pi/12$ (Stable initial condition)

$y = 1.5,\ \dot{y} = 3, \psi = 5\pi/36\,,\ r = -\pi/18$ (Unstable initial condition)

$y = 0.5,\ \dot{y} = 1, \psi = -\pi/12\,,\ r = \pi/36$ (Unstable initial condition).

The cell size is defined as 0.01×0.01. The unstable intial conditions are leaving from the region of interst and back again to the equilibrium point.

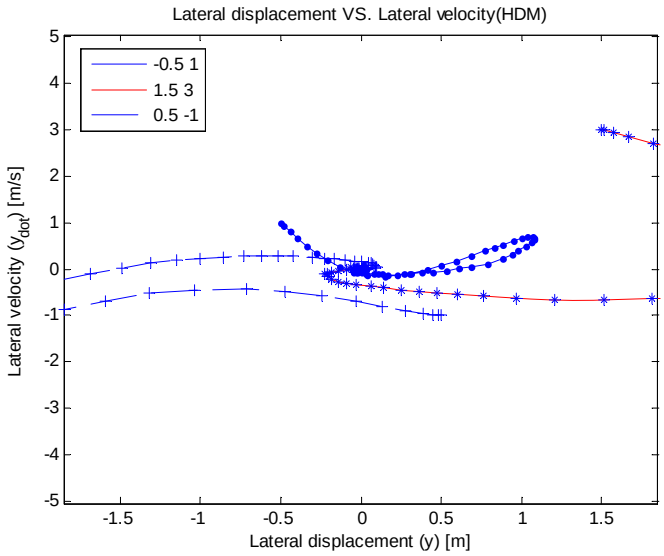

(a) Region of interest

Figure 5.9 Cell-to-Cell Mapping lateral motion trajectories with cell size (0.01×0.01): HDM basd control.

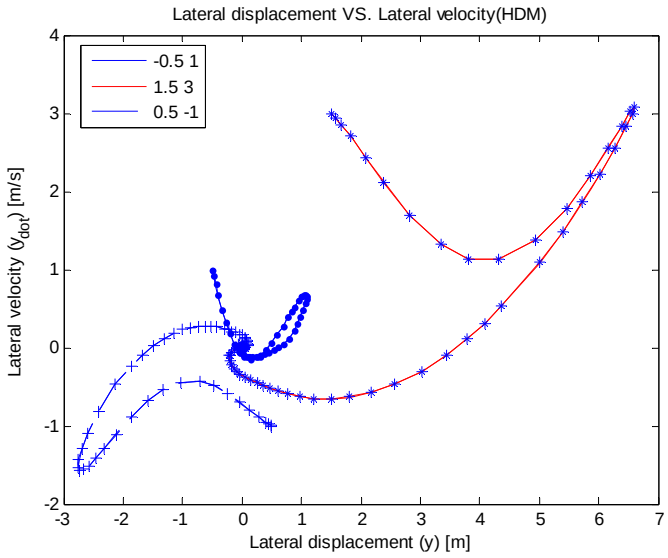

(b) Region of the trajecories

Figure 5.9 Continued.

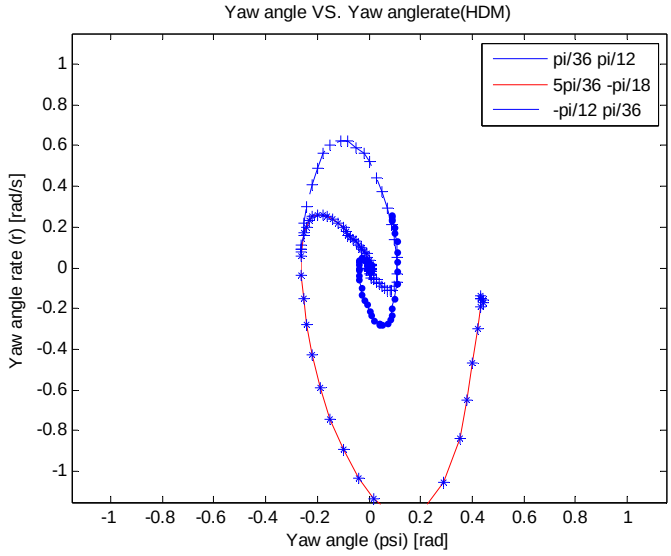

(a) Region of interest

Figure 5.10 Cell-to-Cell Mapping angular motion trajectories with cell size (0.01×0.01): HDM based control.

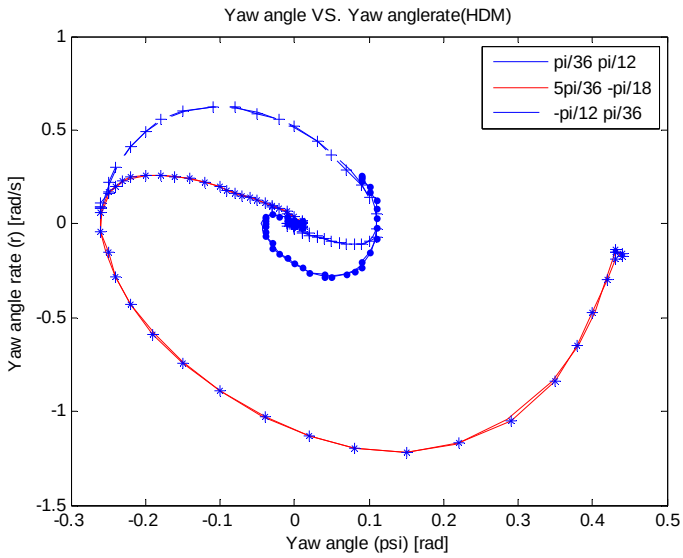

(b) Region of the trajecories

Figure 5.10 Continued.

5.4 Summary

In this Section, the stability of BLS based control is analyzed via Cell-to-Cell Mapping method. BLS based control system cannot be analyzed by conventional Lyapunov's method because of the nonlinearity and complicacy of BLS structure. Cell-to-Cell Mapping applied LCM problem by defining the region of interest as the vehicle operating range.

The resulting cell map indicated the stable and unstable initial conditions on lateral and angular motion plane. In order to display four states, two of the states are fixed. By analyzing the cell map, it is concluded that BLS based LCM is stable under normal driving conditions for lateral motion and angular motion.

Subsequently, the stability of HDM based LCM is analyzed with the same method. By investigating the stable cell numbers of two control strategy, BLS based control has more number of stable states meaning that has larger stability margin in BLS based control. In the resulting cell map, it is observed that stable initial states area of BLS based LCM is a little bit broader than that of HDM.

6. ANALYTIC HIERARCHY PROCESS

6.1 Autonomous Vehicle Decision Making via AHP

In this Section, a multi objective decision making method, Analytic Hierarchy Process (AHP) is explained and the application of AHP to an autonomous vehicle decision making process is provided. AHP provides a comprehensive and rational framework for structuring a problem, for representing and quantifying its elements, for relating those elements to overall goals, and for evaluating alternative solutions [68]. In order to implement AHP, the designer (or user) has to standardize the problem as hierarchies. In AHP based decision making, the highest level is the overall goal and the lowest level of the hierarchy is the final function (or alternative) among available candidates. To make an optimal decision, the designer has to define the objectives as the considerations in decision making. And those objectives form intermediate hierarchies (or hierarchy). After these hierarchies are formalized, the relative importance matrix (RM), relative importance between objectives, has to be defined. Before AHP decision making is done, the consistency of the RM has to be checked to make rational decision. If the RM is not consistent then the decision based on the particular RM cannot be reliable. Therefore by consistency consideration, the acceptability of the defined matrix is investigated. Subsequently, the alternatives' values are evaluated according to the objectives. Numerical priorities are calculated for each of the alternative. And the final decision is made by choosing the function that has maximum value.

6.1.1 Hierarchy Formalizing

In AHP, there are three main hierarchies such as goal, objectives, and alternatives. Figure 6.1 shows the hierarchy of decision making to determine the optimal function. In autonomous vehicle function management problem, the ***goal*** is to select an optimal function among allowed functions; the ***objectives*** (the consideration when the decision is made) are safety, driving speed, and fuel economy; and the ***alternatives*** are LCM_L, LCM_R, and ACC that stand for lane change maneuver to the left lane, lane change maneuver to the right lane, and adaptive cruise control, respectively. In this research, a three lane road is considered. Therefore, the allowed functions are different according to the vehicle position; if the vehicle is located at the 1st lane ACC and LCM_R are allowed; however, if the vehicle is in the 2nd lane it can have all the function; finally by locating at the 3rd lane it only obtains LCM_L and ACC. After the hierarchy is designed, the preferences (or priority among the entries) are determined by

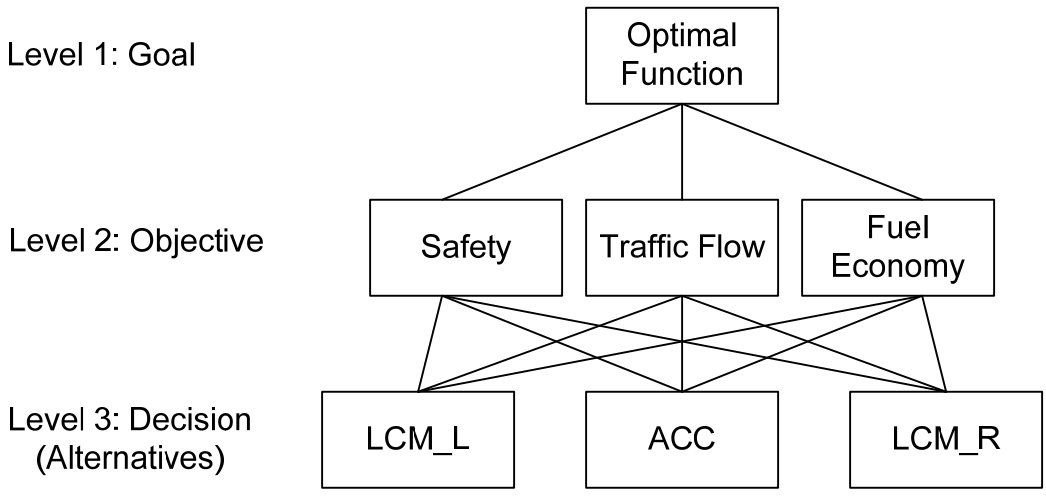

Figure 6.1 Hierarchy for getting optimal function.

the designer according to the importance of each objective. After these levels are decided, AHP chooses the best function which satisfies the defined preferences [45].

6.1.2 Relative Importance Matrix

The first step of using AHP is to decide the relative importance of the objectives. In AHP theory, the pairwise comparison scale is given [46] to define an RM. According to the relative importance of an objective to the other, one can define a scale from 1 to 9. Table 6.1 shows the pair-wise comparison scale that is used in forming an RM.

Table 6.1 The pairwise comparison scale [45].

Intensity of Importance	Definition
1	Equal importance of elements
3	Moderate importance of one element over another
5	Strong importance of one element over another
7	Very Strong importance of one element over another
9	Extreme importance of one element over another
2, 4, 6, 8	Intermediate values between two adjacent judgment

The RM of the objectives is defined O. And the size of an RM matrix is $\kappa \times \kappa$ when κ is the number of objectives. In this research, three objectives are considered. O_1, O_2, and O_3 represent the degree of safety, driving speed, and fuel economy, respectively. In the RM is formalized by the following structure,

$$RM = \begin{bmatrix} O_1/O_1 & O_1/O_2 & O_1/O_3 \\ O_2/O_1 & O_2/O_2 & O_2/O_3 \\ O_3/O_1 & O_3/O_2 & O_3/O_3 \end{bmatrix} = \begin{bmatrix} 1 & a & b \\ 1/a & 1 & c \\ 1/b & 1/c & 1 \end{bmatrix}. \quad (6.1)$$

In Equation (6.1), all diagonal elements are '1' and the same equation shows that an *RM* can be defined by only three elements, *a*, *b*, and *c*. This form of matrix is called as ***reciprocal*** matrix. In order to obtain a weighted objective matrix the *RM* is to be normalized. A normalized matrix of the relative important matrix obtained by the following equation,

$$O_{norm} = \begin{bmatrix} \dfrac{O_{i1}}{\sum_{i=1}^{\kappa} O_{i1}} & \dfrac{O_{i2}}{\sum_{i=1}^{\kappa} O_{i2}} & \cdots & \dfrac{O_{i\kappa}}{\sum_{i=1}^{\kappa} O_{i\kappa}} \end{bmatrix}. \quad (6.2)$$

i.e., $O_{norm(23)} = O_{23} \Big/ \sum_{i=1}^{\kappa} O_{i3}$, where $i = 1, 2, 3, \cdots, \kappa$ and κ is the number of objectives.

And O_{norm} is a $\kappa \times \kappa$ matrix. To get a weighted objective matrix, the average of each row in (6.2) is calculated,

$$W_{obj} = \begin{bmatrix} \dfrac{\sum_{j=1}^{\kappa} O_{norm(1\,j)}}{\kappa} & \dfrac{\sum_{j=1}^{\kappa} O_{norm(2\,j)}}{\kappa} & \cdots & \dfrac{\sum_{j=1}^{\kappa} O_{norm(\kappa\,j)}}{\kappa} \end{bmatrix}, \quad (6.3)$$

where W_{obj} is a $1 \times \kappa$ row vector.

6.1.3 Consistency of Relative Importance Matrix

However, the limitation of Saaty's discrete 9-value scale and the inconsistency of human's judgments make the weight inappropriate [69]. Therefore, Saaty [45] proposed a method to measure the inconsistency. Saaty [70] proved that the consistent of a positive reciprocal matrix. Under the perfect consistency, the largest eigenvalue of the RM is equal to the size of the matrix, i.e., $\lambda_{\max} = n$. It is also possible to estimate the departure from consistency by the consistency index, difference $\lambda_{\max} - n$ dividing by $n-1$. Therefore the consistency index (CI) is defined as

$$CI = \frac{\lambda_{\max} - n}{n-1}, \tag{6.4}$$

where n is the number of objectives. After the CI (consistency index) is obtained, it is divided by the random consistency index to get the consistency ratio,

$$CR = \frac{CI}{RC}, \tag{6.5}$$

where the random consistency index is randomly generated reciprocal matrix using scale $\frac{1}{9}, \frac{1}{8}, \cdots, 1, \cdots, 8, 9$ by Saaty. Saaty [45] suggests that the appropriate measure, consistency ratio, ought to be no more than 0.1. In other words, if CR is greater than 0.1, the result is not accepted and another relative importance matrix is assessed until the consistency ratio satisfies the condition appropriately, $CR < 0.1$. For the acceptability of using 0.1 as the threshold, Vargas [71] figured out that the consistency index follows a truncated normal distribution when uniform distributions are used. He proved this by the 500 times of different size matrices simulation and normality tested. From the results,

Vargas concluded that for a reciprocal random matrix, an acceptable upper bound of the ratio between the consistency index of a reciprocal matrix, and its corresponding average random consistency index is 10% [72]. The average random consistency index of sample size 500 matrices is shown in the table below.

Table 6.2 Random consistency index (RC).

Number of objectives	1	2	3	4	5	6	7	8	9
RC	0	0	0.58	0.90	1.12	1.24	1.32	1.41	1.45

6.1.4 Evaluation of Alternatives

After the weighted objective matrix is obtained and the consistency is investigated, the next step is to evaluate the given three alternatives, LCM_L, LCM_R, and ACC with respect to each objective. To get the evaluation matrix of each objective, the following evaluation is utilized,

$$E(O_i)_{lm} = \frac{O_i(f_l)}{O_i(f_m)}, \tag{6.6}$$

where $O_i(f_l)$ represents the value of l^{th} function in consideration of i^{th} objective, and $l = 1, 2, \cdots, \gamma$, $m = 1, 2, \cdots, \gamma$, where γ is the number of alternatives. Also by the same process of (6.2) – (6.3), normalized matrices and the weighted alternative matrices of each corresponding objectives are obtained. To make the notation simple, (6.6) is reformed to $E(O_i)$, and the normalized form of (6.6) is defined

$$E(O_i)_{norm} = \left[\frac{E(O_i)_{l1}}{\sum_{l=1}^{\gamma} E(O_i)_{l1}} \quad \frac{E(O_i)_{l2}}{\sum_{l=1}^{\gamma} E(O_i)_{l2}} \quad \cdots \quad \frac{E(O_i)_{l\gamma}}{\sum_{l=1}^{\gamma} E(O_i)_{l\gamma}} \right], \tag{6.7}$$

where γ is the number of alternatives and $E(O_i)_{norm}$ is a $\gamma \times \gamma$ matrix. The weighted alternative matrix of each objective is obtained with the following equation

$$W_{alter}(O_i) = \left[\frac{\sum_{m=1}^{\gamma} E(O_i)_{norm(1\,m)}}{\gamma} \quad \frac{\sum_{m=1}^{\gamma} E(O_i)_{norm(2\,m)}}{\gamma} \quad \cdots \quad \frac{\sum_{m=1}^{\gamma} E(O_i)_{norm(\gamma\,m)}}{\gamma} \right], \tag{6.8}$$

where $W_{alter}(O_i)$ is a $1 \times \gamma$ row vector, and O_i represents the i^{th} objective. By considering all the functions that are equipped the following weighted alternative matrix is obtained.

$$W_{alter} = \left[W_{alter}(O_1)^T \quad W_{alter}(O_2)^T \quad \cdots \quad W_{alter}(O_\kappa)^T \right]. \tag{6.9}$$

And W_{alter} is a $\kappa \times \gamma$ matrix for κ is the number of objectives and γ is the number of alternatives.

The optimal function which has the highest value will be suggested by multiplying the two resulting matrices (6.3) and (6.9) composed of weights,

$$Function^{*} = \arg\max_{l} \left(W_{alter} \times W_{obj}^{T} \right). \tag{6.10}$$

Therefore after the hierarchy is formalized, the relative objective matrix is defined by the decision maker possessing consistency. However, an autonomous vehicle has to be operated in real traffic situation which has various traffic conditions.

6.2 Adaptive AHP

In this subsection, adaptive AHP is considered to cope with various traffic situations and driving modes. Before the autonomous vehicle functions are managed by AHP, one have to find the way to set up an RM . Also, the importance of each objective is varying with the situation especially in dynamic traffic environment. Therefore, the fixed RM does not eligible to apply an autonomous vehicle function management problem. To this end, adaptive AHP that can find optimal importance of each objective is developed.

The purpose of adaptive AHP is to select an RM to get optimal function according to the autonomous vehicle encountering situations and driving modes. In this research, the three different modes are defined such as aggressive mode, careful mode, and fuel economy mode. Aggressive mode prioritizes the driving speed by taking an RM that has highest priority in speed. In Careful mode, the algorithm chooses an RM which has highest weighting in safety focusing on the safety factor most. And the fuel economy mode takes an RM that has maximum relative importance in fuel economy. It can be expect that by taking aggressive mode the traveling time is reduced; by taking carful mode the safe travel is guaranteed; and the fuel economy mode can reduce the consumption of gas. Therefore, the suggested adaptive AHP can provide an RM that satisfies the given traffic situation and driving mode.

$$Function^{*}_{mode} = \arg\max_{l}\left(W_{alter} \times \left(W^{*}_{obj} \right)^{T}_{mode} \right). \tag{6.11}$$

In adaptive AHP, Equation (6.11) selects the function that satisfies driving mode and maximum value in the multiplication of the weighted alternative matrix and weighted objective matrix.

6.2.1 Adaptive AHP Algorithm

An *RM* has reciprocal matrix and it can be defined with only three relative importance scales from Equation (6.1). In AHP framework, only 9 numbers are used with respect to the importance degree, i.e. 1 to 9. By the inverse of the numbers, 17 numbers can be used to define an *RM* such as $\left[\frac{1}{9}, \frac{1}{8}, \frac{1}{7}, \cdots 1, 2, \cdots 8, 9\right]$. By choosing three numbers among the available numbers, one can define 4913 matrices. However, the number is reduced to 3835 matrices by removing matrices that have the same ratio.

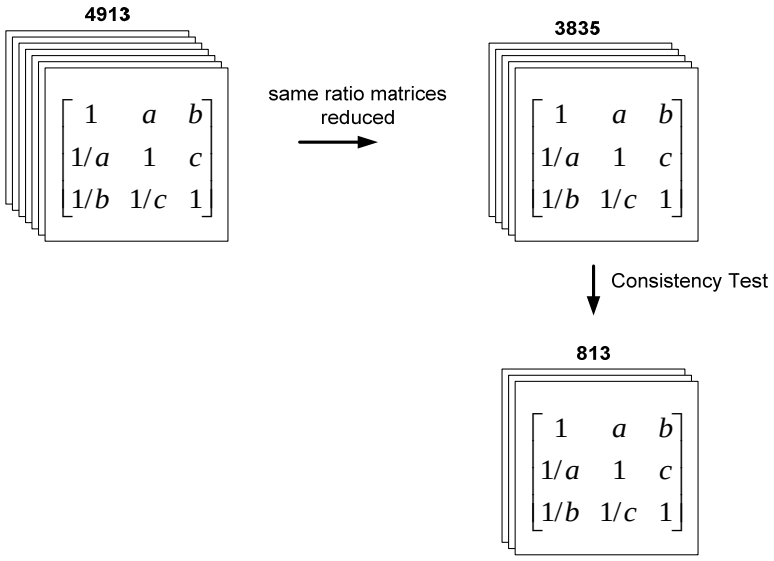

Figure 6.2 The reduction of relative importance matrix candidates.

Finally, the consistency investigation cuts the number of matrix to 813. Figure 6.2 displays the matrix reduction process.

Subsequently, Equation (6.11) is evaluated for the *RM* that satisfies driving modes under traffic situations are evaluated according to the objectives. Therefore, the optimal function is selected by taking the *RM* that creates the maximum value in the multiplication of (6.11). However, the driving mode cannot be always implemented due to the safety issue. If all available functions are above the safety threshold, i.e. $S_{LCM\_L} > 0.5$, $S_{ACC} > 0.5$, and $S_{LCM\_R} > 0.5$, the driving mode can be used. However, the safety condition is not hold, the algorithm takes the safety mode, which is the careful mode. Figure 6.3 displays the adaptive AHP structure. In the structure, *RM* is not a fixed matrix but a flexible variable that can be changed with respect to the traffic situation and driving mode.

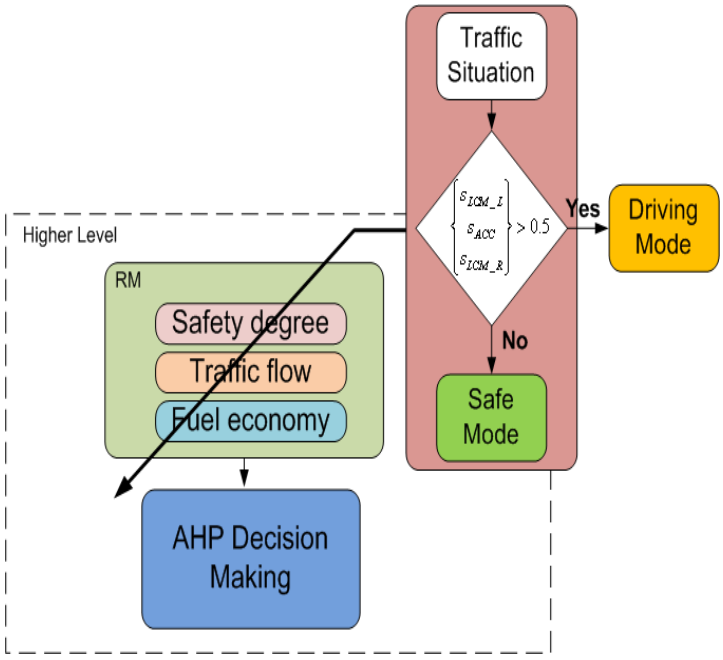

Figure 6.3 An adaptive AHP structure.

6.3 Measurement of Traffic Environment

In order to make an optimal decision for an autonomous vehicle via AHP, the degree of safety of a given action, the traffic flow, and fuel economy are considered; the safety and fuel economy are implemented via a fuzzy logic based method that determines a safer and cheaper function in a given traffic situation. And the traffic flows are defined as f_L, f_F, and f_R representing the traffic flow for left lane, driving lane, and right lane, respectively. The traffic flows of each lane are obtained from the average velocity of each lane. It is assumed that the data measured by LIDAR (**Li**ght **D**etection **A**nd **R**anging). Figure 6.4 displays the traffic situation that the subject vehicle (centered in the figure) encounters. The ellipse represents the sensing range provided by radar measurement systems that is assumed installed on the vehicle. It is further assumed that the sensing data is accurate;

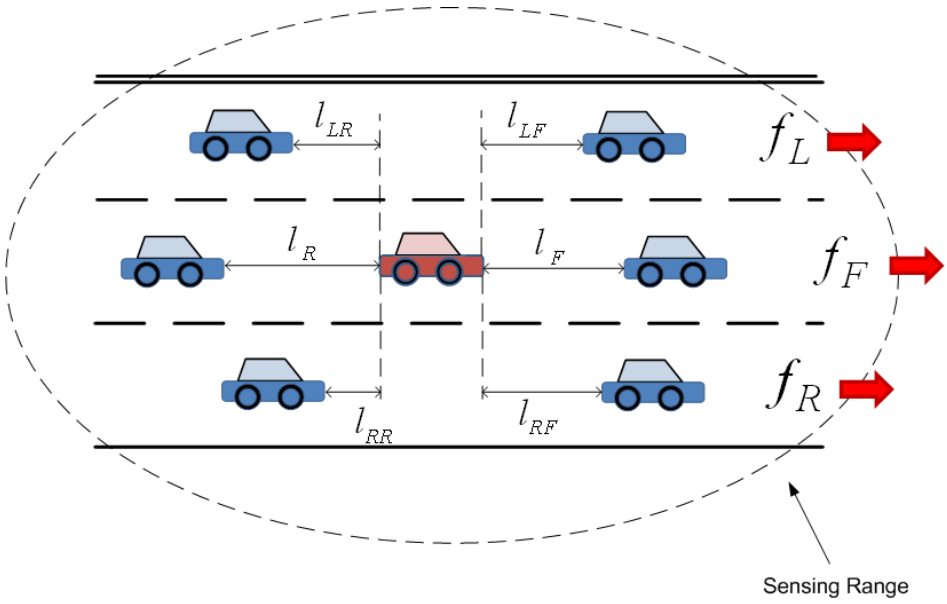

Figure 6.4 Traffic situation of an autonomous vehicle.

l_{LR} , l_{LF} , l_R , l_F , l_{RR} , and l_{RF} represent length from the autonomous car's rear/front sensors to the left rear, left front, rear, front, right rear, and right front, respectively. (Consideration of errors in these measurements is the subject of an upcoming article by the authors[57].)

In this research, two autonomous vehicle functions, LCM and ACC, are considered. In normal highway driving environment, it is assumed that the vehicle is driven via ACC. By monitoring the surrounding traffic situation, the subject vehicle makes a decision among LCM_L, LCM_R, and ACC. Fuzzy logic is used to assess the traffic conditions surrounding the subject vehicle such as safety of each function and fuel economy of each function by taking the corresponding lane.

6.4 Alternative Evaluation

In order to implement (adaptive) AHP, all the possible alternatives need to be evaluated with respect to the objective. In this subsection, the alternative evaluation methods are discussed.

6.4.1 Safety Degree of Lane Change

The safe distance varies according to the vehicle velocity in conjunction with the so called three-second rule for safe distance following policy [73]. To measure the safety degree of the lane change maneuver, the gap between the vehicles (g_i), the ratio between the rear and the front gaps ($\bar{g}_i$), and the gap rate ($\dot{g}_i$) are considered. These quantities are defined as follows:

$$g_i = l_{iR} + l_{iF} + l_{veh} \tag{6.12}$$

$$\bar{g}_i = \frac{\min(l_{iR}, \quad l_{iF})}{\max(l_{iR}, \quad l_{iF})} \tag{6.13}$$

$$\dot{g}_i = v_{iF} - v_{iR}, \tag{6.14}$$

where l_{veh} is the length of controlled vehicle and $i = L, R$. Further, v_{iF} and v_{iR} represent the velocity of the front and rear vehicles in each of the two adjacent lanes.

If the subject vehicle is located too close to its rear or front vehicles in lateral view point, lane change safety cannot be guaranteed even though g_i is large. The gap ratio captures this sense of where the subject vehicle located. The gap rate notifies that two vehicles in next lane are approaching or not. During lane change, the notion of safe distance must vary with the velocity of the subject vehicle, i.e. the faster the velocity of the vehicle, the larger the safe distance required to secure a lane change:

Table 6.3 LCM fuzzy rules.

	Antecedents			Consequent
	g_i	$\bar{g}_i$	$\dot{g}_i$	$s_{\deg}$
Rule 1	Very Short	Near	Extremely Negative	Very Unsafe
Rule 2	Very Short	Near	Negative	Very Unsafe
⋮	⋮	⋮	⋮	⋮
Rule 75	Very Long	Far	Extremely Positive	Very Safe

This is reflected in the definition of the membership functions associated with the gap variable, g_i, in the rule set used to characterize the condition for safe lane change. In this rule set the linguistic variables in the antecedent clause are g_i, $\overline{g}_i$, and $\dot{g}_i$ and while the consequent of each rule states the degree of safety, $s_{\deg}$, of the traffic situation from a lane change perspective. The structure of each rule is given by

$$\textit{If } g_i \textit{ is ( ) and } \overline{g}_i \textit{ is ( ), and } \dot{g}_i \textit{ is ( ), then } s_{\deg} \textit{ is ( ),}$$

which are implemented as a Mamdani fuzzy model, i.e. the truth condition of each rule is the minimum of the truth value of each of the three antecedent conditions. Table 6.3 shows the specific rules developed for LCM safety evaluation and total list of the rules are provided in the Appendix A. The gap g_i has five members such as ‘Very Short’, ‘Short’, ‘Medium’, ‘Long’, and ‘Very Long’. And in the ratio $\overline{g}_i$ has ‘Near’, ‘Medium’, and ‘Far’. $\dot{g}_i$ has ‘Extremely Negative’, ‘Negative’, ‘Medium’, ‘Positive’, and ‘Extremely Positive’. While the safety membership function includes ‘Very Unsafe’, ‘Unsafe’, ‘Medium’, ‘Safe’, and ‘Very Safe’. Figures 6.5 and 6.6 show the membership functions that are applied described above and fuzzy rule surface from fuzzy rules.

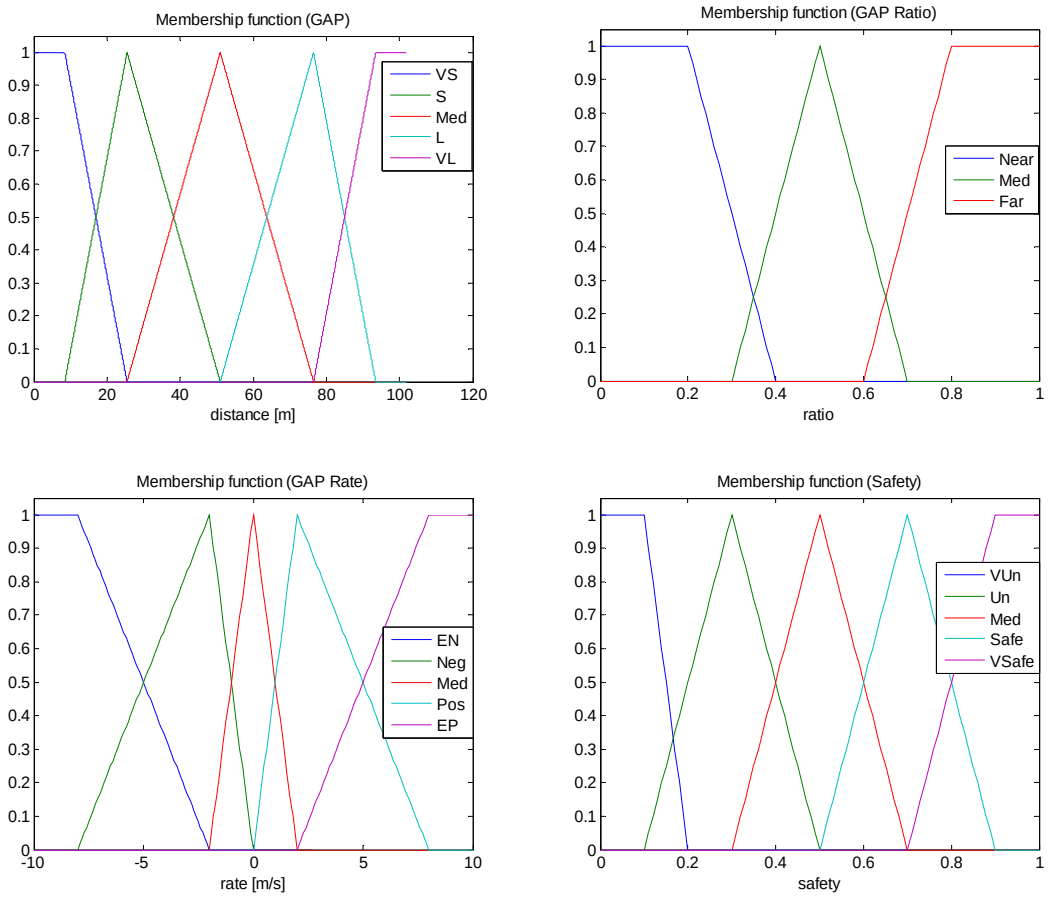

Figure 6.5 Membership functions to get LCM safety degree.

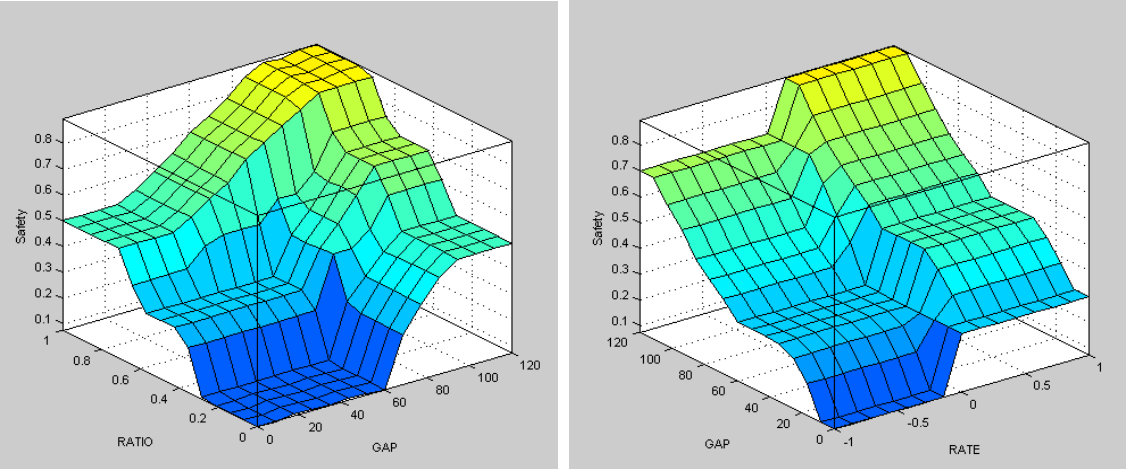

Figure 6.6 Surface of LCM fuzzy rules.

6.4.2 Safety Degree of Adaptive Cruise Control

The degree safety of using ACC is evaluated in this subsection. In this evaluation process, only three vehicles in the same lane are considered. It is further defined the front and rear gaps between the subject vehicle and its front and rear vehicles as follows:

$$g_F = l_F \tag{6.15}$$

$$g_R = l_R . \tag{6.16}$$

The gap rate

$$\dot{g} = -\frac{(v_F - v_R)}{\max(v_F, v_R)}, \tag{6.17}$$

where v_F and v_R represent the velocity of the front and rear vehicle of subject vehicle. To calculate the gap rate, deviation from the maximum velocity is evaluated. And the negative sign in equation (6.17) represents that the positive sign of gap rate has negative effect on safety degree. It is considered that the distance from the front and rear vehicles

and the velocity change of the two vehicles in determining the safety of the ACC maneuver. To this end, 125 fuzzy rules are developed with the linguistic structure of

$$If\ g_F\ is\ (\ )\ and\ g_R\ is\ (\ )\ and\ \dot{g}\ \ is\ (\ ),\ then\ s_{\deg}\ \ is\ (\ ).$$

Table 6.4 lists the sequence of rules for ACC safety evaluation and the full rules are

Table 6.4 ACC fuzzy rules.

	Antecedents			Consequent
	g_F	g_R	$\dot{g}$	$s_{\deg}$
Rule 1	Very Short	Very Short	Extremely Negative	Medium
Rule 2	Very Short	Short	Negative	Safe
Rule 3	Very Short	Medium	Zero	
⋮	⋮	⋮	⋮	⋮
Rule 125	Very Long	Very Long	Extremely Positive	Safe

provided in the Appendix B while Figures 6.7 and 6.8 depicts the membership functions of each antecedent and consequence component and the fuzzy rule surface obtained from fuzzy rules.

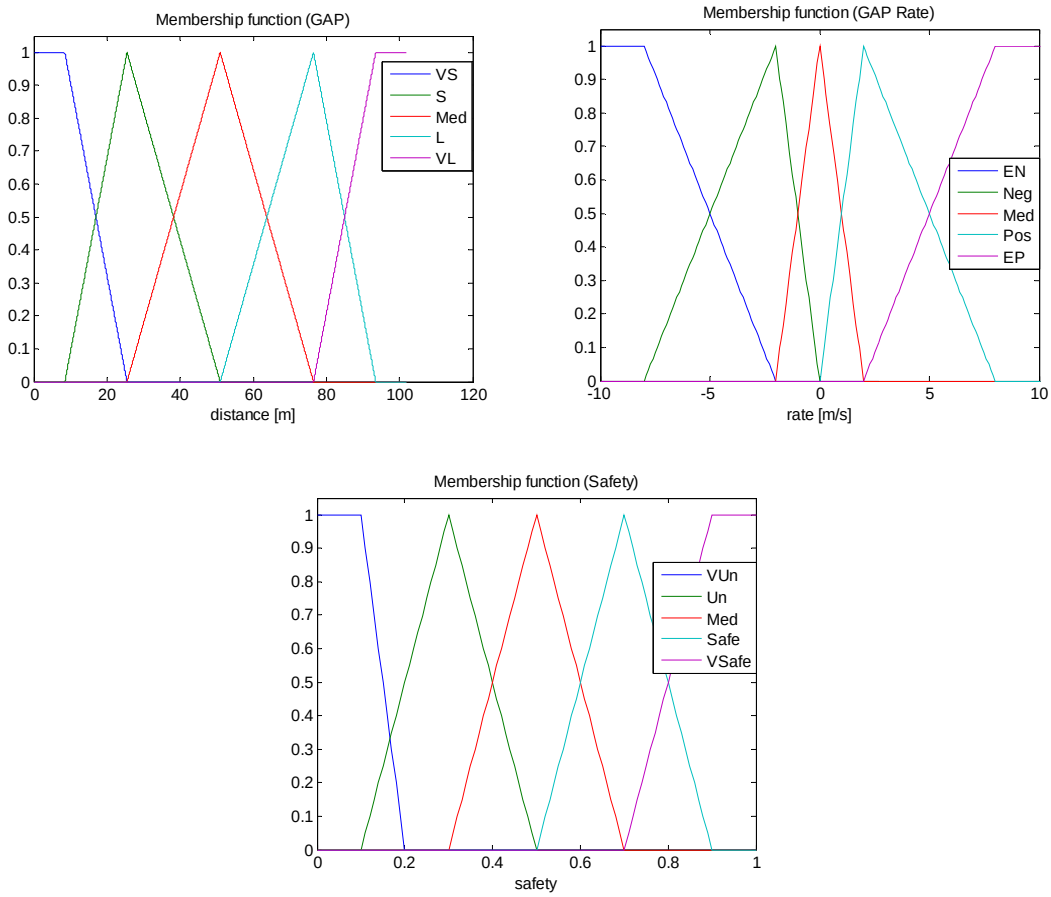

Figure 6.7 Membership functions to get ACC safety degree.

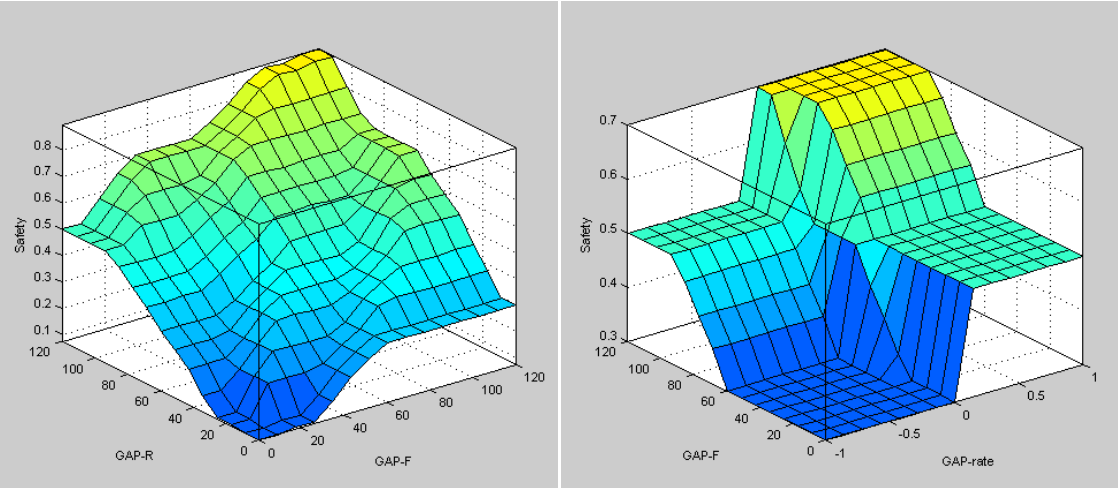

Figure 6.8 Surface of ACC fuzzy rules.

6.4.3 Energy (Fuel) Consumption of Each Lane

In this subsection, the fuel consumption is taken into account as the third objective. In order to adjust the subjective vehicle's velocity to each lane such as left, right, and driving lane, different amount of energy is consumed. However, to hold the consistency about each objective, all the objectives have larger grade for better choice. Therefore, the fuel economy of each lane is calculated by fuzzy logic and fuzzy rules reflect the consistency point of view. By taking the velocity differences between the controlling vehicle and the traffic flow of each lane, the energy consumption is expected. As the velocity difference is larger the vehicle has to be accelerated or decelerated more, i.e. it is assumed that braking energy is 10% higher than accelerating energy in highway driving [74]. If the velocity of the subjective vehicle is higher than comparing lane then braking energy is applied by having 10% more fuel than accelerating situation when the

velocity is lower than the comparing lane. 3 rules are developed to relate the velocity difference and fuel efficiency. Table 6.5 shows the fuzzy rules and membership functions and fuzzy surface are displayed in Figures 6.9 and 6.10, respectively.

Table 6.5 Energy efficiency fuzzy rules (3 rules).

	Antecedents	Consequent
	v_{diff}	F_{eff}
Rule 1	Small	Large
Rule 2	Medium	Medium
Rule 3	Large	Small

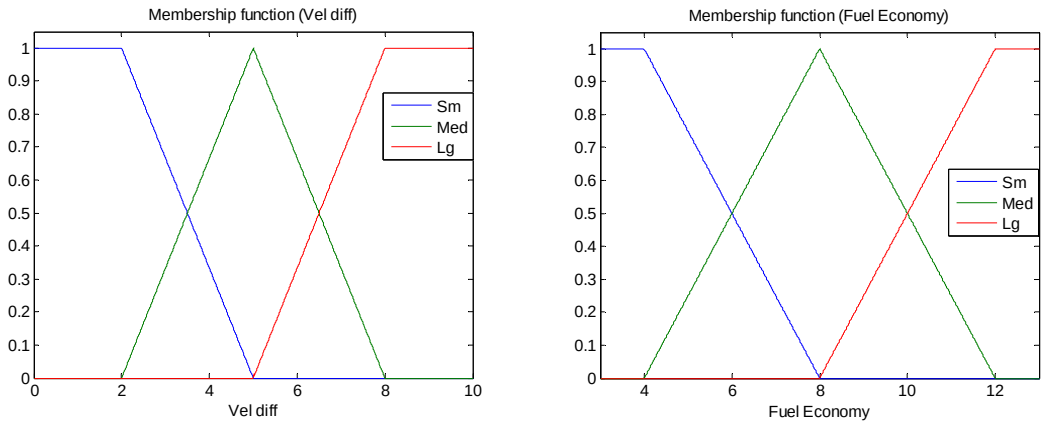

Figure 6.9 Membership functions to get fuel economy degree.

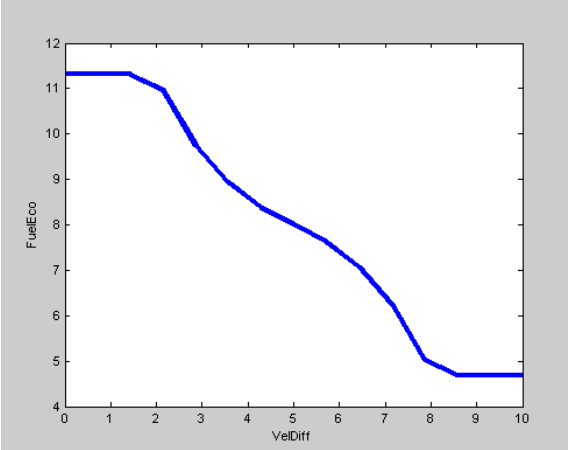

Figure 6.10 Surface of fuel economy fuzzy rules.

6.5 Adaptive AHP Based Decision Making

An adaptive AHP based decision making simulation results are presented. In the simulations, seven vehicles, the autonomous vehicle and surrounding six vehicles, are considered. At first, it is assumed that the vehicle is located in the center lane. Therefore, there are three functions are available such as LCM_L, ACC, and LCM_R. The position of each vehicle is determined as Figure 6.11. From the top right to bottom left, 151.1, 53.3, 151.1, 26.2, 160, and 71.1, respectively in meter scale. The red rectangular represents the autonomous vehicle and the others are surrounding vehicles. The number within the parenthesis represents the velocity of each vehicle when the traffic flows from the left hand side to right hand side. It is assumed that the suggested adaptive AHP makes decision under the given situation.

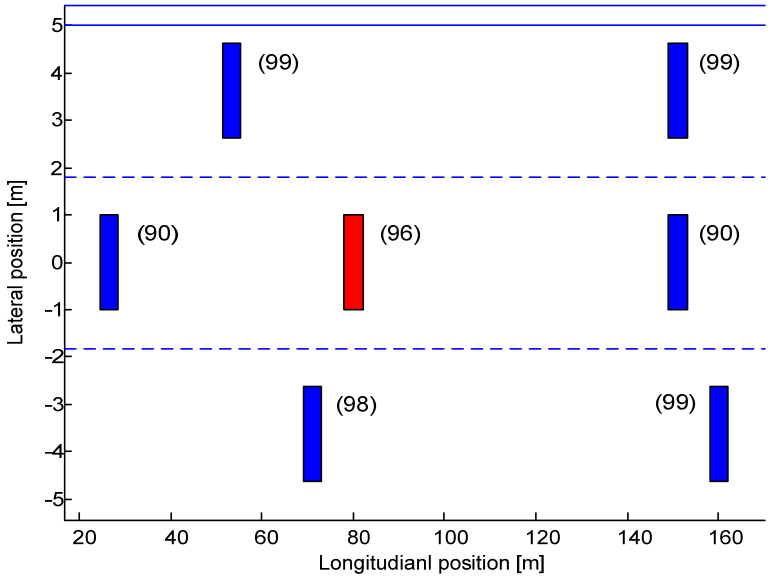

Figure 6.11 Vehicle position and velocity at decision making.

The adaptive AHP makes decision under driving mode, it can be set with three different options. Table 6.6 show the decision made by adaptive AHP. When aggressive and careful driving mode is selected, lane change to the left lane is chosen as the optimal function. However, by selecting fuel economy mode, Adaptive cruise control is suggested as the optimal function. It is obvious that aggressive mode takes the function

Table 6.6 AAHP decision making (center lane).

Driving mode	Decision
Aggressive Mode	LCM_L
Careful Mode	LCM_L
Fuel Economy Mode	ACC

that shifting the vehicle position to the fastest lane; careful mode takes the function that moves the vehicle position to the safest lane; and fuel economy mode takes the function that uses least fuel. After the decision is made, the autonomous vehicle takes different action with respect to the decision. In the simulations, there are four steps in accomplishing the lane changing.

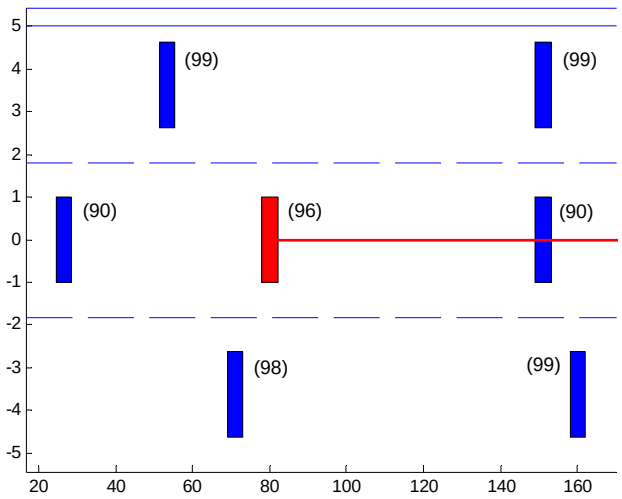

(a) Decision making

Figure 6.12 Adaptive cruise control process (center lane).

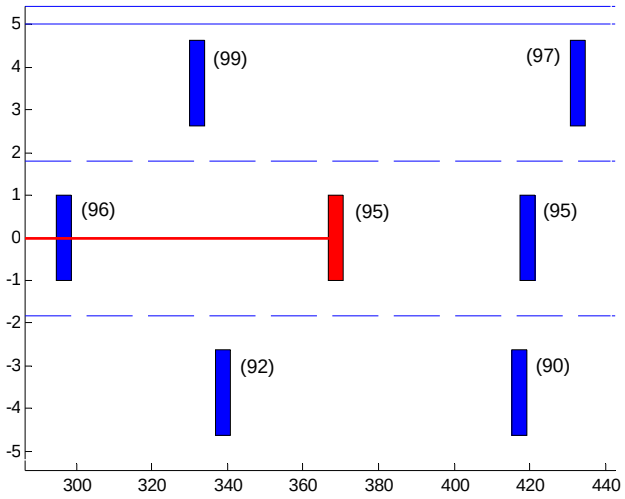

(b) ACC

Figure 6.12 Continued.

When the decision is ACC by choosing fuel economy mode in the vehicle environmental settings Figure 6.12 (a), the autonomous vehicle keeps the function ACC. Figure 6.12 (b) staying at the same lane until the next decision is made. However, LCM_L decision is made from the higher level, the first step of lane change is the velocity adjusting by using ACC. The autonomous vehicle adjusts the velocity to the left front vehicle, Figure 6.13 (b). After the velocity is matched to new targeting vehicle, it changes the lateral position by the steering angle input (LCM), Figure 6.13 (c). When the vehicle finished the lane change, ACC function is activated until next decision is made as shown in Figure 6.13 (d).

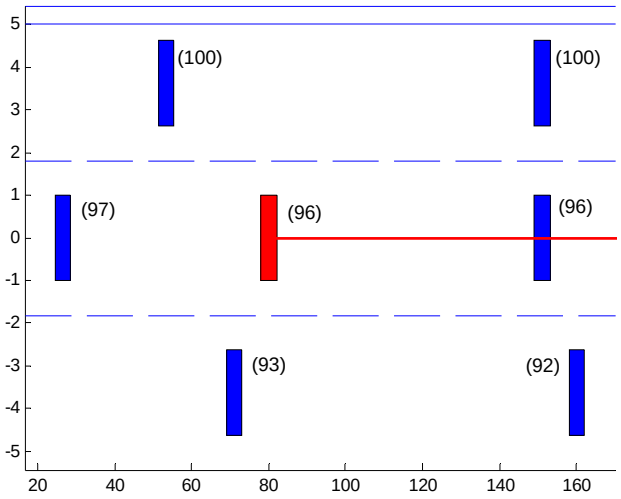

(a) Decision making

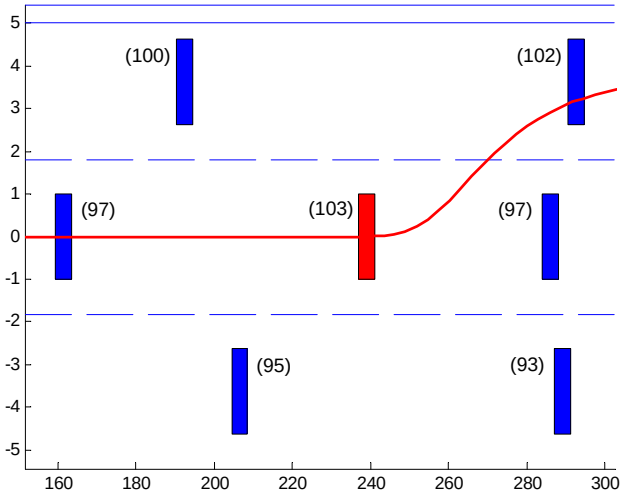

(b) Velocity adjusting

Figure 6.13 Lane change to the left process.

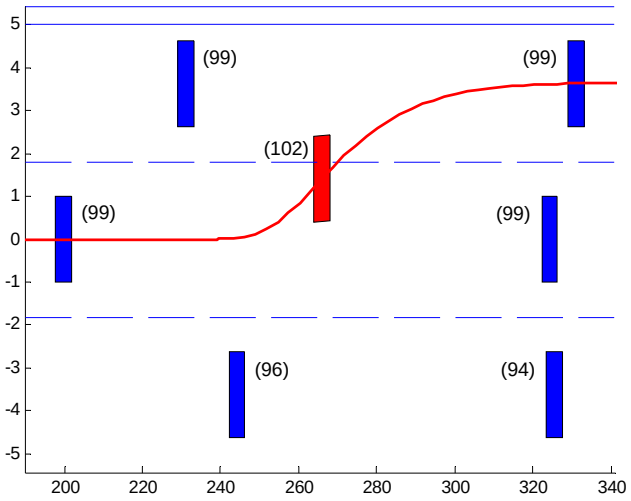

(c) Lane changing

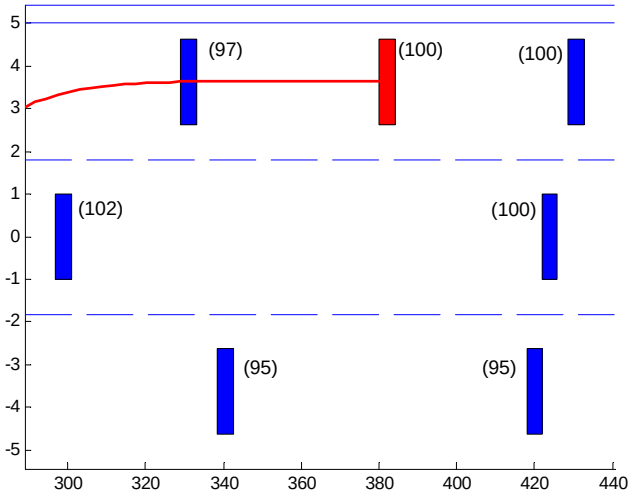

(d) Adaptive cruise control

Figure 6.13 Continued.

Figures 6.14 and 6.15 show the decision making result when the vehicle is located at the 1st lane. By locating at the 1st lane the autonomous vehicle has only two available functions, i.e. ACC and LCM_R. Therefore, in AHP structure there are two

alternatives while three objectives considering. According to the driving mode, the adaptive AHP decides different function.

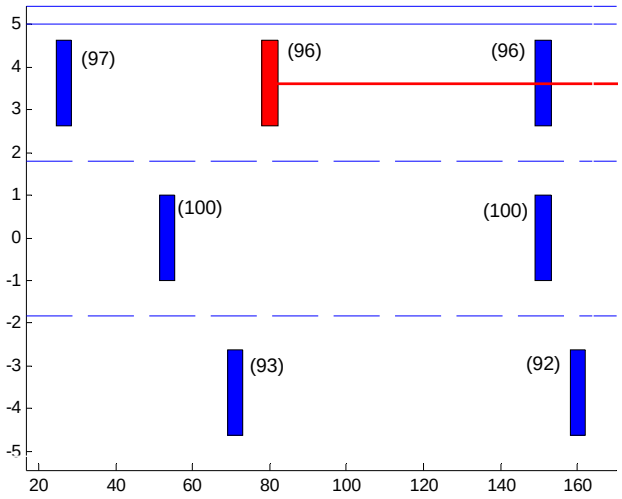

(a) Decision making

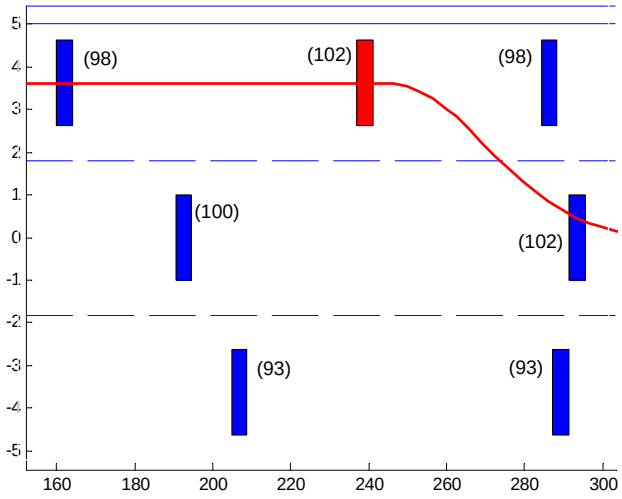

(b) Velocity adjusting

Figure 6.14 Lane change to the right process.

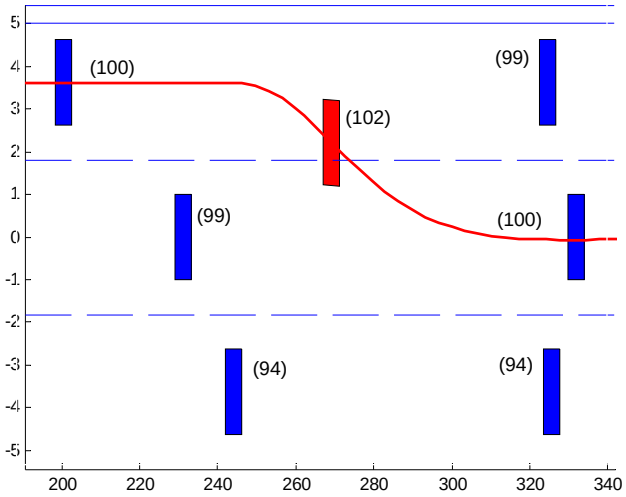

(c) Lane changing

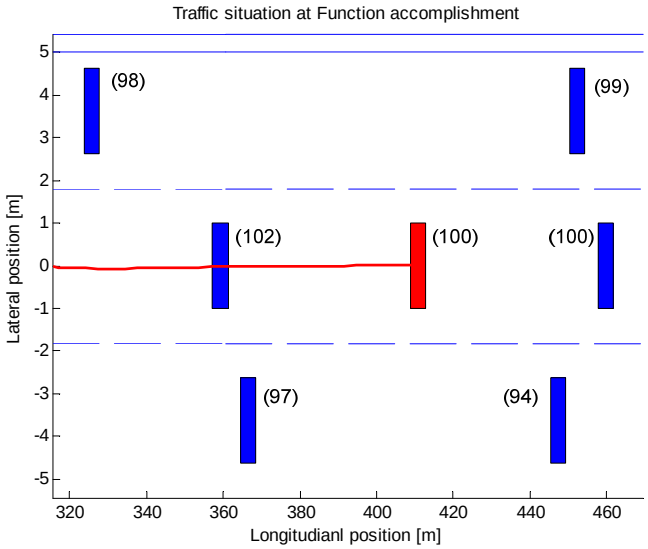

(d) Adaptive cruise control

Figure 6.14 Continued.

Table 6.7 AAHP decision making (left lane).

Driving mode	Decision
Aggressive Mode	LCM_R
Careful Mode	ACC
Fuel Economy Mode	ACC

Aggressive mode selects LCM_R while the other driving modes choose ACC as shown in Table 6.7. The lane change step is very similar to the lane change decision when the vehicle is located at the center lane. After the decision is made in Figure 6.14 (a), the autonomous vehicle set the right front vehicle as a new target while following up the velocity, Figure 6.14(b). Lane change is performed subsequently when the velocity is enough to cut into the center lane (2^{nd} lane). Again ACC is followed the LCM_R until the next decision making. Careful mode and fuel economy mode decide to follow the preceding vehicle without lane change therefore the autonomous vehicle keep the function, adaptive cruise control.

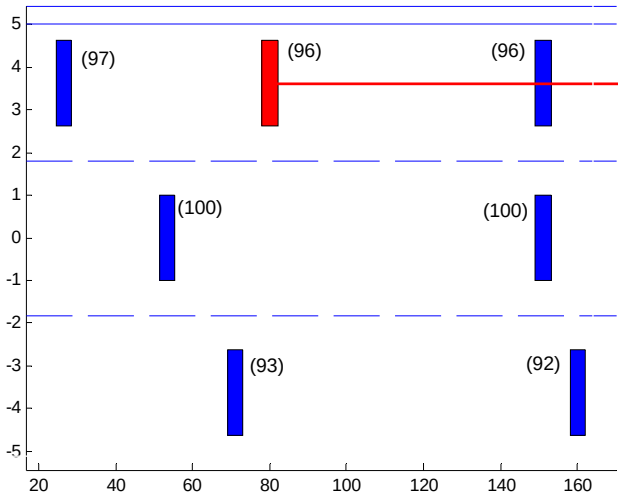

(a) Lane changing

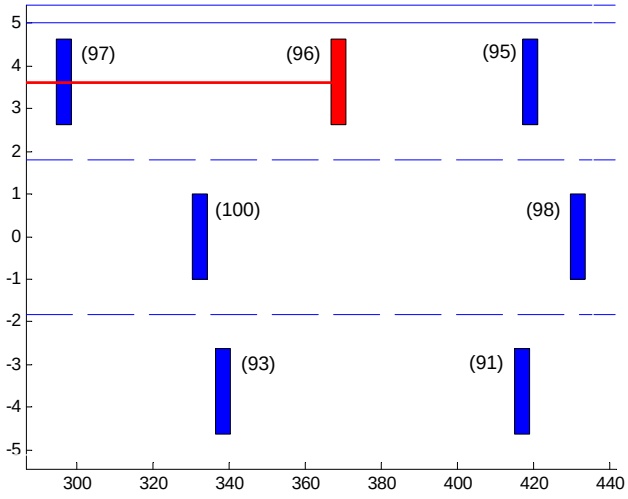

(b) Adaptive cruise control

Figure 6.15 Adaptive cruise control process (left lane).

6.6 Summary

In this Section, a multi objective decision making method Analytic Hierarchy Process (AHP) is explained and the application of AHP to an autonomous vehicle decision making process is provided. After the hierarchy is formalized, relative importance matrix generating method is explained.

To cope with the real traffic situation, an adaptive AHP algorithm that selects a relative importance matrix satisfying the driving modes and AHP optimality is suggested. The simulation results demonstrate that the adaptive AHP decides an optimal function with respect to the driving mode and traffic situation that an autonomous vehicle encounters.

7. CONCLUSIONS AND FUTURE WORK

7.1 Conclusions

In this research, control and management strategy of autonomous vehicle is studied. The lower level control functions are developed by Brain Limbic System based control and the higher level decision making structure is implemented by Analytic Hierarchy Process.

In the Section 2, the structure of Brain Limbic System is explained by providing the functions of each component. The emotional learning mechanism is studied as an adaptive controller.

Subsequently, BLS based control method is applied to develop autonomous vehicle functions such as lane change maneuver and adaptive cruise control. First of all, LCM function is implemented by BLS control scheme. The performance of BLS based LCM is compared with human driver model. The simulation results demonstrate that BLS based control LCM has better performance with and without disturbance.

Adaptive cruise control function also developed by means of the same control method and the performance is compared with PD like control and fuzzy logic control. The BLS based ACC is simulated on various traffic situations. From the simulation results, it is observed that the BLS based control shows better inter-vehicle distance tracking performance. While in terms of velocity tracking, fuzzy logic method has best performance among them. However, from the performance measure for each simulation,

the results demonstrate effective performance of the BLS based control approach for an autonomous vehicle.

The stability of BLS based control is analyzed via Cell-to-Cell Mapping method. Cell-to-Cell Mapping is a global dynamics system analyzing tool. This method successfully analyzed BLS based control system that hardly investigated by Lyapunov method. By analyzing cell map, it is concluded that BLS based LCM is stable under normal driving conditions for lateral motion and angular motion. Subsequently, the stability of HDM based LCM is investigated and it is observed that BLS based control has more stable margin having more stable initial condition under the same region of interests.

After BLS based control and its stability is considered, AHP method is applied to make decision under rapidly changing traffic situations. The procedure of AHP developing in an autonomous vehicle is explained. By the demand of operating real traffic situation that cannot expectable, adaptive AHP algorithm is suggested. The simulation results show the decision that is made by adaptive AHP considering driving mode.

7.2 Future Work

This research mainly focused on autonomous vehicle. From this research, the application of BLS control method and control function managing strategy is studied. First of all, another autonomous vehicle functions can be developed by the same

controller. And the function management under more complex situation will be considered.

Also, in the following researches, the systematic method to design a BLS controller will be studied. And energy based system will be targeted to apply the same controller and by means of (adaptive) AHP, the optimal operating method of a multi control functioned system will be studied.

REFERENCES

[1] C. Mathers, T. Boerma, and D. M. Fat, *The Global Burden of Disease: 2004 Update*. Geneva, Switzerland: World Health Organization, 2008.

[2] N. A. Stanton and P. M. Salmon, "Human error taxonomies applied to driving: A generic driver error taxonomy and its implications for intelligent transport systems," *Safety Science*, vol. 47, pp. 227-237, Feb 2009.

[3] T. D. Peterson, J. B. Tilman, J. W. Runge, and R. C. Hunt, "Motor vehicle safety: Current concepts and challenges for the emergency physician," *Annals of Emergency Medicine*, vol. 34, pp. 384-393, Dec 1999.

[4] K. Lee and H. Peng, "Evaluation of automotive forward collision warning and collision avoidance algorithms," *Vehicle System Dynamics*, vol. 43, pp. 735-751, Oct 2005.

[5] H. S. Tan and J. Huang, "DGPS-based vehicle-to-vehicle cooperative collision warning: Engineering feasibility viewpoints," *IEEE Transactions on Intelligent Transportation Systems*, vol. 7, pp. 415-428, Dec 2006.

[6] J. Lu, D. Messih, A. Salib, and D. Harmison, "An enhancement to an electronic stability control system to include a rollover control function," *Society of Automotive Engineers Transactions*, vol. 116, pp. 303-313, 2007.

[7] J. J. Martinez and C. Canudas-De-Wit, "A safe longitudinal control for adaptive cruise control and stop-and-go scenarios," *IEEE Transactions on Control Systems Technology*, vol. 15, pp. 246-258, Mar 2007.

[8] D. Hong, I. Hwang, K. Huh, "Development of a vehicle stability control system using brake-by-wire actuators," *Journal of Dynamic Systems Measurement and Control-Transactions of the ASME*, vol. 130, 011008 (9 pages), Jan 2008.

[9] R. Bishop, "Intelligent vehicles: A global perspective," *National Institute of Standards and Technology*, Gaithersburg, MD, 2009.

[10] O. H. Mowrer, *Learning Theory and Behavior*, New York:Wiley, 1960.

[11] E. T. Rolls, “A theory of emotion, and its application to understanding the neural basis of emotion,” in Emotions: Neural and Chemical Control, Y. Oomura, Ed., Tokyo: Japan Scientific Societies Press, 1986, pp. 325-344.

[12] J. E. LeDoux, “In search of an emotional system in the brain: leaping from fear to emotion and consciousness,” in The Cognitive Neurosciences, M. S. Gazzaniga, Ed., Cambridge, MA: MIT Press, 1995, pp. 1049-1061.

[13] E. T. Rolls, “A theory of emotion and consciousness, and its application to understanding the neural basis of emotion,” in The Cognitive Neurosciences, M. S. Gazzaniga, Ed., Cambridge, MA: MIT Press, 1995, pp. 1091-1106.

[14] J. Moren and C. Balkenius, “A computational model of emotional learning in the amygdale,” in Animals to Animats 6: Proceedings of the 6th International Conference on the Simulation of Adaptive Behaviour, J. A. Meyer, A. Berthoz, D. Floreano, H.L. Roitblat, and S.W. Wilson, Ed.. MA: MIT Press, 2000, pp. 383–391.

[15] J. Moren, “Emotion and learning - A computational model of the amygdale,” Ph.D. dissertation, Cognitive Science, Lund University, Sweden, 2002.

[16] C. Lucas, D. Shahmirzadi, and N. S.Aleslami, "Introducing BELBIC: Brain emotional learning based intelligent controller," *Intelligent Automation and Soft Computing*, vol. 10, pp. 11-21, 2004.

[17] A. R. Mehrabian and C. Lucas, "Emotional learning based intelligent robust adaptive controller for stable uncertain nonlinear systems," *International Journal of Computational Intelligence*, vol. 2, pp. 246-252, 2005.

[18] M. Chandra and R. Langari, "Analytical study of a control algorithm based on emotional processing," in *Proceedings of American Control Conference*, Minneapolis, MN, 2006, pp. 3433-3438.

[19] D. Shahmirzadi, R. Langari, L. J. Ricalde, and E. N. Sanchez, "Intelligent vs. sliding mode control in rollover prevention of tractor-semitrailers," *International Journal of Vehicle Autonomous Systems*, vol. 4, pp. 68-87, 2006.

[20] C. Lucas, R. M. Milasi, and B. N. Araabi, "Intelligent modeling and control of washing machine using locally linear neuro-fuzzy (LLNF) modeling and modified brain emotional learning based intelligent controller (BELBIC)," *Asian Journal of Control*, vol. 8, pp. 393-400, Dec 2006.

[21] N. Sheikholeslami, D. Shahmirzadi, E. Semsarc, C. Lucas, and M. J. Yazdanpanah, "Applying brain emotional learning algorithm for multivariable control of HVAC systems," *Journal of Intelligent & Fuzzy Systems*, vol. 17, pp. 35-46, 2006.

[22] A. R. Mehrabian, C. Lucas, and J. Roshanian, "Aerospace launch vehicle control: An intelligent adaptive approach," *Aerospace Science and Technology*, vol. 10, pp. 149-155, Mar 2006.

[23] H. Rouhani, M. Jalili, B. N. Araabi, W. Eppler, and C. Lucas, "Brain emotional learning based intelligent controller applied to neurofuzzy model of micro-heat exchanger," *Expert Systems with Applications*, vol. 32, pp. 911-918, Apr 2007.

[24] S. Jafarzadeh, R. Mirheidari, M. R. J. Motlagh, and M. Barkhordari, "Designing PID and BELBIC controllers in path tracking problem," *International Journal of Computers Communications & Control*, vol. 3, pp. 343-348, 2008.

[25] C. Kim and R. Langari, "Target tracking control of a mobile robot using a brain limbic system based control strategy," in *Proceedings of IEEE/RSJ International*

Conference on Intelligent Robots and Systems, St. Louis, MO, 2009, pp. 5059-5064.

[26] M. R. Jamali, M. Dehyadegari, A. Arami, C. Lucas, and Z. Navabi, "Real-time embedded emotional controller," *Neural Computing & Applications*, vol. 19, pp. 13-19, February 2010.

[27] Y. Kim, C. Kim, and R. Langari, "Novel bio-inspired smart control for hazard mitigation of civil structures," *Smart Materials and Structures*, vol. 19, no. 11, 115009, 2010.

[28] J. K. Hedrick, M. Tomizuka, and P. Varaiya, "Control issues in automated highway systems," *IEEE Control Systems Magazine*, vol. 14, pp. 21-32, Dec 1994.

[29] W. Chee and M. Tomizuka, "Vehicle lane change maneuver in automated highway systems," California Partners for Advanced Transit and Highways, Berkery, CA, UCB-ITS-PRR-94-22, October 1994

[30] H. S. Tan, J. Guldner, C. Chen, S. Patwardhan, and B. Bougler, "Lane changing with look-down reference systems on automated highways," *Control Engineering Practice*, vol. 8, pp. 1033-1043, Sep 2000.

[31] C. Hatipoglu, U. Ozguner, and K. A. Redmill, "Automated lane change controller design," *IEEE Transactions on Intelligent Transportation Systems*, vol. 4, pp. 13-22, Mar 2003.

[32] J. Feng, J. Ruan, and Y. Li, "Study on intelligent vehicle lane change path planning and control simulation," in *Proceedings of IEEE International Conference on Information Acquisition*, Weihai, China, 2006, pp. 683-688.

[33] S. S. You, H. S. Choi, H. S. Kim, and T. W. Lim, "Active steering for intelligent vehicles using advanced control synthesis," *International Journal of Vehicle Design*, vol. 42, pp. 244-262, 2006.

[34] J. E. Naranjo, C. Gonzalez, R. Garcia, and T. de Pedro, "Lane-change fuzzy control in autonomous vehicles for the overtaking maneuver," *IEEE Transactions on Intelligent Transportation Systems*, vol. 9, pp. 438-450, Sep 2008.

[35] M. Abe, *Vehicle Handling Dynamics: Theory and Application*, 1st ed. Amsterdam; Boston: Butterworth-Heinemann, 2009.

[36] D. Swaroop and R. Huandra, "Intelligent cruise control system design based on a traffic flow specification," California Partners for Advanced Transit and Highways, Berkery, CA, UCB-ITS-PRR-99-5, 1999.

[37] L. Vlacic, M. Parent, and F. Harashima, *Intelligent Vehicle Technologies: Theory and Applications*. Warrendale, PA: SAE International, 2001.

[38] K. Santhanakrishnan and R. Rajamani, "On spacing policies for highway vehicle automation," *IEEE Transactions on Intelligent Transportation Systems*, vol. 4, pp. 198-204, Dec 2003.

[39] P. A. Ioannou and C. C. Chien, "Autonomous intelligent cruise control," *IEEE Transactions on Vehicular Technology*, vol. 42, pp. 657-672, Nov 1993.

[40] C. Y. Liang and H. Peng, "Optimal adaptive cruise control with guaranteed string stability," *Vehicle System Dynamics*, vol. 32, pp. 313-330, Nov 1999.

[41] D. Swaroop and J. K. Hedrick, "Constant spacing strategies for platooning in automated highway systems," *Journal of Dynamic Systems Measurement and Control-Transactions of the ASME*, vol. 121, pp. 462-470, Sep 1999.

[42] V. L. Bageshwar, W. L. Garrard, and R. Rajamani, "Model predictive control of transitional maneuvers for adaptive cruise control vehicles," *IEEE Transactions on Vehicular Technology*, vol. 53, pp. 1573-1585, Sep 2004.

[43] A. Ferrara and C. Vecchio, "Second order sliding mode control of vehicles with distributed collision avoidance capabilities," *Mechatronics*, vol. 19, pp. 471-477, Jun 2009.

[44] C. C. Tsai, S. M. Hsieh, and C. T. Chen, “Fuzzy longitudinal controller design and experimentation for adaptive cruise control and Stop&Go,” *Journal of Intelligent Robot System*, vol. 59, pp. 167-189, 2010.

[45] T. L. Saaty, *The Analytic Hierarchy Process*. New York: McGraw Hill, 1980.

[46] T. L. Saaty, *Decision Making for Leaders: The Analytical Hierarchy Process for Decisions in a Complex World*. Belmont, CA: Lifetime Learning Publications, 1982.

[47] T. D. Gillespie, *Fundamentals of Vehicle Dynamics*. Warrendale, PA: Society of Automotive Engineers, 1992.

[48] G. Genta, *Motor Vehicle Dynamics: Modeling and Simulation*., Singapore: World Scientific Publishing, 1997.

[49] R. Rajamani, *Vehicle Dynamics and Control*. New York: Springer Verlag, 2005.

[50] C. J. Taylor, J. Košecká, R. Blasi, and J. Malik, "A comparative study of vision-based lateral control strategies for autonomous highway driving," *International Journal of Robotics Research*, vol. 18, pp. 442-453, May 1999.

[51] J. P. Switkes, E. J. Rossetter, I. A. Coe, and J. C. Gerdes, "Handwheel force feedback for lanekeeping assistance: Combined dynamics and stability," *Journal of Dynamic Systems Measurement and Control-Transactions of the ASME*, vol. 128, pp. 532-542, Sep 2006.

[52] A. Broggi, M. Bertozzi, A. Fascioli, G. L. Bianco, and A. Piazzi, "Visual perception of obstacles and vehicles for platooning," *IEEE Transactions on Intelligent Transportation Systems*, vol. 1, no.3, pp. 164-176, 2000.

[53] J. R. Ragazzini, “Engineering aspects of the human being as a servo mechanism,” paper read at Amer. Psychol. Assn. Meeting, Boston, Sep. 1948.

[54] M. A. Marek, *Roadway Design Manual*. Austin, TX: Texas Department of Transportation, March, 2009.

[55] W. Sienel, “Estimation of the tire cornering stiffness and its application to active car steering,” in *Proceedings of the 36th Conference on Decision and Control*, San Diego, CA, December 1997, pp. 4744-4748.

[56] A. R. Girard, J. B. de Sousa, J .A. Misener, and J. K. Hedrick, "A control architecture for integrated cooperative cruise control and collision warning systems," in *Proceedings of the 40th IEEE Conference on Decision and Control*, Orlando, FL, 2001, pp. 1491-1496.

[57] R. Sharifi, Y. Kim, and R. Langari, “Sensor fault isolation and detection of smart structures,” *Smart Materials and Structures*, vol. 19, no. 10, 105001, 2010.

[58] P. Fancher and Z. Bareket, "Evaluating headway control using range versus range-rate relationships," *Vehicle System Dynamics*, vol. 23, no.1, pp. 575-596, 1994.

[59] K. Yi and J. Chung, "Nonlinear brake control for vehicle CW/CA systems," *IEEE/ASME Transactions on Mechatronics*, vol. 6, no.1, pp. 17-25, 2001.

[60] D. Shahmirzadi and R. Langari, “Stability of amygdala learning system using Cell-to-Cell Mapping algorithm,” in *Proceeding of the 8th IASTED International Conference on Intelligent system and Control*, Cambridge, MA, 2005, pp. 54-59.

[61] C. Hsu, "A theory of Cell-to-Cell Mapping dynamical systems," *Journal of Applied Mechanics*, vol. 47, pp. 931-939, 1980.

[62] C. Hsu, "A generalized theory of Cell-to-Cell Mapping for nonlinear dynamical systems," *Journal of Applied Mechanics*, vol. 48, pp. 634-642, 1981.

[63] J. A. W. Spek, C. A. L. Hoon, A. Kraker, and D. H. Campen, "Application of cell mapping methods to a discontinuous dynamic system," *Nonlinear Dynamics*, vol. 6, no.1, pp. 87-99, 1994.

[64] J. Levitas, "Global stability analysis of fuzzy controllers using cell mapping methods," *Fuzzy Sets and Systems*, vol. 106, no.1, pp. 85-97, 1999.

[65] G. Patel, and K. Ashenayi, “Power system stability analysis using Cell to Cell Mapping,” in *45th Midwest Symposium on Circuits and Systems*, Tulsa, OK, 2002, pp. 671-674.

[66] S. M. Smith and D. J. Comer, “Automated calibration of a fuzzy logic controller using a cell state space algorithm,” *IEEE Control Systems Magazine*, vol. 11, no.5, pp. 18-28, 1991.

[67] J. T. Spooner, M. Maggiore, R. Ordonez, and K. M. Passino, *Stable Adaptive Control and Estimation for Nonlinear Systems: Neural and Fuzzy Approximator Techniques*. New York: Wiley, 2002.

[68] C. Wang, F. Zhou, and Joris Vergeest, “Multi-objective optimization for the functional configuration design of mobile devices using analytic hierarchy process,” in *Proceedings of the Second International Symposium on Intelligent Information Technology and Security Informatics*, Moscow, Russia, pp. 137– 142, 2009.

[69] C. C. Lin, W. C. Wang, and W. D. Yu, "Improving AHP for construction with an adaptive AHP approach (A3)," *Automation in Construction*, vol. 17, no.2, pp. 180-187, 2008.

[70] T. Saaty, *Multicriteria Decision Making: The Analytic Hierarchy Process: Planning, Priority Setting, Resource Allocation*. Pittsburgh, PA: RWS PUBLICATIONS, 1990.

[71] L. Vargas, "Reciprocal matrices with random coefficients," *Mathematical Modeling*, vol. 3, no.1, pp. 69-81, 1982.

[72] R. Banuelas and J. Antony, "Modified analytic hierarchy process to incorporate uncertainty and managerial aspects," *International Journal of Production Research*, vol. 42, no.18, pp. 3851-3872, 2004.

[73] Maintain a Safe Following Distance (The 3 Second Rule), May, 2010, [Online]. Available: http://www.smartmotorist.com/traffic-and-safety-guideline/maintain-a-safe-following-dista nce-the-3-second-rule.html.

[74] Advanced Technologies & Energy Efficiency, June, 2010, [Online]. Available: http://www.Fueleconom y.gov/ feg/atv.shtml.

APPENDIX A

FUZZY RULES FOR LANE CHANGE MANEUVER

Rule statement: *If* g_i *is ( ) and* $\overline{g}_i$ *is ( ), and* $\dot{g}_i$ *is ( ), then* $s_{\deg}$ *is ( )*

Table A.1 LCM fuzzy rules (75 rules).

	Antecedents			Consequent
	g_i	$\overline{g}_i$	$\dot{g}$	S
1	Very short	Near	Extremely negative	Very unsafe
2	Very short	Near	Negative	Very unsafe
3	Very short	Near	Zero	Very unsafe
4	Very short	Near	Positive	Very unsafe
5	Very short	Near	Extremely positive	Very unsafe
6	Very short	Medium	Extremely negative	Very unsafe
7	Very short	Medium	Negative	Unsafe
8	Very short	Medium	Zero	Unsafe
9	Very short	Medium	Positive	Unsafe
10	Very short	Medium	Extremely positive	Unsafe
11	Very short	Far	Extremely negative	Unsafe
12	Very short	Far	Negative	Medium
13	Very short	Far	Zero	Medium
14	Very short	Far	Positive	Medium
15	Very short	Far	Extremely positive	Medium
16	Short	Near	Extremely negative	Very unsafe
17	Short	Near	Negative	Very unsafe
18	Short	Near	Zero	Very unsafe
19	Short	Near	Positive	Unsafe
20	Short	Near	Extremely positive	Unsafe

21	Short	Medium	Extremely negative	Unsafe
22	Short	Medium	Negative	Unsafe
23	Short	Medium	Zero	Unsafe
24	Short	Medium	Positive	Medium
25	Short	Medium	Extremely positive	Medium
26	Short	Far	Extremely negative	Medium
27	Short	Far	Negative	Medium
28	Short	Far	Zero	Medium
29	Short	Far	Positive	Medium
30	Short	Far	Extremely positive	Safe
31	Medium	Near	Extremely negative	Very unsafe
32	Medium	Near	Negative	Very unsafe
33	Medium	Near	Zero	Very unsafe
34	Medium	Near	Positive	Unsafe
35	Medium	Near	Extremely positive	Unsafe
36	Medium	Medium	Extremely negative	Unsafe
37	Medium	Medium	Negative	Unsafe
38	Medium	Medium	Zero	Unsafe
39	Medium	Medium	Positive	Medium
40	Medium	Medium	Extremely positive	Medium
41	Medium	Far	Extremely negative	Medium
42	Medium	Far	Negative	Safe
43	Medium	Far	Zero	Safe
44	Medium	Far	Positive	Safe
45	Medium	Far	Extremely positive	Safe
46	Long	Near	Extremely negative	Unsafe
47	Long	Near	Negative	Medium
48	Long	Near	Zero	Medium
49	Long	Near	Positive	Medium
50	Long	Near	Extremely positive	Medium
51	Long	Medium	Extremely negative	Medium

52	Long	Medium	Negative	Medium
53	Long	Medium	Zero	Safe
54	Long	Medium	Positive	Safe
55	Long	Medium	Extremely positive	Safe
56	Long	Far	Extremely negative	Safe
57	Long	Far	Negative	Safe
58	Long	Far	Zero	Very safe
59	Long	Far	Positive	Very safe
60	Long	Far	Extremely positive	Very safe
61	Extremely long	Near	Extremely negative	Medium
62	Extremely long	Near	Negative	Medium
63	Extremely long	Near	Zero	Medium
64	Extremely long	Near	Positive	Medium
65	Extremely long	Near	Extremely positive	Safe
66	Extremely long	Medium	Extremely negative	Safe
67	Extremely long	Medium	Negative	Safe
68	Extremely long	Medium	Zero	Safe
69	Extremely long	Medium	Positive	Safe
70	Extremely long	Medium	Extremely positive	Very safe
71	Extremely long	Far	Extremely negative	Very safe
72	Extremely long	Far	Negative	Very safe
73	Extremely long	Far	Zero	Very safe
74	Extremely long	Far	Positive	Very safe
75	Extremely long	Far	Extremely positive	Very safe

APPENDIX B

FUZZY RULES FOR ADAPTIVE CRUISE CONTROL

Rule statement: *If* g_F *is ( ) and* g_R *is ( ) and* $\dot{g}$ *is ( ), then* $s_{\deg}$ *is ( ).*

Table A.2 ACC fuzzy rules (125 rules)

	Antecedents			Consequent
Rule	g_F	g_R	$\dot{g}$	$s_{\deg}$
1	Very Short	Very Short	Extremely negative	Very unsafe
2	Very Short	Very Short	Negative	Very unsafe
3	Very Short	Very Short	Zero	Very unsafe
4	Very Short	Very Short	Positive	Very unsafe
5	Very Short	Very Short	Extremely positive	Very unsafe
6	Very Short	Short	Extremely negative	Very unsafe
7	Very Short	Short	Negative	Very unsafe
8	Very Short	Short	Zero	Very unsafe
9	Very Short	Short	Positive	Unsafe
10	Very Short	Short	Extremely positive	Unsafe
11	Very Short	Medium	Extremely negative	Unsafe
12	Very Short	Medium	Negative	Unsafe
13	Very Short	Medium	Zero	Unsafe
14	Very Short	Medium	Positive	Unsafe
15	Very Short	Medium	Extremely positive	Medium
16	Very Short	Long	Extremely negative	Unsafe
17	Very Short	Long	Negative	Medium
18	Very Short	Long	Zero	Medium
19	Very Short	Long	Positive	Medium
20	Very Short	Long	Extremely positive	Medium
21	Very Short	Very long	Extremely negative	Medium
22	Very Short	Very long	Negative	Medium
23	Very Short	Very long	Zero	Medium
24	Very Short	Very long	Positive	Safe

25	Very Short	Very long	Extremely positive	Safe
26	Short	Very Short	Extremely negative	Very unsafe
27	Short	Very Short	Negative	Very unsafe
28	Short	Very Short	Zero	Very unsafe
29	Short	Very Short	Positive	Very unsafe
30	Short	Very Short	Extremely positive	Unsafe
31	Short	Short	Extremely negative	Very unsafe
32	Short	Short	Negative	Very unsafe
33	Short	Short	Zero	Unsafe
34	Short	Short	Positive	Unsafe
35	Short	Short	Extremely positive	Unsafe
36	Short	Medium	Extremely negative	Unsafe
37	Short	Medium	Negative	Unsafe
38	Short	Medium	Zero	Unsafe
39	Short	Medium	Positive	Medium
40	Short	Medium	Extremely positive	Medium
41	Short	Long	Extremely negative	Medium
42	Short	Long	Negative	Medium
43	Short	Long	Zero	Medium
44	Short	Long	Positive	Medium
45	Short	Long	Extremely positive	Safe
46	Short	Very long	Extremely negative	Medium
47	Short	Very long	Negative	Medium
48	Short	Very long	Zero	Safe
49	Short	Very long	Positive	Safe
50	Short	Very long	Extremely positive	Safe
51	Medium	Very Short	Extremely negative	Very unsafe
52	Medium	Very Short	Negative	Very unsafe
53	Medium	Very Short	Zero	Unsafe
54	Medium	Very Short	Positive	Unsafe
55	Medium	Very Short	Extremely positive	Unsafe
56	Medium	Short	Extremely negative	Unsafe
57	Medium	Short	Negative	Unsafe
58	Medium	Short	Zero	Unsafe

59	Medium	Short	Positive	Unsafe
60	Medium	Short	Extremely positive	Medium
61	Medium	Medium	Extremely negative	Unsafe
62	Medium	Medium	Negative	Medium
63	Medium	Medium	Zero	Medium
64	Medium	Medium	Positive	Medium
65	Medium	Medium	Extremely positive	Medium
66	Medium	Long	Extremely negative	Medium
67	Medium	Long	Negative	Medium
68	Medium	Long	Zero	Safe
69	Medium	Long	Positive	Safe
70	Medium	Long	Extremely positive	Safe
71	Medium	Very long	Extremely negative	Safe
72	Medium	Very long	Negative	Safe
73	Medium	Very long	Zero	Safe
74	Medium	Very long	Positive	Safe
75	Medium	Very long	Extremely positive	Very safe
76	Long	Very Short	Extremely negative	Very unsafe
77	Long	Very Short	Negative	Unsafe
78	Long	Very Short	Zero	Unsafe
79	Long	Very Short	Positive	Unsafe
80	Long	Very Short	Extremely positive	Medium
81	Long	Short	Extremely negative	Unsafe
82	Long	Short	Negative	Unsafe
83	Long	Short	Zero	Medium
84	Long	Short	Positive	Medium
85	Long	Short	Extremely positive	Medium
86	Long	Medium	Extremely negative	Medium
87	Long	Medium	Negative	Medium
88	Long	Medium	Zero	Medium
89	Long	Medium	Positive	Safe
90	Long	Medium	Extremely positive	Safe
91	Long	Long	Extremely negative	Medium
92	Long	Long	Negative	Safe

93	Long	Long	Zero	Safe
94	Long	Long	Positive	Safe
95	Long	Long	Extremely positive	Very safe
96	Long	Very long	Extremely negative	Safe
97	Long	Very long	Negative	Safe
98	Long	Very long	Zero	Very safe
99	Long	Very long	Positive	Very safe
100	Long	Very long	Extremely positive	Very safe
101	Very long	Very Short	Extremely negative	Unsafe
102	Very long	Very Short	Negative	Unsafe
103	Very long	Very Short	Zero	Unsafe
104	Very long	Very Short	Positive	Medium
105	Very long	Very Short	Extremely positive	Medium
106	Very long	Short	Extremely negative	Unsafe
107	Very long	Short	Negative	Medium
108	Very long	Short	Zero	Medium
109	Very long	Short	Positive	Medium
110	Very long	Short	Extremely positive	Medium
111	Very long	Medium	Extremely negative	Medium
112	Very long	Medium	Negative	Medium
113	Very long	Medium	Zero	Safe
114	Very long	Medium	Positive	Safe
115	Very long	Medium	Extremely positive	Safe
116	Very long	Long	Extremely negative	Safe
117	Very long	Long	Negative	Safe
118	Very long	Long	Zero	Safe
119	Very long	Long	Positive	Very safe
120	Very long	Long	Extremely positive	Very safe
121	Very long	Very long	Extremely negative	Safe
122	Very long	Very long	Negative	Very safe
123	Very long	Very long	Zero	Very safe
124	Very long	Very long	Positive	Very safe
125	Very long	Very long	Extremely positive	Very safe

VITA

Chang Won Kim was born in Korea. He received his B.S. degree from the School of Mechanical Engineering, Pusan National University in February 2003. He received his M.S. degree in the Department of Mechanical and Intelligent Systems Engineering at the same University in August 2005. During his master's course, Feb. 2004 – Feb. 2005, he was granted Abroad Cooperative Research funding by the Korean Science and Engineering Foundation, and worked in the Delft University of Technology, the Netherlands. He received his Doctor of Philosophy degree in mechanical engineering at Texas A&M University in 2010. His research interests include bio-inspired control and distributed control and control function management.

His address is

Department of Mechanical Engineering
c/o Dr. Reza Langari
Texas A&M University
College Station, TX 77843-3123

And his e-mail addresses

cwkim@tamu.edu, wonnyday@gmail.com